

**Geometric Nonlinear Controls for Multiple Cooperative Quadrotor
UAVs Transporting a Rigid Body**

Farhad A. Goodarzi

B.S. in Mechanical Engineering, December 2009, Sharif University of Technology
M.S. in Mechanical Engineering, December 2011, Santa Clara University

A Dissertation submitted to

The Faculty of
The School of Engineering and Applied Science
of The George Washington University
in partial satisfaction of the requirements
for the degree of Doctor of Philosophy

August 31, 2015

Dissertation directed by

Taeyoung Lee
Professor of Engineering and Applied Science

The School of Engineering and Applied Science of The George Washington University certifies that Farhad A. Goodarzi has passed the Final Examination for the degree of Doctor of Philosophy as of August 31, 2015. This is the final and approved form of the dissertation.

Geometric Nonlinear Control for Multiple Cooperative Quadrotor UAVs
Transporting a Rigid Body

Farhad A. Goodarzi

Dissertation Research Committee:

Taeyoung Lee, Associate Professor, Dissertation Director

Azim Eskandarian, Professor, Committee Chairman

Adam Wickenheiser, Assistant Professor, Committee Member

Evan Drumwright, Assistant Professor, Committee Member

Jinglai Shen, Associate Professor, Committee Member

© Copyright 2015 by Farhad A. Goodarzi
All rights reserved

Dedication

I dedicate my dissertation work to my family and many friends. A special feeling of gratitude to my loving mother Giti Moradi who has always loved me unconditionally and whose good examples have taught me to work hard for the things that I aspire to achieve. This work is also dedicated to my deceased father who I lost at the begging of my Ph.D. program and his words of encouragement and push for tenacity ring in my ears.

My twin sister Shirin has never left my side and is very special. I also dedicate this dissertation to my many friends who have supported me throughout the process. I will always appreciate all they have done, especially Naeem Masnadi and Parisa Abdollahi for a constant source of support and encouragement during the challenges of graduate school and life. I am truly thankful for having you in my life.

To Dr. Taeyoung Lee, my advisor, whose passion for excellence is apparent in all that he does. His motivational guidance, intellectual tenacity, and editing skills are unsurpassed.

Abstract

Geometric Nonlinear Control for Multiple Cooperative Quadrotor UAVs Transporting a Rigid Body

This dissertation presents nonlinear tracking control systems for quadrotor unmanned aerial vehicles (UAV) under the influence of uncertainties. Assuming that there exist unstructured disturbances in the translational dynamics and the attitude dynamics, a geometric nonlinear adaptive controller is developed directly on the special Euclidean group. In particular, a new form of an adaptive control term is proposed to guarantee stability while compensating the effects of uncertainties in quadrotor dynamics. Next, we derived a coordinate-free form of equations of motion for a complete model of a quadrotor UAV with a payload which is connected via a flexible cable according to Lagrangian mechanics on a manifold. The flexible cable is modeled as a system of serially-connected links and has been considered in the full dynamic model. A geometric nonlinear control system is presented to asymptotically stabilize the position of the quadrotor while aligning the links to the vertical direction below the quadrotor. Finally, we focused on the dynamics and control of arbitrary number of quadrotor UAVs transporting a rigid body payload. The rigid body payload is connected to quadrotors via flexible cables. It is shown that a coordinate-free form of equations of motion can be derived for arbitrary numbers of quadrotors and links according to Lagrangian mechanics on a manifold. A geometric nonlinear controller is presented to transport the rigid body to a fixed desired position while aligning all of the links along the vertical direction. Numerical simulation and experimental results are presented and rigorous mathematical stability analysis are provided. These results will be particularly useful for aggressive load transportation that involves large deformation of the cable.

Table of Contents

Dedication	iv
Abstract	v
List of Figures	viii
Chapter 1: Introduction	1
1.1 Motivation	1
1.2 Literature Review	2
1.3 Proposed Approches	6
1.4 Contributions	7
1.5 Publications	9
Chapter 2-Quadrotor Autonomous Trajectory Tracking	10
2.1 Quadrotor Dynamic Model	11
2.2 Attitude Controlled Flight Mode	14
2.2.1 Attitude Tracking Errors	14
2.2.2 Attitude Tracking Controller	16
2.3 Position Controlled Flight Mode	18
2.3.1 Position Tracking Errors	18
2.3.2 Position Tracking Controller	20
2.3.3 Direction of the First Body-Fixed Axis	23
2.4 Numerical Example	24
Chapter 3: Quadrotor UAV Transporting a Payload with Flexible Cable 27	
3.1 Quadrotor Dynamic Model	27
3.1.1 Lagrangian	29
3.1.2 Euler-Lagrange equations	30
3.2 Control System Design for a Simplified Dynamic Model	33
3.2.1 Control Problem Formulation	33
3.2.2 Linear Control System	34
3.3 Controller Design for a Quadrotor with a Flexible Cable	36
3.3.1 Controller Design	37
3.3.2 Stability Analysis	39
3.4 Numerical Example	40
Chapter 4: Multiple Quadrotor UAVs Transporting a Rigid Body . . .	46
4.1 Quadrotor Dynamic Model	48
4.1.1 Lagrangian	49
4.1.2 Euler-Lagrange equations	50
4.2 Controlled System Design for Simplified Dynamic Model	53
4.2.1 Simplified Dynamic Model	54
4.2.2 Linear Control System	54

4.3	Controlled System Design for Full Dynamic Model	58
4.4	Numerical Example	60
	4.4.1 Stabilization of the Rigid Body	60
	4.4.2 Payload Stabilization with Large Initial Attitude Errors	64
	4.4.3 Two Quadrotors Stabilizing a Rod	67
	Chapter 5: Experiment	71
5.1	CAD Model and Calibration	71
5.2	Building Quadrotor	72
	5.2.1 Hardware Configuration	73
	5.2.2 Software Development	74
5.3	Autonomous Trajectory Tracking	76
	5.3.1 Attitude Tracking Test	76
	5.3.2 Lissajous Curve Trajectory Tracking	77
	5.3.3 Flipping 360 Degree Maneuver	78
5.4	Payload Stabilization with one Quadrotor	82
	Chapter 6: Conclusions	86
6.1	Conclusions	86
6.2	Challenges & Future Work	87
	Bibliography	89
	Appendix- Proofs	97
A.1	Proof for Proposition 1	97
A.2	Proof for Proposition 2	100
A.3	Proof for Proposition 3	102
A.4	Proof for Proposition 4	107
A.5	Proof for Proposition 5	107
A.6	Proof for Proposition 6	110
A.7	Proof for Proposition 7	111
A.8	Proof for Proposition 8	121
A.9	Proof for Proposition 9	125
A.10	Proof for Proposition 10	127

List of Figures

1	Aerial payload transportation	1
2	Quadrotor model	11
3	Controller loops	19
4	Adaptive control law	21
5	Snapshots of a flipping maneuver: the red line denotes the rotation axis $e_r = [\frac{1}{\sqrt{2}}, \frac{1}{\sqrt{2}}, 0]$. The quadrotor UAV rotates about the e_r axis by 360° . The trajectory of its mass center is denoted by blue, dotted lines.	25
6	Flipping without adaptive term (dotted:desired, solid:actual) .	26
7	Flipping with adaptive term (dotted:desired, solid:actual) . . .	26
8	Quadrotor UAV with a cable-suspended load. Cable is modeled as a serial connection of arbitrary number of links (only 5 are illustrated).	28
9	Stabilization of a payload connected to a quadrotor with 5 links without Integral term	41
10	Stabilization of a payload connected to a quadrotor with 5 links with Integral term	43
11	Snapshots of the controlled maneuver	45
12	Quadrotor UAVs with a rigid body payload. Cables are modeled as a serial connection of an arbitrary number of links (only 4 quadrotors with 5 links in each cable are illustrated).	47
13	Stabilization of a rigid-body connected to multiple quadrotors	62
14	Snapshots of controlled maneuver	63
15	Stabilization of a payload with multiple quadrotors connected with flexible cables.	65
16	Snapshots of the controlled maneuver.	66
17	Two quadrotor with a rod	67

18	Stabilization of a rod with two quadrotors without Integral term.	68
19	Stabilization of a rod with two quadrotors with Integral term.	69
20	Snapshots of the controlled maneuver for two quadrotors stabilizing a rod.	70
21	Hardware development for a quadrotor UAV	71
22	Hardware development	72
23	Motion capture Laboratory	72
24	Hardware parts for a quadrotor UAV	73
25	Motors and speed controllers	74
26	Hardware connections	74
27	Quadrotors	75
28	Information flow of overall system	75
29	Information flow of overall system	75
30	Attitude tracking test(dotted:desired, solid:actual)	76
31	Quadrotor on a stand	77
32	Lissajous curve $x - y$ plane trajectory	78
33	Lissajous curve tracking(dotted:desired, solid:actual)	79
34	Flipping flight test results (dotted:desired, solid:actual)	81
35	Snapshots for flipping maneuver.	82
36	Experimental results (x_d :black, x :red, $x + l_1 q_1$:blue)	84
37	Snapshot of a quadrotor UAV stabilizing a payload	85
38	Experimental results: link deflection angles	85

Chapter 1: Introduction

1.1 Motivation

Quadrotor unmanned aerial vehicles (UAVs) are becoming increasingly popular. They offer flight characteristics comparable to traditional helicopters, namely stationary, vertical, and lateral flights in a wide range of speeds, with a much simpler mechanical structure. With their small-diameter rotors driven by electric motors, these multi-rotor platforms are safer to operate than helicopters in indoor environments. Also, they have sufficient payload transporting capability and flight endurance for various missions [1, 2, 3, 4]. UAVs have been studied for different applications such as surveillance or mobile sensor networks as well as for educational purposes. Quadrotors are very popular due to their dynamic simplicity, maneuverability and high performance. Aerial transportation of a cable-suspended load has been studied traditionally for helicopters [5, 6]. Recently, small-size single or multiple autonomous vehicles are considered for load transportation and deployment [7, 8, 9, 10], and trajectories with minimum swing and oscillation of payload are generated [11, 12, 13].

Safe cooperative transportation of possibly large or bulky payloads is extremely important in various missions, such as military operations, search and rescue, mars surface explorations and personal assistance.



Figure 1: Aerial payload transportation

However, these results are based on the common and restrictive assumption that the cable connecting the payload to the quadrotor UAV is always taut and rigid. Also, the dynamic of the cable and payload are ignored and they are considered as bounded disturbances to the transporting vehicle. Therefore, they cannot be applied to aggressive, rapid load transportations where the cable is deformed or the tension along the cable is low, thereby restricting its applicability. As such, it is impossible to guarantee safety operations.

It is challenging to incorporate the effects of a deformable cable, since the dimension of the configuration space becomes infinite. Finite element approximation of a cable often yields complicated equations of motion that make dynamic analysis and controller design extremely difficult.

1.2 Literature Review

Several control systems have been proposed for quadrotors. In many cases, disturbances and uncertainties are eliminated in the model for simplicity. There are other limitations of quadrotor control systems, such as complexities in controller structures or lack of stability proof. For example, tracking control of a quadrotor UAV has been considered in [14, 15], but the control system in [14] has a complex structure since it is based on a multiple-loop backstepping approach, and no stability proof is presented in [15]. Robust tracking control systems are studied in [16, 17], but the quadrotor dynamics is simplified by considering planar motion only [16], or by ignoring the rotational dynamics by timescale separation assumption [17].

In other studies, disturbances and uncertainties have been considered into the dynamics of the quadrotors [18, 19, 20, 21]. Several controllers have been

designed and presented to eliminate these disturbances such as PID [22], sliding mode [23], or robust controllers [24]. In one example, proportional-derivative controllers are developed with consideration of blade flapping for operations under wind disturbances [25]. A backstepping control method is proposed in [26] by considering an aggressive perturbation with bounded signals. These approaches have certain limitations on handling uncertainties. For example, it is well known that sliding mode controller causes chattering problems that may excite high-frequency unmodeled dynamics. Nonlinear robust tracking control systems in [27, 28] guarantee ultimate boundedness of tracking errors only, and they are also prone to chattering if the required ultimate bound is smaller. PID controllers are adopted widely, but it is required that the uncertainties are fixed.

Due to the limitations mentioned above, adaptive controllers have been developed [29, 30, 31, 32]. Although adaptive controllers compensate the effects of disturbances and uncertainties for quadrotor controls, most of the studies are based on linearization [29, 30] or simplification [31, 32]. In [31] only the constant external disturbances is considered into the system dynamics and the stability analysis. In [32] an adaptive block backstepping controller is presented to stabilize the attitude of a quadrotor, however this method only guarantees the boundedness of errors. A nonlinear adaptive state feedback controller is also presented in [33], where the proposed controller only assumes constant known disturbance forces. An adaptive sliding mode controller is developed for under-actuated quadrotor dynamics in [34]. This controller uses slack variables to overcome the under-actuated property of a quadrotor system while simplifying the dynamics to reduce the higher-order derivative terms which makes it very sensitive to the noise. A robust adaptive control of a

quadrotor is also presented in [35], where linear-in-the-parameter uncertainties and bounded disturbances are considered. These simplifications [31, 33], linearization [29, 30], and assumptions [32] in the dynamics and controller design process of adaptive controllers restrict the quadrotor to maintain complex or aggressive missions such as a flipping maneuver [35].

The other critical issue in designing controllers for quadrotors is that they are mostly based on local coordinates. Local coordinates such as Euler angles and quaternions produce singularities and the dynamic model needs to be examined and studied more explicitly [36]. For quadrotor UAV's dynamics, some aggressive maneuvers are demonstrated at [37] which are based on Euler angles. Therefore they involve complicated expressions for trigonometric functions, and they exhibit singularities in representing quadrotor attitudes, thereby restricting their ability to achieve complex rotational maneuvers significantly. A quaternion-based feedback controller for attitude stabilization was shown in [38]. By considering the Coriolis and gyroscopic torques explicitly, this controller guarantees exponential stability. Quaternions do not have singularities but, as the three-sphere double-covers the special orthogonal group, one attitude may be represented by two antipodal points on the three-sphere. This ambiguity should be carefully resolved in quaternion-based attitude control systems, otherwise they may exhibit unwinding, where a rigid body unnecessarily rotates through a large angle even if the initial attitude error is small [39]. To avoid these, an additional mechanism to lift attitude onto the unit-quaternion space is introduced [40].

The dynamics of a quadrotor UAV is globally expressed on the special Euclidean group, $SE(3)$, and nonlinear control systems are developed to track

outputs of several flight modes [41]. There are also several studies using the estimations for dynamical objects developed on the special Euclidean group [42, 43, 44]. Several aggressive maneuvers of a quadrotor UAV or spacecrafts are demonstrated based on a hybrid control architecture, and a nonlinear robust control system is also considered in [27, 45]. As they are directly developed on the special Euclidean/Orthogonal group, complexities, singularities, and ambiguities associated with minimal attitude representations or quaternions are completely avoided [46, 47, 48].

In most of the prior works, the dynamics of aerial transportation has been simplified due to the inherent dynamic complexities. For example, it is assumed that the dynamics of the payload is considered completely decoupled from quadrotors, and the effects of the payload and the cable are regarded as arbitrary external forces and moments exerted to the quadrotors [11, 12, 13], thereby making it challenging to suppress the swinging motion of the payload actively, particularly for agile aerial transportations.

Recently, the coupled dynamics of the payload or cable has been explicitly incorporated into control system design [49]. In particular, a complete model of a quadrotor transporting a payload modeled as a point mass, connected via a flexible cable is presented, where the cable is modeled as serially connected links to represent the deformation of the cable [2]. In another distinct study, multiple quadrotors transporting a rigid body payload has been studied [50], but it is assumed that the cables connecting the rigid body payload and quadrotors are always taut. These assumptions and simplifications in the dynamics of the system reduce the stability of the controlled system, particularly in rapid and aggressive load transportation where the motion of the cable and payload

is excited nontrivially.

1.3 Proposed Approches

Geometric nonlinear controllers are developed to follow an attitude tracking command and a position tracking command. In particular, a new form of an adaptive control term is proposed to guarantee asymptotical convergence of tracking error variables when there exist uncertainties at the translational dynamics and the rotational dynamics of quadrotors. The corresponding stability properties are analyzed mathematically, and they are verified by several experiments [51]. The robustness of the proposed tracking control systems are critical in generating complex maneuvers, as the impact of the several aerodynamic effects resulting from the variation in air speed is significant even at moderate velocities [25].

A coordinate-free form of the equations of motion for a chain pendulum connected a cart that moves on a horizontal plane is presented according to Lagrangian mechanics on a manifold [52]. The cable is modeled as an arbitrary number of links with different sizes and masses that are serially-connected by spherical joints. The resulting configuration manifold is the product of the special Euclidean group for the position and the attitude of the quadrotor, and a number of two-spheres that describe the direction of each link. We present Euler-Lagrange equations of the presented quadrotor model that are globally defined on the nonlinear configuration manifold.

The coupled dynamics of the payload or cable has been explicitly incorporated into control system design [49]. In particular, a complete model of a quadrotor transporting a payload modeled as a point mass, connected via

a flexible cable is presented. In another distinct study, multiple quadrotors transporting a rigid body payload has been studied [50], but it is assumed that the cables connecting the rigid body payload and quadrotors are always taut. These assumptions and simplifications in the dynamics of the system reduce the stability of the controlled system, particularly in rapid and aggressive load transportation where the motion of the cable and payload is excited nontrivially.

Quadrotor UAV is under-actuated as the direction of the total thrust is always fixed relative to its body. By utilizing geometric control systems for quadrotor [41, 28, 45], we show that the hanging equilibrium of the links can be asymptotically stabilized while translating the quadrotor to a desired position. In contrast to existing papers where the force and the moment exerted by the payload to the quadrotor are considered as disturbances, the control systems proposed in this work explicitly consider the coupling effects between the cable/load dynamics and the quadrotor dynamics.

1.4 Contributions

The first distinct feature of the proposed approach is that the equations of motion and the control systems are developed directly on the nonlinear configuration manifold in a coordinate-free fashion. This yields remarkably compact expressions for the dynamic model and controllers, compared with local coordinates that often require symbolic computational tools due to complexity of multi-body systems. Furthermore, singularities of local parameterization are completely avoided to generate agile maneuvers in a uniform way.

This work presents a rigorous Lyapunov stability analysis to establish sta-

bility properties without any timescale separation assumptions or singular perturbation, and a new nonlinear integral and adaptive control term are designed to guarantee robustness against unstructured uncertainties in both rotational and translational dynamics.

The other distinct contribution of this dissertation is presenting the complete dynamic model of an arbitrary number of quadrotors transporting a rigid body where each quadrotor is connected to the rigid body via a flexible cable. Each flexible cable is modeled as an arbitrary number of serially connected links, and it is valid for various masses and lengths. A coordinate free form of equations of motion is derived according to Lagrange mechanics on a nonlinear manifold for the full dynamic model. These sets of equations of motion are presented in a complete and organized manner without any simplification.

Another contribution of this study is designing a control system to stabilize the rigid body at desired position. Geometric nonlinear controller is utilized [41, 28, 45], and they are generalized for the presented model. More explicitly, we show that the rigid body payload is asymptotically transported into a desired location, while aligning all of the links along the vertical direction corresponding to a hanging equilibrium.

The unique property of the proposed control system is that the nontrivial coupling effects between the dynamics of rigid payload, flexible cables, and multiple quadrotors are explicitly incorporated into control system design, without any simplifying assumption. Also, the equations of motion and the control systems are developed directly on the nonlinear configuration manifold intrinsically. Therefore, singularities of local parameterization are completely

avoided to generate agile maneuvers of the payload in a uniform way. In short, the proposed control system is particularly useful for rapid and safe payload transportation in complex terrain, where the position of the payload should be controlled concurrently while suppressing the deformation of the cables.

1.5 Publications

The contributions in this dissertation have been published in the following journals and conference proceedings.

- Farhad A. Goodarzi, Daewon Lee, Taeyoung Lee, Geometric Control of a Quadrotor UAV Transporting a Payload Connected via Flexible Cable, International Journal of Control, Automation and Systems, Vol. 13, No. 6, December 2015.
- Farhad A. Goodarzi, Daewon Lee, Taeyoung Lee, Geometric Adaptive Tracking Control of a Quadrotor UAV on $SE(3)$ for Agile Maneuvers, ASME Journal of Dynamic Systems, Measurement and Control, 137(9), 091007-12, Sep 01, 2015
- Farhad A. Goodarzi, Taeyoung Lee, Dynamic and Control of Quadrotor UAVs Transporting a Rigid Body Connected via Flexible Cables, in Proceeding of American Control Conference, pp. 4677-4682, Chicago, IL, July 2015
- Farhad A. Goodarzi, Daewon Lee, Taeyoung Lee, Geometric Stabilization of a Quadrotor UAV with a Payload Connected by flexible Cable, in Proceeding of American Control Conference, pp. 4925-4930, Portland, OR, June 2014
- Farhad A. Goodarzi, Daewon Lee, Taeyoung Lee, Geometric Nonlinear PID Control of a Quadrotor UAV on $SO(3)$, in Proceeding of European Control Conference, pp. 3845-3850, Zurich, Switzerland, February 2013

Chapter 2-Quadrotor Autonomous Trajectory Tracking

In this chapter, we present a complete model of a quadrotor transporting a payload connecting with a flexible cable. The flexible cable is modeled as an arbitrary number of serially connected links. Geometric nonlinear controller presented for the full dynamic model considering the coupling effects of payload and the cable.

New contributions and the unique features of the control system proposed in this chapter compared with other studies are as follows: (i) it is developed for the full six degrees of freedom dynamic model of a quadrotor UAV on $SE(3)$, including the coupling effects between the translational dynamics and the rotational dynamics on a nonlinear manifold without any simplification or assumptions, (ii) the control systems are developed directly on the nonlinear configuration manifold in a coordinate-free fashion. Thus, singularities of local parameterization are completely avoided to generate agile maneuvers in a uniform way, (iii) a rigorous Lyapunov analysis is presented to establish stability properties without any timescale separation assumption, and (iv) a new form of an adaptive control term is proposed to guarantee asymptotical convergence of tracking error variables in the presence of uncertainties, (v) in contrast to hybrid control systems [53], complicated reachability set analysis is not required to guarantee safe switching between different flight modes, as the region of attraction for each flight mode covers the configuration space almost globally, (vi) the proposed algorithm is validated with experiments for agile maneuvers. A rigorous mathematical analysis of nonlinear adaptive controllers for a quadrotor UAV on $SE(3)$ with experimental validations for complex and aggressive maneuvers is unprecedented.

The chapter is organized as follows. We develop a globally defined model for a quadrotor UAV in Section 2.1. Adaptive tracking control systems are developed in Sections 2.2 and 2.3, followed by numerical examples in Section 2.4.

2.1 Quadrotor Dynamic Model

Consider a quadrotor UAV model illustrated in Figure 2. We choose an inertial reference frame $\{\vec{e}_1, \vec{e}_2, \vec{e}_3\}$ and a body-fixed frame $\{\vec{b}_1, \vec{b}_2, \vec{b}_3\}$. The origin of the body-fixed frame is located at the center of mass of this vehicle. The first and the second axes of the body-fixed frame, \vec{b}_1, \vec{b}_2 , lie in the plane defined by the centers of the four rotors.

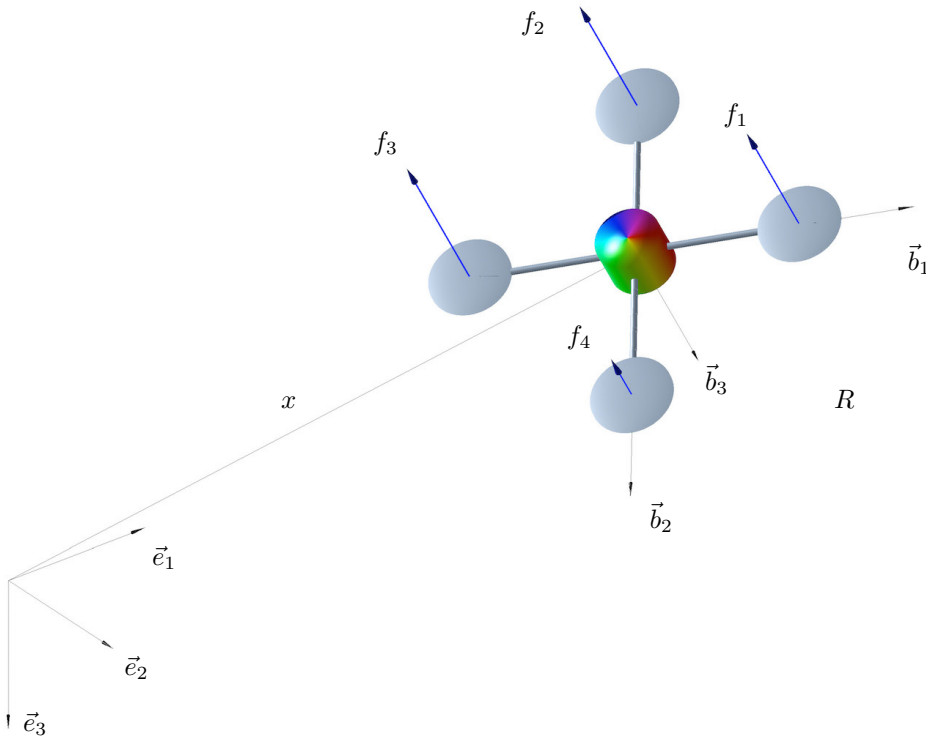


Figure 2: Quadrotor model

The configuration of this quadrotor UAV is defined by the location of the center of mass and the attitude with respect to the inertial frame. Therefore, the configuration manifold is the special Euclidean group $\text{SE}(3)$, which is the semi-direct product of \mathbb{R}^3 and the special orthogonal group $\text{SO}(3) = \{R \in \mathbb{R}^{3 \times 3} \mid R^T R = I, \det R = 1\}$.

The mass and the inertial matrix of a quadrotor UAV are denoted by $m \in \mathbb{R}$ and $J \in \mathbb{R}^{3 \times 3}$. Its attitude, angular velocity, position, and velocity are

defined by $R \in \text{SO}(3)$, $\Omega, x, v \in \mathbb{R}^3$, respectively, where the rotation matrix R represents the linear transformation of a vector from the body-fixed frame to the inertial frame and the angular velocity Ω is represented with respect to the body-fixed frame. The distance between the center of mass to the center of each rotor is $d \in \mathbb{R}$, and the i -th rotor generates a thrust f_i and a reaction torque τ_i along $-\vec{b}_3$ for $1 \leq i \leq 4$. The magnitude of the total thrust and the total moment in the body-fixed frame are denoted by $f \in \mathbb{R}$, $M \in \mathbb{R}^3$, respectively.

The following conventions are assumed for the rotors and propellers, and the thrust and moment that they exert on the quadrotor UAV. We assume that the thrust of each propeller is directly controlled, and the direction of the thrust of each propeller is normal to the quadrotor plane. The first and third propellers are assumed to generate a thrust along the direction of $-\vec{b}_3$ when rotating clockwise; the second and fourth propellers are assumed to generate a thrust along the same direction of $-\vec{b}_3$ when rotating counterclockwise. Thus, the thrust magnitude is $f = \sum_{i=1}^4 f_i$, and it is positive when the total thrust vector acts along $-\vec{b}_3$, and it is negative when the total thrust vector acts along \vec{b}_3 . By the definition of the rotation matrix $R \in \text{SO}(3)$, the direction of the i -th body-fixed axis \vec{b}_i is given by Re_i in the inertial frame, where $e_1 = [1; 0; 0]$, $e_2 = [0; 1; 0]$, $e_3 = [0; 0; 1] \in \mathbb{R}^3$. Therefore, the total thrust vector is given by $-fRe_3 \in \mathbb{R}^3$ in the inertial frame.

We also assume that the torque generated by each propeller is directly proportional to its thrust. Since it is assumed that the first and the third propellers rotate clockwise and the second and the fourth propellers rotate counterclockwise to generate a positive thrust along the direction of $-\vec{b}_3$, the torque generated by the i -th propeller about \vec{b}_3 can be written as $\tau_i = (-1)^i c_{\tau f} f_i$ for a fixed constant $c_{\tau f}$. All of these assumptions are fairly common in many

quadrotor control systems [38, 54].

Under these assumptions, the thrust of each propeller f_1, f_2, f_3, f_4 is directly converted into f and M , or vice versa. In this paper, the thrust magnitude $f \in \mathbb{R}$ and the moment vector $M \in \mathbb{R}^3$ are viewed as control inputs. The corresponding equations of motion are given by

$$\dot{x} = v, \quad (1)$$

$$m\dot{v} = mge_3 - fRe_3 + W_x(x, v, R, \Omega)\theta_x, \quad (2)$$

$$\dot{R} = R\hat{\Omega}, \quad (3)$$

$$J\dot{\Omega} + \Omega \times J\Omega = M + W_R(x, v, R, \Omega)\theta_R, \quad (4)$$

where the *hat map* $\hat{\cdot} : \mathbb{R}^3 \rightarrow \text{SO}(3)$ is defined by the condition that $\hat{x}y = x \times y$ for all $x, y \in \mathbb{R}^3$. More explicitly, for a vector $x = [x_1, x_2, x_3]^T \in \mathbb{R}^3$, the matrix \hat{x} is given by

$$\hat{x} = \begin{bmatrix} 0 & -x_3 & x_2 \\ x_3 & 0 & -x_1 \\ -x_2 & x_1 & 0 \end{bmatrix}. \quad (5)$$

This identifies the Lie algebra $\text{SO}(3)$ with \mathbb{R}^3 using the vector cross product in \mathbb{R}^3 . The inverse of the hat map is denoted by the *vee* map, $\vee : \text{SO}(3) \rightarrow \mathbb{R}^3$.

The modeling error and uncertainties in the translational dynamics and the rotational dynamics are given by $W_x(x, v, R, \Omega)\theta_x$, and $W_R(x, v, R, \Omega)\theta_R$, respectively. Where $W_x(x, v, R, \Omega), W_R(x, v, R, \Omega) \in \mathbb{R}^{3 \times P}$ are known functions of the state, and $\theta_x, \theta_R \in \mathbb{R}^{P \times 1}$ are fixed unknown parameters. It is assumed that the bounds of unknown parameters are given by

$$\|W_x\| \leq B_{W_x}, \quad \|\theta_x\| \leq B_\theta, \quad \|\theta_R\| \leq B_\theta, \quad (6)$$

for $B_{W_x}, B_\theta > 0$. Throughout this chapter, $\lambda_m(A)$ and $\lambda_M(A)$ denote the minimum eigenvalue and the maximum eigenvalue of a square matrix A , respectively, and λ_m and λ_M are the minimum eigenvalue and the maximum eigenvalue of the inertia matrix J . i.e., $\lambda_m = \lambda_m(J)$ and $\lambda_M = \lambda_M(J)$. The two-norm of a matrix A is denoted by $\|A\|$. The standard dot product in \mathbb{R}^n is denoted by \cdot , i.e., $x \cdot y = x^T y$ for any $x, y \in \mathbb{R}^n$.

2.2 Attitude Controlled Flight Mode

Since the quadrotor UAV has four inputs, it is possible to achieve asymptotic output tracking for at most four quadrotor UAV outputs. The quadrotor UAV has three translational and three rotational degrees of freedom; it is not possible to achieve asymptotic output tracking of both attitude and position of the quadrotor UAV. This motivates us to introduce two flight modes, namely (1) an attitude controlled flight mode, and (2) a position controlled flight mode. While a quadrotor UAV is under-actuated, a complex flight maneuver can be defined by specifying a concatenation of flight modes together with conditions for switching between them. This will be further illustrated by a numerical example and experimental results later. In this section, the attitude controlled flight mode is considered.

2.2.1 Attitude Tracking Errors

Suppose that a smooth attitude command $R_d(t) \in \text{SO}(3)$ satisfying the following kinematic equation is given:

$$\dot{R}_d = R_d \hat{\Omega}_d, \tag{7}$$

where $\Omega_d(t) \in \mathbb{R}^3$ is the desired angular velocity, which is assumed to be uniformly bounded. We first define errors associated with the attitude dynamics as follows [55, 56].

Proposition 1 *For a given tracking command (R_d, Ω_d) , and the current attitude and angular velocity (R, Ω) , we define an attitude error function $\Psi : \text{SO}(3) \times \text{SO}(3) \rightarrow \mathbb{R}$, an attitude error vector $e_R \in \mathbb{R}^3$, and an angular velocity error vector $e_\Omega \in \mathbb{R}^3$ as follows [56]:*

$$\Psi(R, R_d) = \frac{1}{2} \text{tr}[G(I - R_d^T R)], \quad (8)$$

$$e_R = \frac{1}{2}(GR_d^T R - R^T R_d G)^\vee, \quad (9)$$

$$e_\Omega = \Omega - R^T R_d \Omega_d, \quad (10)$$

where the matrix $G \in \mathbb{R}^{3 \times 3}$ is given by $G = \text{diag}[g_1, g_2, g_3]$ for distinct, positive constants $g_1, g_2, g_3 \in \mathbb{R}$. Then, the following properties hold:

- (i) Ψ is positive-definite about $R = R_d$.
- (ii) The directional derivative of Ψ with respect to R along $\delta R = R\hat{\eta}$ for any $\eta \in \mathbb{R}^3$ is given by

$$\left. \frac{d}{d\epsilon} \right|_{\epsilon=0} \Psi(R \exp(\epsilon \hat{\eta}), R_d) = e_R \cdot \eta. \quad (11)$$

- (iii) The critical points of Ψ , where $e_R = 0$, are $\{R_d\} \cup \{R_d \exp(\pi \hat{s}), s \in \mathbb{S}^2\}$, where $\mathbb{S}^2 = \{s \in \mathbb{R}^3 \mid \|s\| = 1\}$.

- (iv) A lower bound of Ψ is given as follows:

$$b_1 \|e_R\|^2 \leq \Psi(R, R_d), \quad (12)$$

where the constant b_1 is given by $b_1 = \frac{h_1}{h_2+h_3}$ for

$$\begin{aligned} h_1 &= \min\{g_1 + g_2, g_2 + g_3, g_3 + g_1\}, \\ h_2 &= \max\{(g_1 - g_2)^2, (g_2 - g_3)^2, (g_3 - g_1)^2\}, \\ h_3 &= \max\{(g_1 + g_2)^2, (g_2 + g_3)^2, (g_3 + g_1)^2\}. \end{aligned}$$

(v) Let ψ be a positive constant that is strictly less than 2. If $\Psi(R, R_d) < \psi < h_1$, then an upper bound of Ψ is given by

$$\Psi(R, R_d) \leq b_2 \|e_R\|^2, \quad (13)$$

where the constant b_2 is given by $b_2 = \frac{h_1 h_4}{h_5(h_1 - \psi)}$ for

$$\begin{aligned} h_4 &= \max\{g_1 + g_2, g_2 + g_3, g_3 + g_1\}, \\ h_5 &= \min\{(g_1 + g_2)^2, (g_2 + g_3)^2, (g_3 + g_1)^2\}. \end{aligned}$$

(vi) The time-derivative of Ψ and e_R satisfies:

$$\dot{\Psi} = e_R \cdot e_\Omega, \quad \|\dot{e}_R\| \leq \|e_\Omega\|. \quad (14)$$

Proof 1 See Appendix A.1 .

2.2.2 Attitude Tracking Controller

We now introduce a nonlinear controller for the attitude controlled flight mode:

$$M = -k_R e_R - k_\Omega e_\Omega - \mathbb{W}_R \bar{\theta}_R + (R^T R_d \Omega_d)^\wedge J R^T R_d \Omega_d + J R^T R_d \dot{\Omega}_d, \quad (15)$$

and adaptive law

$$\dot{\bar{\theta}}_R = \gamma_R \mathbf{W}_R^T (e_\Omega + c_2 e_R), \quad (16)$$

where $k_R, k_\Omega, c_2, \gamma_R$ are positive constants and $\bar{\theta}_R \in \mathbb{R}^p$ denotes the estimated value of θ_R . The adaptive gains for e_Ω and e_R correspond to γ_R and $c_2\gamma_R$, respectively.

The control moment is composed of proportional, derivative, and adaptive terms, augmented with additional terms to cancel out the angular acceleration caused by the desired angular velocity.

Proposition 2 (*Attitude Controlled Flight Mode*) Consider the control moment M defined in (15)-(16). For positive constants k_R, k_Ω , the constants c_2, B_2 are chosen such that

$$\|(2J - \text{tr}[J]I)\|\|\Omega_d\| \leq B_2, \quad (17)$$

$$c_2 < \min \left\{ \frac{\sqrt{k_R \lambda_m}}{\lambda_M}, \frac{4k_\Omega}{8k_R \lambda_M + (k_\Omega + B_2)^2} \right\}, \quad (18)$$

Then, the zero equilibrium of tracking errors and the estimation errors is stable in the sense of Lyapunov, and $e_R, e_\Omega \rightarrow 0$ as $t \rightarrow \infty$. Furthermore the estimation error, $\tilde{\theta}_R = \theta_R - \bar{\theta}_R$, is uniformly bounded.

Proof 2 See Appendix A.2 .

While these results are developed for the attitude dynamics of a quadrotor UAV, they can be applied to the attitude dynamics of any rigid body. Nonlinear adaptive controllers have been developed for attitude stabilization in terms of modified Rodriguez parameters [57] and quaternions [58], and for attitude tracking in terms of Euler-angles [59]. The proposed tracking control

system is developed on $\text{SO}(3)$, therefore it avoids singularities of Euler-angles and Rodriguez parameters, as well as unwinding of quaternions.

Asymptotic tracking of the quadrotor attitude does not require specification of the thrust magnitude. As an auxiliary problem, the thrust magnitude can be chosen in many different ways to achieve an additional translational motion objective. For example, it can be used to asymptotically track a quadrotor altitude command [28]. Since the translational motion of the quadrotor UAV can only be partially controlled; this flight mode is most suitable for short time periods where an attitude maneuver is to be completed.

2.3 Position Controlled Flight Mode

We introduce a nonlinear controller for the position controlled flight mode in this section.

2.3.1 Position Tracking Errors

Suppose that an arbitrary smooth position tracking command $x_d(t) \in \mathbb{R}^3$ is given. The position tracking errors for the position and the velocity are given by:

$$e_x = x - x_d, \quad e_v = \dot{e}_x = v - \dot{x}_d. \quad (19)$$

In the position controlled tracking mode, the attitude dynamics is controlled to follow the computed attitude $R_c(t) \in \text{SO}(3)$ as illustrated in Figure 3 and the computed angular velocity $\Omega_c(t)$ defined as

$$R_c = [b_{1c}; b_{3c} \times b_{1c}; b_{3c}], \quad \hat{\Omega}_c = R_c^T \dot{R}_c, \quad (20)$$

where $b_{3_c} \in \mathbf{S}^2$ is given by

$$b_{3_c} = -\frac{-k_x e_x - k_v e_v - \mathbb{W}_x \bar{\theta}_x - m g e_3 + m \ddot{x}_d}{\| -k_x e_x - k_v e_v - \mathbb{W}_x \bar{\theta}_x - m g e_3 + m \ddot{x}_d \|}, \quad (21)$$

for positive constants k_x, k_v and $\bar{\theta}_x \in \mathbb{R}^p$ denotes the estimate value of θ_x . The

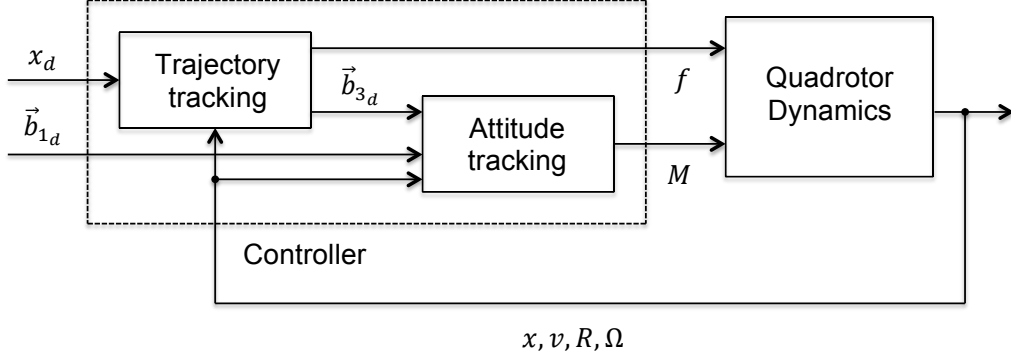


Figure 3: Controller loops

unit vector $b_{1_c} \in \mathbf{S}^2$ is selected to be orthogonal to b_{3_c} , thereby guaranteeing that $R_c \in \text{SO}(3)$. It can be chosen to specify the desired heading direction, and the detailed procedure to select b_{1_c} is described later at Section 2.3.3. Following the prior definition of the attitude error and the angular velocity error given at (9) and (10), and assume that the commanded acceleration is uniformly bounded:

$$\| -m g e_3 + m \ddot{x}_d \| < B_1 \quad (22)$$

for a given positive constant B_1 . These imply that the given desired position command is distinctive from free-fall, where no control input is required.

2.3.2 Position Tracking Controller

The nonlinear controller for the position controlled flight mode, described by control expressions for the thrust magnitude and the moment vector, are:

$$f = (k_x e_x + k_v e_v + \mathbb{W}_x \bar{\theta}_x + m g e_3 - m \ddot{x}_d) \cdot R e_3, \quad (23)$$

$$M = -k_R e_R - k_\Omega e_\Omega - \mathbb{W}_R \bar{\theta}_R + (R^T R_c \Omega_c)^\wedge J R^T R_c \Omega_c + J R^T R_c \dot{\Omega}_c. \quad (24)$$

In 23, we can show that the total thrust is always positive. The first term in this equation is the projection into b_3 and while controller works perfectly we can guarantee that the angle between two terms in 23 is always less than 90 degree and it happens when R is close to R_c . Similar with (16), an adaptive control law for the position tracking controller is defined as

$$\dot{\theta}_x = \begin{cases} \gamma_x \mathbb{W}_x^T (e_v + c_1 e_x) & \text{if } \|\bar{\theta}_x\| < B_\theta \\ & \text{or } \|\bar{\theta}_x\| = B_\theta \\ & \text{and } \bar{\theta}_x^T \mathbb{W}_x^T (e_v + c_1 e_x) \leq 0, \\ \gamma_x \left(I - \frac{\bar{\theta}_x \bar{\theta}_x^T}{\bar{\theta}_x^T \bar{\theta}_x} \right) \mathbb{W}_x^T (e_v + c_1 e_x) & \text{Otherwise} \end{cases} \quad (25)$$

for a positive adaptive gain γ_x and a weighting parameter c_1 . The corresponding effective adaptive gain for e_x corresponds to $c_1 \gamma_x$. The above expression correspond adaptive controls with projection [60] and it is included to restrict the effects of attitude tracking errors on the translational dynamics as shown in Figure 4

The nonlinear controller given by equations (23), (24) can be given a back-stepping interpretation. The computed attitude R_c given in equation (20) is selected so that the thrust axis $-b_3$ of the quadrotor UAV tracks the computed

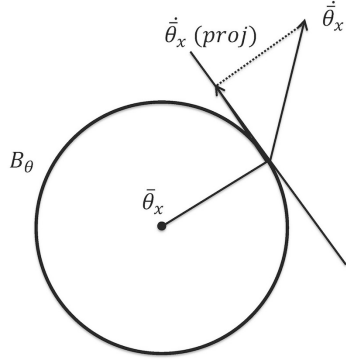


Figure 4: Adaptive control law

direction given by $-b_{3_c}$ in (21), which is a direction of the thrust vector that achieves position tracking. The moment expression (24) causes the attitude of the quadrotor UAV to asymptotically track R_c and the thrust magnitude expression (23) achieves asymptotic position tracking.

Proposition 3 (*Position Controlled Flight Mode*) *Suppose that the initial conditions satisfy*

$$\Psi(R(0), R_c(0)) < \psi_1 < 1, \quad (26)$$

for positive constant ψ_1 . Consider the control inputs f, M defined in (23)-(24). For positive constants k_x, k_v , we choose positive constants c_1, c_2, k_R, k_Ω such that

$$c_1 < \min \left\{ \frac{4k_x k_v (1 - \alpha)^2}{k_v^2 (1 + \alpha)^2 + 4m k_x (1 - \alpha)}, \sqrt{\frac{k_x}{m}} \right\}, \quad (27)$$

$$\lambda_m(W_2) > \frac{\|W_{12}\|^2}{4\lambda_m(W_1)}, \quad (28)$$

and (237) is satisfied, where $\alpha = \sqrt{\psi_1(2 - \psi_1)}$, and the matrices $W_1, W_{12}, W_2 \in \mathbb{R}^{2 \times 2}$

are given by

$$W_1 = \begin{bmatrix} c_1 k_x (1 - \alpha) & -\frac{c_1 k_v}{2} (1 + \alpha) \\ -\frac{c_1 k_v}{2} (1 + \alpha) & k_v (1 - \alpha) - m c_1 \end{bmatrix}, \quad (29)$$

$$W_{12} = \begin{bmatrix} c_1 (B_{W_x} B_\theta + B_1) & 0 \\ B_{W_x} B_\theta + B_1 + k_x e_{x_{\max}} & 0 \end{bmatrix}, \quad (30)$$

$$W_2 = \begin{bmatrix} c_2 k_R & -\frac{c_2}{2} (k_\Omega + B_2) \\ -\frac{c_2}{2} (k_\Omega + B_2) & k_\Omega - 2c_2 \lambda_M \end{bmatrix}. \quad (31)$$

This implies that the zero equilibrium of the tracking errors and the estimation errors is stable in the sense of Lyapunov and all of the tracking error variables asymptotically converge to zero. Also, the estimation errors are uniformly bounded.

Proof 3 See Appendix A.3 .

Proposition 3 requires that the initial attitude error is less than 90° in (26). Suppose that this is not satisfied, i.e. $1 \leq \Psi(R(0), R_c(0)) < 2$. We can still apply Proposition 2, which states that the attitude error is asymptotically decreases to zero for almost all cases, and it satisfies (26) in a finite time. Therefore, by combining the results of Proposition 2 and 3, we can show attractiveness of the tracking errors when $\Psi(R(0), R_c(0)) < 2$.

Proposition 4 (*Position Controlled Flight Mode with a Larger Initial Attitude Error*) Suppose that the initial conditions satisfy

$$1 \leq \Psi(R(0), R_c(0)) < 2, \quad \|e_x(0)\| < e_{x_{\max}}, \quad (32)$$

for a constant $e_{x_{\max}}$. Consider the control inputs f, M defined in (23)-(24), where the control parameters satisfy (26)-(28) for a positive constant $\psi_1 < 1$. Then the zero equilibrium of the tracking errors is attractive, i.e., $e_x, e_v, e_R, e_\Omega \rightarrow 0$ as $t \rightarrow \infty$.

Proof 4 See Appendix A.4 .

Linear or nonlinear PID and adaptive controllers have been widely used for a quadrotor UAV. But, they have been applied in an *ad-hoc* manner without stability analysis. This paper provides a new form of nonlinear adaptive controller on SE(3) that guarantees almost global attractiveness in the presence of uncertainties.

Compared with other PID controllers requiring that uncertain terms should be fixed, the proposed adaptive control system can handle more general class of uncertainties. The nonlinear robust tracking control system in [27, 28] provides ultimate boundedness of tracking errors, and the control input may be prone to chattering if the required ultimate bound is smaller. Compared with [28], the control system in this paper guarantees stronger asymptotic stability, and there is no concern for chattering.

2.3.3 Direction of the First Body-Fixed Axis

As described above, the construction of the orthogonal matrix R_c involves having its third column b_{3_c} specified by (21), and its first column b_{1_c} is arbitrarily chosen to be orthogonal to the third column, which corresponds to a one-dimensional degree of choice.

By choosing b_{1_c} properly, we constrain the asymptotic direction of the first body-fixed axis. Here, we propose to specify the *projection* of the first body-fixed axis onto the plane normal to b_{3_c} . In particular, we choose a desired direction $b_{1_d} \in \mathbf{S}^2$, that is not parallel to b_{3_c} , and b_{1_c} is selected as $b_{1_c} = \text{Proj}[b_{1_d}]$, where $\text{Proj}[\cdot]$ denotes the normalized projection onto the plane perpendicular to b_{3_c} . In this case, the first body-fixed axis does not converge to b_{1_d} , but it converges to the projection of b_{1_d} , i.e. $b_1 \rightarrow b_{1_c} = \text{Proj}[b_{1_d}]$ as $t \rightarrow \infty$. This can be used to specify the heading direction of a quadrotor UAV in the horizontal

plane [28].

2.4 Numerical Example

An aggressive flipping maneuver is considered for a numerical simulation. The quadrotor parameters are chosen as

$$J = \begin{bmatrix} 5.5711 & 0.0618 & -0.0251 \\ 0.06177 & 5.5757 & 0.0101 \\ -0.02502 & 0.01007 & 1.05053 \end{bmatrix} \times 10^{-2} \text{ kgm}^2,$$

$$m = 0.755 \text{ kg}, \quad d = 0.169 \text{ m}, \quad c_{\tau f} = 0.1056.$$

Also, controller parameters are selected as follows: $k_x = 6.0$, $k_v = 3.0$, $k_R = 0.7$, $k_\Omega = 0.12$, $c_1 = 0.1$, $c_2 = 0.1$.

In this simulation, initial state of the quadrotor UAV is at a hovering condition: $x(0) = v(0) = \Omega(0) = 0_{3 \times 1}$, and $R(0) = I_{3 \times 3}$. The desired trajectory is a flipping maneuver where the quadrotor rotates about rotation axis $e_r = [\frac{\sqrt{2}}{2}, \frac{\sqrt{2}}{2}, 0]$ by 360° . This is a complex maneuver combining a nontrivial pitching maneuver with a yawing motion. It is achieved by concatenating the following two control modes:

- (i) Attitude tracking to rotate the quadrotor ($t \leq 0.375$)

$$R_d(t) = I + \sin(4\pi t)\hat{e}_r + (1 - \cos(4\pi t))(e_r e_r^T - I), \quad \Omega_d = 4\pi \cdot e_r.$$

- (ii) Trajectory tracking to make it hover after completing the preceding rotation ($0.375 < t \leq 2$)

$$x_d(t) = [0, 0, 0]^T, \quad b_{1_d} = [1, 0, 0]^T.$$

We considered two cases for this numerical simulation to compare the effect of the proposed adaptive term in the presence of disturbances. In this numerical simulation we considered a special case of $W_x = I_{3 \times 3}$ and $W_R = I_{3 \times 3}$. Two cases are as follows: (i) with adaptive term and (ii) without the adaptive term, where constant disturbances are defined as

$$\theta_R = [0.03, -0.06, 0.09]^T, \quad \theta_x = [0.25, 0.125, 0.2]^T$$

The switching time is determined as follows. The desired angular velocity of the first attitude tracking mode is 4π , which means it requires 0.5 sec for one revolution but the control mode is switched to trajectory tracking mode at $t = 0.375$ sec to compensate rotational inertia. It is also assumed that the maximum thrust at each rotor is given by $f_{i_{\max}} = 3.2$ N, and any thrust command above the maximum thrust is saturated to represent the actual motor limitation in the numerical simulation. Snapshots of the maneuver

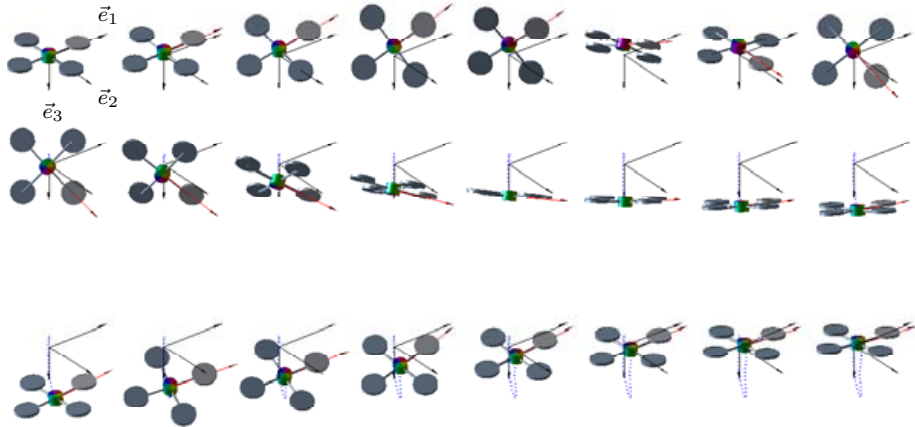


Figure 5: Snapshots of a flipping maneuver: the red line denotes the rotation axis $e_r = [\frac{1}{\sqrt{2}}, \frac{1}{\sqrt{2}}, 0]$. The quadrotor UAV rotates about the e_r axis by 360° . The trajectory of its mass center is denoted by blue, dotted lines.

are presented at Figure 5 and numerical results are illustrated at Figures 6 and 7, where it is shown that the adaptive terms eliminate the steady state error. The altitude drop during the flipping maneuver is reduced noticeably.

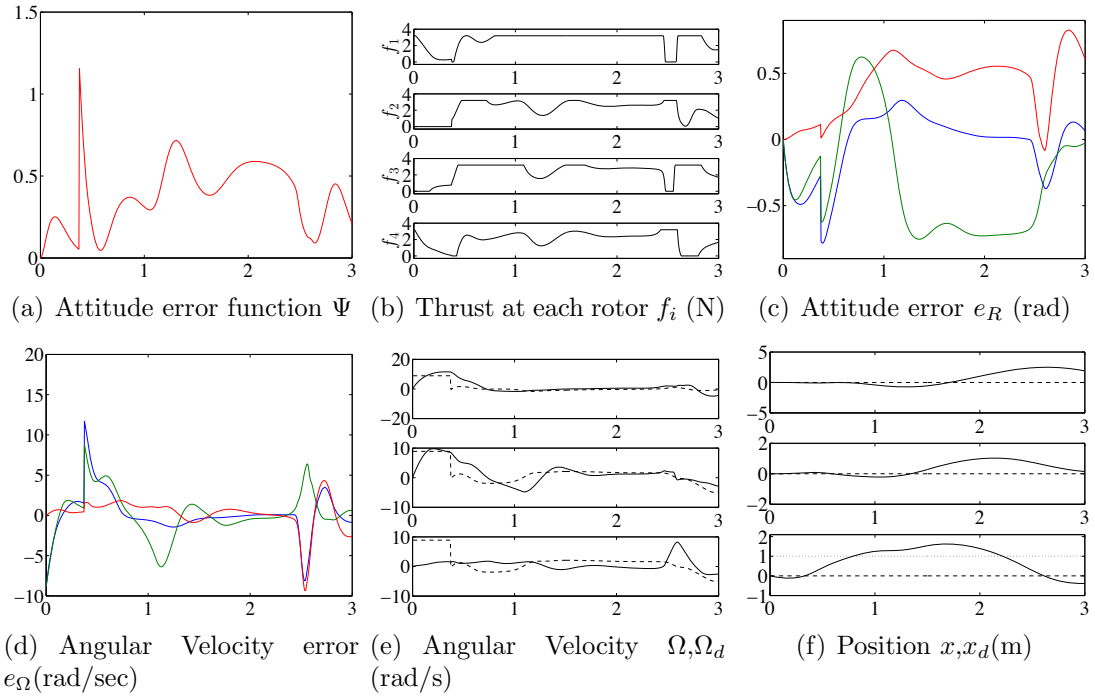


Figure 6: Flipping without adaptive term (dotted:desired, solid:actual)

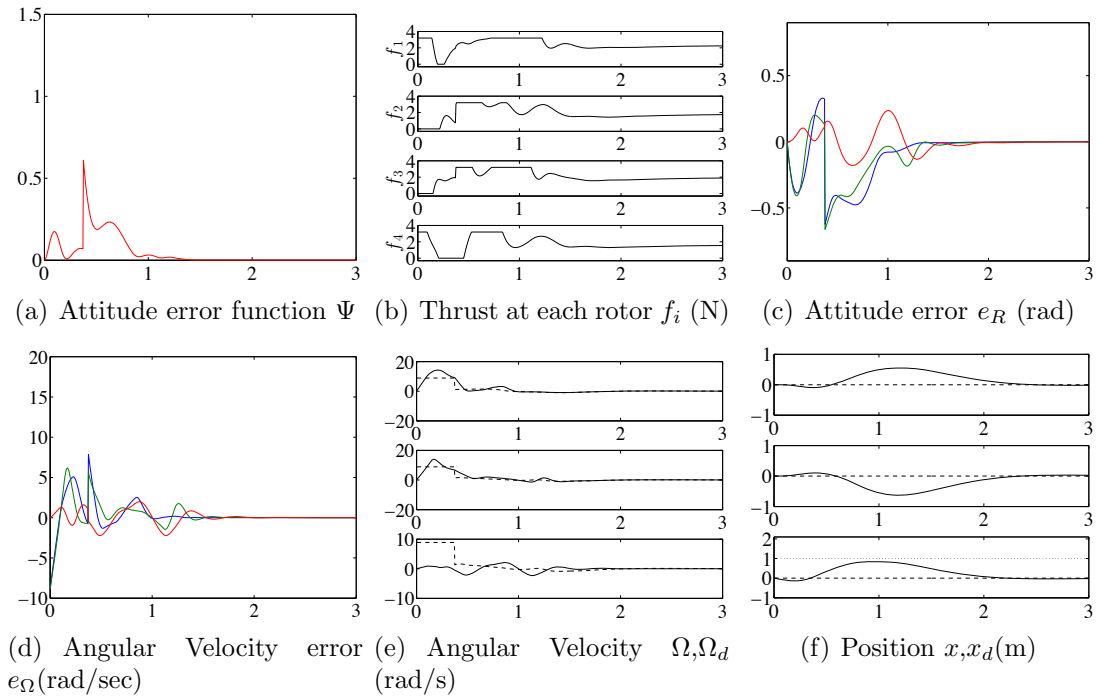


Figure 7: Flipping with adaptive term (dotted:desired, solid:actual)

Chapter 3: Quadrotor UAV Transporting a Payload with Flexible Cable

The main contribution of this chapter is presenting a nonlinear dynamic model and a control system for a quadrotor UAV with a cable-suspended load, that explicitly incorporate the effects of deformable cable.

This chapter is organized as follows. In section 3.1, equations of motion in 3D space for a chain pendulum on a quadrotor are derived. Section 3.2, talks about the dynamics equation, linearization, and linear control design for a chain pendulum on a cart moving in 3D. Section 3.3 presents the proposed geometric nonlinear controller and stability analysis to asymptotically stabilize the chain pendulum on a quadrotor. In section 3.4, we provide numerical simulations results to validate our work.

3.1 Quadrotor Dynamic Model

Consider a quadrotor UAV with a payload that is connected via a chain of n links, as illustrated at Figure 22. The inertial frame is defined by the unit vectors $e_1 = [1; 0; 0]$, $e_2 = [0; 1; 0]$, and $e_3 = [0; 0; 1] \in \mathbb{R}^3$, and the third axis e_3 corresponds to the direction of gravity. Define a body-fixed frame $\{\vec{b}_1, \vec{b}_2, \vec{b}_3\}$ whose origin is located at the center of mass of the quadrotor, and its third axis \vec{b}_3 is aligned to the axis of symmetry.

The location of the mass center, and the attitude of the quadrotor are denoted by $x \in \mathbb{R}^3$ and $R \in \text{SO}(3)$, respectively, where the special orthogonal group is $\text{SO}(3) = \{R \in \mathbb{R}^{3 \times 3} \mid R^T R = I_{3 \times 3}, \det[R] = 1\}$. A rotation matrix represents the linear transformation of a representation of a vector from the body-fixed frame to the inertial frame.

The dynamic model of the quadrotor is identical to [41]. The mass and the inertia matrix of the quadrotor are denoted by $m \in \mathbb{R}$ and $J \in \mathbb{R}^{3 \times 3}$, respectively. The quadrotor can generate a thrust $-fRe_3 \in \mathbb{R}^3$ with respect

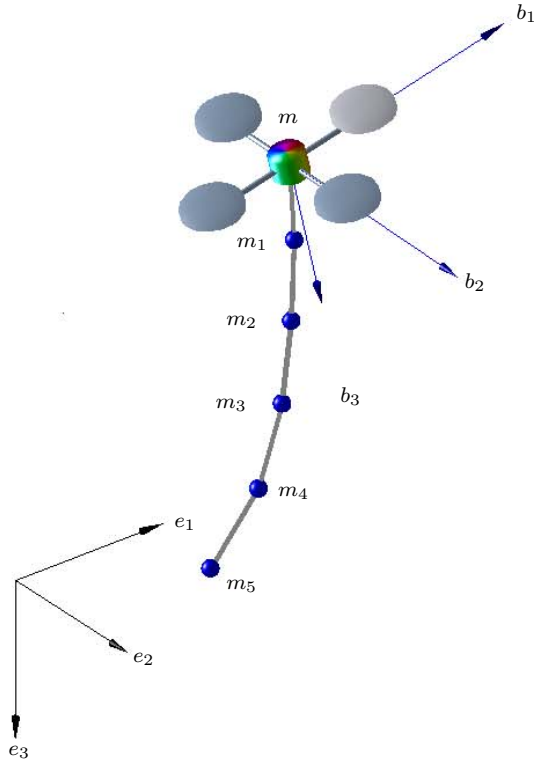


Figure 8: Quadrotor UAV with a cable-suspended load. Cable is modeled as a serial connection of arbitrary number of links (only 5 are illustrated).

to the inertial frame, where $f \in \mathbb{R}$ is the total thrust magnitude. It also generates a moment $M \in \mathbb{R}^3$ with respect to its body-fixed frame. The pair (f, M) is considered as control input of the quadrotor.

Let $q_i \in \mathbb{S}^2$ be the unit-vector representing the direction of the i -th link, measured outward from the quadrotor toward the payload, where the two-sphere is the manifold of unit-vectors in \mathbb{R}^3 , i.e., $\mathbb{S}^2 = \{q \in \mathbb{R}^3 \mid \|q\| = 1\}$. For simplicity, we assume that the mass of each link is concentrated at the outboard end of the link, and the point where the first link is attached to the quadrotor corresponds to the mass center of the quadrotor. The mass and the length of the i -th link are defined by m_i and $l_i \in \mathbb{R}$, respectively. Thus, the mass of the payload corresponds to m_n . The corresponding configuration manifold of this system is given by $\text{SO}(3) \times \mathbb{R}^3 \times (\mathbb{S}^2)^n$.

Next, we show the kinematics equations. Let $\Omega \in \mathbb{R}^3$ be the angular velocity of the quadrotor represented with respect to the body fixed frame, and let $\omega_i \in \mathbb{R}^3$ be the angular velocity of the i -th link represented with respect to the inertial frame. The angular velocity is normal to the direction of the link, i.e., $q_i \cdot \omega_i = 0$. The kinematics equations are given by

$$\dot{R} = R\hat{\Omega}, \quad (33)$$

$$\dot{q}_i = \omega_i \times q_i = \hat{\omega}_i q_i. \quad (34)$$

Throughout this chapter, the 2-norm of a matrix A is denoted by $\|A\|$, and the dot product is denoted by $x \cdot y = x^T y$. Also $\lambda_{\min}(\cdot)$ and $\lambda_{\max}(\cdot)$ denotes the minimum and maximum eigenvalue of a square matrix respectively, and λ_m and λ_M are shorthand for $\lambda_m = \lambda_m(J)$ and $\lambda_M = \lambda_M(J)$.

3.1.1 Lagrangian

We derive the equations of motion according to Lagrangian mechanics. The kinetic energy of the quadrotor is given by

$$T_Q = \frac{1}{2}m\|\dot{x}\|^2 + \frac{1}{2}\Omega \cdot J\Omega. \quad (35)$$

Let $x_i \in \mathbb{R}^3$ be the location of m_i in the inertial frame. It can be written as

$$x_i = x + \sum_{a=1}^i l_a q_a. \quad (36)$$

Then, the kinetic energy of the links are given by

$$\begin{aligned}
T_L &= \frac{1}{2} \sum_{i=1}^n m_i \left\| \dot{x} + \sum_{a=1}^i l_a \dot{q}_a \right\|^2 \\
&= \frac{1}{2} \sum_{i=1}^n m_i \|\dot{x}\|^2 + \dot{x} \cdot \sum_{i=1}^n \sum_{a=i}^n m_a l_i \dot{q}_i + \frac{1}{2} \sum_{i=1}^n m_i \left\| \sum_{a=1}^i l_a \dot{q}_a \right\|^2.
\end{aligned} \tag{37}$$

From (35) and (37), the total kinetic energy can be written as

$$T = \frac{1}{2} M_{00} \|\dot{x}\|^2 + \dot{x} \cdot \sum_{i=1}^n M_{0i} \dot{q}_i + \frac{1}{2} \sum_{i,j=1}^n M_{ij} \dot{q}_i \cdot \dot{q}_j + \frac{1}{2} \Omega^T J \Omega, \tag{38}$$

where the inertia values $M_{00}, M_{0i}, M_{ij} \in \mathbb{R}$ are given by

$$\begin{aligned}
M_{00} &= m + \sum_{i=1}^n m_i, & M_{0i} &= \sum_{a=i}^n m_a l_i, & M_{i0} &= M_{0i}, \\
M_{ij} &= \left\{ \sum_{a=\max\{i,j\}}^n m_a \right\} l_i l_j,
\end{aligned} \tag{39}$$

for $1 \leq i, j \leq n$. The gravitational potential energy is given by

$$\begin{aligned}
V &= -mgx \cdot e_3 - \sum_{i=1}^n m_i g x_i \cdot e_3 \\
&= - \sum_{i=1}^n \sum_{a=i}^n m_a g l_i e_3 \cdot q_i - M_{00} g e_3 \cdot x,
\end{aligned} \tag{40}$$

From (38) and (40), the Lagrangian is $L = T - V$.

3.1.2 Euler-Lagrange equations

Coordinate-free form of Lagrangian mechanics on the two-sphere S^2 and the special orthogonal group $SO(3)$ for various multi-body systems has been studied in [61, 62]. The key idea is representing the infinitesimal variation of

$R \in \text{SO}(3)$ in terms of the exponential map

$$\delta R = \left. \frac{d}{d\epsilon} \right|_{\epsilon=0} \exp R(\epsilon \hat{\eta}) = R \hat{\eta}, \quad (41)$$

for $\eta \in \mathbb{R}^3$. The corresponding variation of the angular velocity is given by $\delta \Omega = \dot{\eta} + \Omega \times \eta$. Similarly, the infinitesimal variation of $q_i \in \mathbf{S}^2$ is given by

$$\delta q_i = \xi_i \times q_i, \quad (42)$$

for $\xi_i \in \mathbb{R}^3$ satisfying $\xi_i \cdot q_i = 0$. This lies in the tangent space as it is perpendicular to q_i . Using these, we obtain the following Euler-Lagrange equations.

Proposition 5 *Consider a quadrotor with a cable suspended payload whose Lagrangian is given by (38) and (40). The Euler-Lagrange equations on $\mathbb{R}^3 \times \text{SO}(3) \times (\mathbf{S}^2)^n$ are as follows*

$$M_{00}\ddot{x} + \sum_{i=1}^n M_{0i}\ddot{q}_i = -fRe_3 + M_{00}ge_3 + \Delta_x, \quad (43)$$

$$M_{ii}\ddot{q}_i - \hat{q}_i^2(M_{i0}\ddot{x} + \sum_{\substack{j=1 \\ j \neq i}}^n M_{ij}\ddot{q}_j) = -M_{ii}\|\dot{q}_i\|^2 q_i - \sum_{a=i}^n m_a g l_i \hat{q}_i^2 e_3, \quad (44)$$

$$J\dot{\Omega} + \hat{\Omega}J\Omega = M + \Delta_R, \quad (45)$$

where M_{ij} is defined at (39). Therefore Δ_x and $\Delta_R \in \mathbb{R}^3$ are fixed disturbances applied to the translational and rotational dynamics of the quadrotor respectively. Equations

(43) and (44) can be rewritten in a matrix form as follows:

$$\begin{aligned}
& \begin{bmatrix} M_{00} & M_{01} & M_{02} & \cdots & M_{0n} \\ -\hat{q}_1^2 M_{10} & M_{11} I_3 & -M_{12} \hat{q}_1^2 & \cdots & -M_{1n} \hat{q}_1^2 \\ -\hat{q}_2^2 M_{20} & -M_{21} \hat{q}_2^2 & M_{22} I_3 & \cdots & -M_{2n} \hat{q}_2^2 \\ \vdots & \vdots & \vdots & & \vdots \\ -\hat{q}_n^2 M_{n0} & -M_{n1} \hat{q}_n^2 & -M_{n2} \hat{q}_n^2 & \cdots & M_{nn} I_3 \end{bmatrix} \begin{bmatrix} \ddot{x} \\ \ddot{q}_1 \\ \ddot{q}_2 \\ \vdots \\ \ddot{q}_n \end{bmatrix} \\
& = \begin{bmatrix} -fRe_3 + M_{00}ge_3 + \Delta_x \\ -\|\dot{q}_1\|^2 M_{11}q_1 - \sum_{a=1}^n m_a gl_1 \hat{q}_1^2 e_3 \\ -\|\dot{q}_2\|^2 M_{22}q_2 - \sum_{a=2}^n m_a gl_2 \hat{q}_2^2 e_3 \\ \vdots \\ -\|\dot{q}_n\|^2 M_{nn}q_n - m_n gl_n \hat{q}_n^2 e_3 \end{bmatrix}. \tag{46}
\end{aligned}$$

Or equivalently, it can be written in terms of the angular velocities as

$$\begin{aligned}
& \begin{bmatrix} M_{00} & -M_{01} \hat{q}_1 & -M_{02} \hat{q}_2 & \cdots & -M_{0n} \hat{q}_n \\ \hat{q}_1 M_{10} & M_{11} I_3 & -M_{12} \hat{q}_1 \hat{q}_2 & \cdots & -M_{1n} \hat{q}_1 \hat{q}_n \\ \hat{q}_2 M_{20} & -M_{21} \hat{q}_2 \hat{q}_1 & M_{22} I_3 & \cdots & -M_{2n} \hat{q}_2 \hat{q}_n \\ \vdots & \vdots & \vdots & & \vdots \\ \hat{q}_n M_{n0} & -M_{n1} \hat{q}_n \hat{q}_1 & -M_{n2} \hat{q}_n \hat{q}_2 & \cdots & M_{nn} I_3 \end{bmatrix} \begin{bmatrix} \ddot{x} \\ \dot{\omega}_1 \\ \dot{\omega}_2 \\ \vdots \\ \dot{\omega}_n \end{bmatrix} \\
& = \begin{bmatrix} \sum_{j=1}^n M_{0j} \|\omega_j\|^2 q_j - fRe_3 + M_{00}ge_3 + \Delta_x \\ \sum_{j=2}^n M_{1j} \|\omega_j\|^2 \hat{q}_1 q_j + \sum_{a=1}^n m_a gl_1 \hat{q}_1 e_3 \\ \sum_{j=1, j \neq 2}^n M_{2j} \|\omega_j\|^2 \hat{q}_2 q_j + \sum_{a=2}^n m_a gl_2 \hat{q}_2 e_3 \\ \vdots \\ \sum_{j=1}^{n-1} M_{nj} \|\omega_j\|^2 \hat{q}_n q_j + m_n gl_n \hat{q}_n e_3 \end{bmatrix}, \tag{47}
\end{aligned}$$

$$\dot{q}_i = \omega_i \times q_i. \tag{48}$$

Proof 5 See Appendix A.5

These provide a coordinate-free form of the equations of motion for the presented quadrotor UAV that is uniformly defined for any number of links n , and that is globally defined on the nonlinear configuration manifold. Compared with equations of motion derived in terms of local coordinates, such as Euler-angles, these avoid singularities completely, and they provide a compact form of equations that are suitable for control system design.

However, the presented finite element model may not capture the certain dynamic characteristics of the actual cable dynamics represented by partial differential equations. Designing a control system for such infinite-dimensional system is beyond the scope of this dissertation.

3.2 Control System Design for a Simplified Dynamic Model

Let $x_d \in \mathbb{R}^3$ be a fixed desired location of the quadrotor UAV. Assuming that all of the links are pointing downward, i.e., $q_i = e_3$, the resulting location of the payload is given by

$$x_n = x_d + \sum_{i=1}^n l_i e_3. \quad (49)$$

We wish to design the control force f and the control moment M such that this hanging equilibrium configuration at the desired location becomes asymptotically stable.

3.2.1 Control Problem Formulation

For the given equations of motion (43) for x , the control force is given by $-fRe_3$. This implies that the total thrust magnitude f can be arbitrarily chosen, but the direction of the thrust vector is always along the third body-fixed axis. Also, the rotational attitude dynamics of the quadrotor is not

affected by the translational dynamics of the quadrotor or the dynamics of links.

To overcome the under-actuated property of a quadrotor, in this section, we first replace the term $-fRe_3$ of (43) by a fictitious control input $u \in \mathbb{R}^3$, and design an expression for u to asymptotically stabilize the desired equilibrium. This is equivalent to assuming that the attitude R of the quadrotor can be instantaneously controlled. The effects of the attitude dynamics are incorporated at the next section. Also Δ_x is ignored in the simplified dynamic model. In short, the equations of motion for the simplified dynamic model considered in the section are given by

$$M_{00}\ddot{x} + \sum_{i=1}^n M_{0i}\ddot{q}_i = u + M_{00}ge_3, \quad (50)$$

and (44).

3.2.2 Linear Control System

The fictitious control input is designed from the linearized dynamics about the desired hanging equilibrium. The variation of x and u are given by

$$\delta x = x - x_d, \quad \delta u = u - M_{00}ge_3. \quad (51)$$

From (78), the variation of q_i from the equilibrium can be written as

$$\delta q_i = \xi_i \times e_3, \quad (52)$$

where $\xi_i \in \mathbb{R}^3$ with $\xi_i \cdot e_3 = 0$. The variation of ω_i is given by $\delta\omega \in \mathbb{R}^3$ with $\delta\omega_i \cdot e_3 = 0$. Therefore, the third element of each of ξ_i and $\delta\omega_i$ for any equilibrium configuration is zero, and they are omitted in the following

linearized equation, i.e., the state vector of the linearized equation is composed of $C^T \xi_i \in \mathbb{R}^2$, where $C = [e_1, e_2] \in \mathbb{R}^{3 \times 2}$.

Proposition 6 *The linearized equations of the simplified dynamic model (50) and (44) can be written as follows*

$$\mathbf{M}\ddot{\mathbf{x}} + \mathbf{G}\dot{\mathbf{x}} = \mathbf{B}\delta u + \mathbf{g}(\mathbf{x}, \dot{\mathbf{x}}), \quad (53)$$

where $\mathbf{g}(\mathbf{x}, \dot{\mathbf{x}})$ corresponds to the higher order terms where $\mathbf{x} = [\delta x, \mathbf{x}_q]^T \in \mathbb{R}^{2n+3}$, $\mathbf{M} \in \mathbb{R}^{2n+3 \times 2n+3}$, $\mathbf{G} \in \mathbb{R}^{2n+3 \times 2n+3}$, $\mathbf{B} \in \mathbb{R}^{2n+3 \times 3}$, and (53) can equivalently be written as

$$\begin{bmatrix} \mathbf{M}_{xx} & \mathbf{M}_{xq} \\ \mathbf{M}_{qx} & \mathbf{M}_{qq} \end{bmatrix} \begin{bmatrix} \delta \ddot{x} \\ \ddot{\mathbf{x}}_q \end{bmatrix} + \begin{bmatrix} 0_3 & 0_{3 \times 2n} \\ 0_{2n \times 3} & \mathbf{G}_{qq} \end{bmatrix} \begin{bmatrix} \delta \dot{x} \\ \dot{\mathbf{x}}_q \end{bmatrix} = \begin{bmatrix} I_3 \\ 0_{2n \times 3} \end{bmatrix} \delta u + \mathbf{g}(\mathbf{x}, \dot{\mathbf{x}}),$$

where the corresponding sub-matrices are defined as

$$\begin{aligned} \mathbf{x}_q &= [C^T \xi_1; \dots; C^T \xi_n], \\ \mathbf{M}_{xx} &= M_{00} I_3, \\ \mathbf{M}_{xq} &= \begin{bmatrix} -M_{01} \hat{e}_3 C & -M_{02} \hat{e}_3 C & \dots & -M_{0n} \hat{e}_3 C \end{bmatrix}, \\ \mathbf{M}_{qx} &= \mathbf{M}_{xq}^T, \\ \mathbf{M}_{qq} &= \begin{bmatrix} M_{11} I_2 & M_{12} I_2 & \dots & M_{1n} I_2 \\ M_{21} I_2 & M_{22} I_2 & \dots & M_{2n} I_2 \\ \vdots & \vdots & & \vdots \\ M_{n1} I_2 & M_{n2} I_2 & \dots & M_{nn} I_2 \end{bmatrix}, \\ \mathbf{G}_{qq} &= \text{diag} \left[\sum_{a=1}^n m_a g l_1 I_2, \dots, m_n g l_n I_2 \right]. \end{aligned}$$

Proof 6 *See Appendix A.6*

For the linearized dynamics (53), the following control system is chosen

$$\begin{aligned}\delta u &= -k_x \delta x - k_{\dot{x}} \delta \dot{x} - \sum_{a=1}^n k_{q_i} C^T (e_3 \times q_i) - k_{\omega_i} C^T \delta \omega_i \\ &= -K_x \mathbf{x} - K_{\dot{x}} \dot{\mathbf{x}},\end{aligned}\tag{54}$$

for controller gains $K_x = [k_x I_3, k_{q_1} I_{3 \times 2}, \dots, k_{q_n} I_{3 \times 2}] \in \mathbb{R}^{3 \times (3+2n)}$ and $K_{\dot{x}} = [k_{\dot{x}} I_3, k_{\omega_1} I_{3 \times 2}, \dots, k_{\omega_n} I_{3 \times 2}] \in \mathbb{R}^{3 \times (3+2n)}$. Provided that (53) is controllable, we can choose the controller gains $K_x, K_{\dot{x}}$ such that the equilibrium is asymptotically stable for the linearized equation (53). Then, the equilibrium becomes asymptotically stable for the nonlinear Euler Lagrange equation (50) and (44) [63]. The controlled linearized system can be written as

$$\dot{z}_1 = \mathbb{A} z_1 + \mathbb{B} \mathbf{g}(\mathbf{x}, \dot{\mathbf{x}}),\tag{55}$$

where $z_1 = [\mathbf{x}, \dot{\mathbf{x}}]^T \in \mathbb{R}^{4n+6}$ and the matrices $\mathbb{A} \in \mathbb{R}^{4n+6 \times 4n+6}$ and $\mathbb{B} \in \mathbb{R}^{4n+6 \times 2n+3}$ are defined as

$$\mathbb{A} = \begin{bmatrix} 0 & I \\ -\mathbf{M}^{-1}(\mathbf{G} + \mathbf{B}K_x) & -(\mathbf{M}^{-1}\mathbf{B}K_{\dot{x}}) \end{bmatrix}, \mathbb{B} = \begin{bmatrix} 0 \\ \mathbf{M}^{-1} \end{bmatrix}.\tag{56}$$

We can also choose $K_{\mathbf{x}}$ and $K_{\dot{\mathbf{x}}}$ such that \mathbb{A} is Hurwitz. Then for any positive definite matrix $Q \in \mathbb{R}^{4n+6 \times 4n+6}$, there exist a positive definite and symmetric matrix $P \in \mathbb{R}^{4n+6 \times 4n+6}$ such that $\mathbb{A}^T P + P \mathbb{A} = -Q$ according to [63, Thm 3.6].

3.3 Controller Design for a Quadrotor with a Flexible Cable

The control system designed in the previous section is generalized to the full dynamic model that includes the attitude dynamics. The central idea is that

the attitude R of the quadrotor is controlled such that its total thrust direction $-Re_3$ that corresponds to the third body-fixed axis asymptotically follows the direction of the fictitious control input u . By choosing the total thrust magnitude properly, we can guarantee that the total thrust vector $-fRe_3$ asymptotically converges to the fictitious ideal force u , thereby yielding asymptotic stability of the full dynamic model.

3.3.1 Controller Design

Consider the full nonlinear equations of motion, let $A \in \mathbb{R}^3$ be the ideal total thrust of the quadrotor system that asymptotically stabilize the desired equilibrium. From (51), we have

$$A = M_{00}ge_3 + \delta u = -K_x \mathbf{x} - K_{\dot{x}} \dot{\mathbf{x}} - K_z \text{sat}_\sigma(e_{\mathbf{x}}) + M_{00}ge_3, \quad (57)$$

where the following integral term $e_{\mathbf{x}} \in \mathbb{R}^{2n+3}$ is added to eliminate the effect of disturbance Δ_x in the full dynamic model

$$e_{\mathbf{x}} = \int_0^t (PB)^T z_1(\tau) d\tau, \quad (58)$$

where $K_z = [k_z I_3, k_{z_1} I_{3 \times 2}, \dots, k_{z_n} I_{3 \times 2}] \in \mathbb{R}^{3 \times (3+2n)}$ is an integral gain. For a positive constant $\sigma \in \mathbb{R}$, a saturation function $\text{sat}_\sigma : \mathbb{R} \rightarrow [-\sigma, \sigma]$ is introduced as

$$\text{sat}_\sigma(y) = \begin{cases} \sigma & \text{if } y > \sigma \\ y & \text{if } -\sigma \leq y \leq \sigma \\ -\sigma & \text{if } y < -\sigma \end{cases}$$

If the input is a vector $y \in \mathbb{R}^n$, then the above saturation function is applied element by element to define a saturation function $\text{sat}_\sigma(y) : \mathbb{R}^n \rightarrow [-\sigma, \sigma]^n$ for a vector. It is also assumed that an upper bound of the infinite norm of the uncertainty is known

$$\|\Delta_x\|_\infty \leq \delta, \quad (59)$$

for positive constant δ . The desired direction of the third body-fixed axis $b_{3_c} \in \mathbf{S}^2$ is given by

$$b_{3_c} = -\frac{A}{\|A\|}. \quad (60)$$

This provides a two-dimensional constraint for the desired attitude of quadrotor, and there is additional one-dimensional degree of freedom that corresponds to rotation about the third body-fixed axis, i.e., yaw angle. A desired direction of the first body-fixed axis, namely $b_{1_d} \in \mathbf{S}^2$ is introduced to resolve it, and it is projected onto the plane normal to b_{3_c} . The desired direction of the second body-fixed axis is chosen to constitute an orthonormal frame. More explicitly, the desired attitude is given by

$$R_c = \left[-\frac{\hat{b}_{3_c}^2 b_{1_d}}{\|\hat{b}_{3_c}^2 b_{1_d}\|}, \frac{\hat{b}_{3_c} b_{1_d}}{\|\hat{b}_{3_c} b_{1_d}\|}, b_{3_c} \right], \quad (61)$$

which is guaranteed to lie in $\mathbf{SO}(3)$ by construction, assuming that b_{1_d} is not parallel to b_{3_c} [28]. The desired angular velocity $\Omega_c \in \mathbb{R}^3$ is obtained by the attitude kinematics equation

$$\Omega_c = (R_c^T \dot{R}_c)^\vee. \quad (62)$$

Next, we introduce the tracking error variables for the attitude and the angular velocity $e_R, e_\Omega \in \mathbb{R}^3$ as follows [64]

$$e_R = \frac{1}{2}(R_c^T R - R^T R_c)^\vee, \quad (63)$$

$$e_\Omega = \Omega - R^T R_c \Omega_c. \quad (64)$$

The thrust magnitude and the moment vector of quadrotor are chosen as

$$f = -A \cdot R e_3, \quad (65)$$

and

$$M = -k_R e_R - k_\Omega e_\Omega - k_I e_I + \Omega \times J \Omega - J(\hat{\Omega} R^T R_c \Omega_c - R^T R_c \dot{\Omega}_c), \quad (66)$$

where k_R, k_Ω , and k_I are positive constants and the following integral term is introduced to eliminate the effect of fixed disturbance Δ_R

$$e_I = \int_0^t e_\Omega(\tau) + c_2 e_R(\tau) d\tau, \quad (67)$$

where c_2 is a positive constant.

3.3.2 Stability Analysis

Proposition 7 *Consider control inputs f, M defined in (105) and (106). There exist controller parameters and gains such that, (i) the zero equilibrium of tracking error is stable in the sense of Lyapunov; (ii) the tracking errors $e_R, e_\Omega, \mathbf{x}, \dot{\mathbf{x}}$ asymptotically converge to zero as $t \rightarrow \infty$; (iii) the integral terms e_I and $e_{\mathbf{x}}$ are uniformly bounded.*

Proof 7 *See Appendix A.7*

By utilizing geometric control systems for quadrotor, we show that the hanging equilibrium of the links can be asymptotically stabilized while translating the quadrotor to a desired position. The control systems proposed explicitly consider the coupling effects between the cable/load dynamics and the quadrotor dynamics. We presented a rigorous Lyapunov stability analysis to establish stability properties without any timescale separation assumptions or singular perturbation, and a new nonlinear integral control term is designed to guarantee robustness against unstructured uncertainties in both rotational and translational dynamics.

3.4 Numerical Example

The desirable properties of the proposed control system are illustrated by a numerical example. Properties of a quadrotor are chosen as

$$m = 0.5 \text{ kg}, \quad J = \text{diag}[0.557, 0.557, 1.05] \times 10^{-2} \text{ kgm}^2.$$

Five identical links with $n = 5$, $m_i = 0.1 \text{ kg}$, and $l_i = 0.1 \text{ m}$ are considered. Controller parameters are selected as follows: $k_x = 12.8$, $k_v = 4.22$, $k_R = 0.65$, $k_\Omega = 0.11$, $k_I = 1.5$, $c_1 = c_2 = 0.7$. Also k_q and k_ω are defined as

$$k_q = [11.01, 6.67, 1.97, 0.41, 0.069],$$

$$k_\omega = [0.93, 0.24, 0.032, 0.030, 0.025].$$

The desired location of the quadrotor is selected as $x_d = 0_{3 \times 1}$. The initial

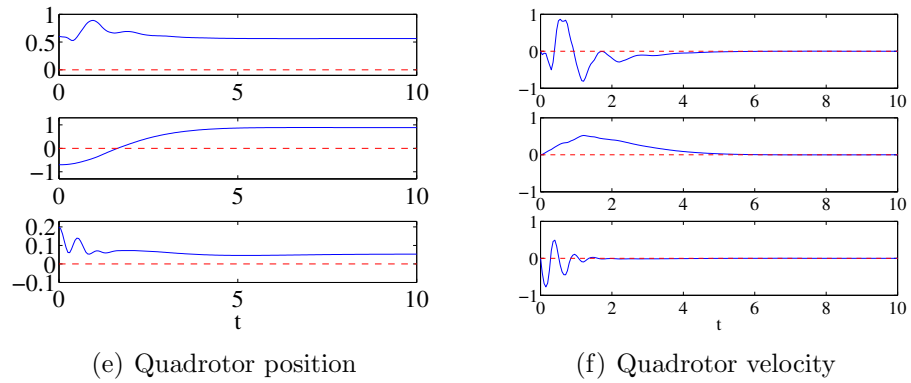
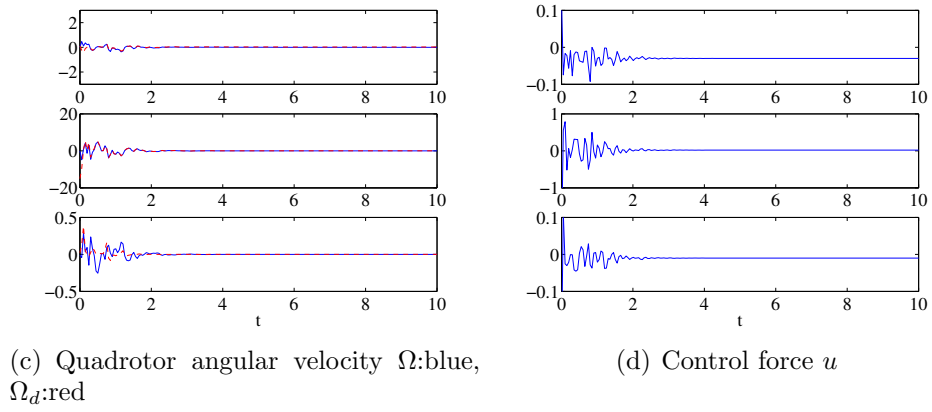
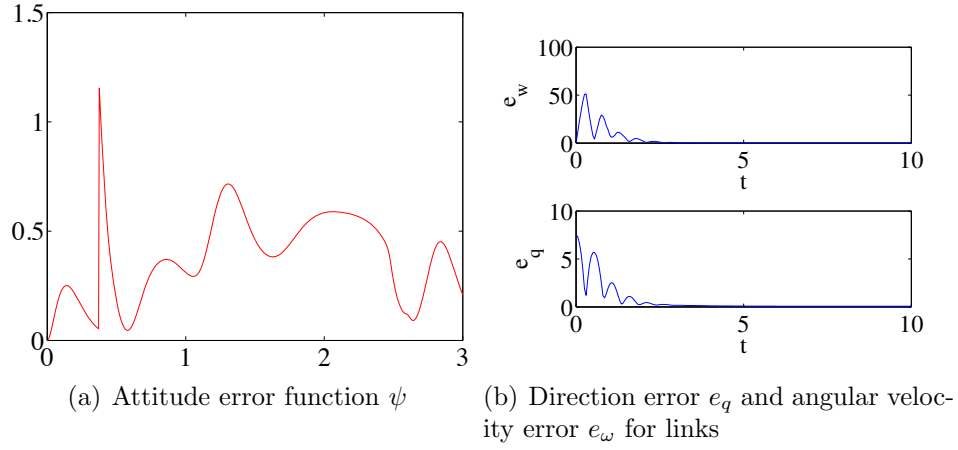


Figure 9: Stabilization of a payload connected to a quadrotor with 5 links without Integral term

conditions for the quadrotor are given by

$$\begin{aligned} x(0) &= [0.6; -0.7; 0.2], \quad \dot{x}(0) = 0_{3 \times 1}, \\ R(0) &= I_{3 \times 3}, \quad \Omega(0) = 0_{3 \times 1}. \end{aligned}$$

The initial direction of the links are chosen such that the cable is curved along the horizontal direction, as illustrated at Figure 11(a), and the initial angular velocity of each link is chosen as zero. The following two fixed disturbances are included in the numerical simulation.

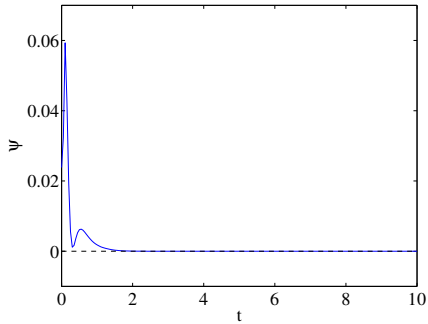
$$\begin{aligned} \Delta_R &= [0.03, -0.02, 0.01]^T, \\ \Delta_x &= [-0.0125, 0.0125, 0.01]^T. \end{aligned}$$

We considered two cases for this numerical simulation to compare the effect of the proposed integral term in the presence of disturbances as follows: (i) with integral term and (ii) without integral term, to emphasize the effect of the integral term. The simulation results for each case are illustrated at Figures 9 and 10, respectively. The corresponding maneuvers of the quadrotor and the links for the second case are illustrated at Figure 11.

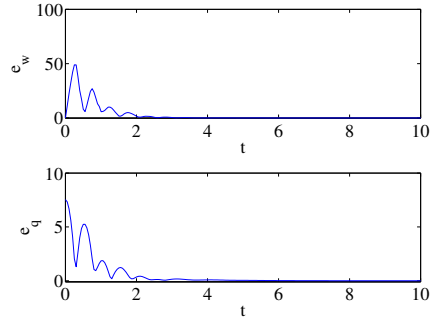
Figures 9(a) and 10(a) show the attitude error function defined as

$$\psi(R, R_d) = \frac{1}{2} \text{tr}[[I - R_c^T R]], \quad (68)$$

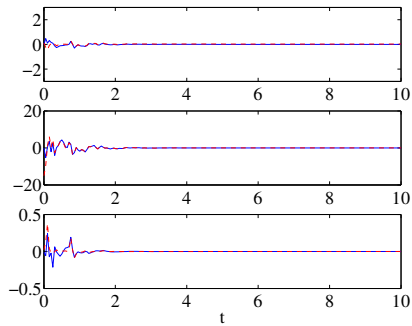
which represents the difference between the desired attitude and the actual attitude of the quadrotor. It is shown that there is a steady state error for the first case without the integral control term, but the error is eliminated at Figure 10(a) for the second case. Next, we define the two following error



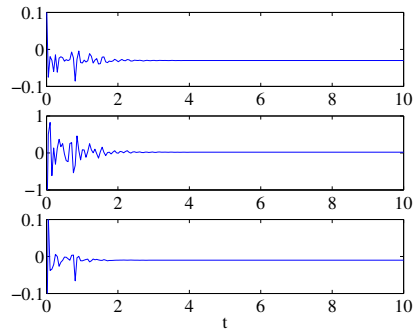
(a) Attitude error function ψ



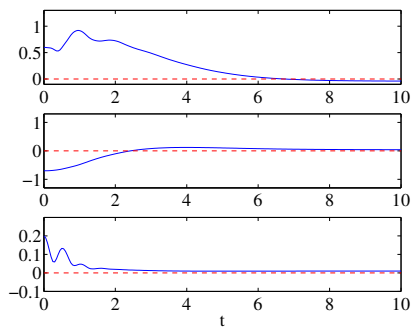
(b) Direction error e_q and angular velocity error e_ω for links



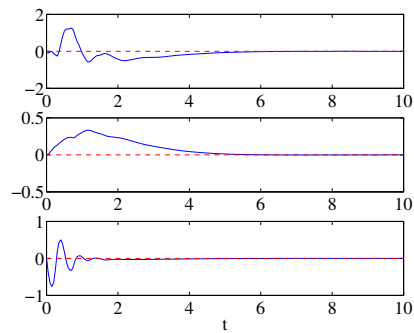
(c) Quadrotor angular velocity Ω :blue, Ω_d :red



(d) Control force u



(e) Quadrotor position



(f) Quadrotor velocity

Figure 10: Stabilization of a payload connected to a quadrotor with 5 links with Integral term

cumulative variables to show the stabilizing performance for all links:

$$e_q = \sum_{i=1}^n \|q_i - e_3\|, \quad e_\omega = \sum_{i=1}^n \|\omega_i\|, \quad (69)$$

and the results of numerical simulation for these error functions are presented in 9(b) and 10(b) for each case. The initial errors for the links are quite large, but they converge to zero nicely. For the first case, there exist a small steady state error in both e_w and e_q . Figures 9(e) and 10(e) show the desired location of the quadrotor (dashed line) and the actual location (solid like) for each case.

These numerical examples verifies that under the proposed control system, all of the position and attitude of the quadrotor, the direction of links, and the location of the payload asymptotically converge to their desire values, and the presented integral terms are effective in eliminating steady state errors caused by disturbances.

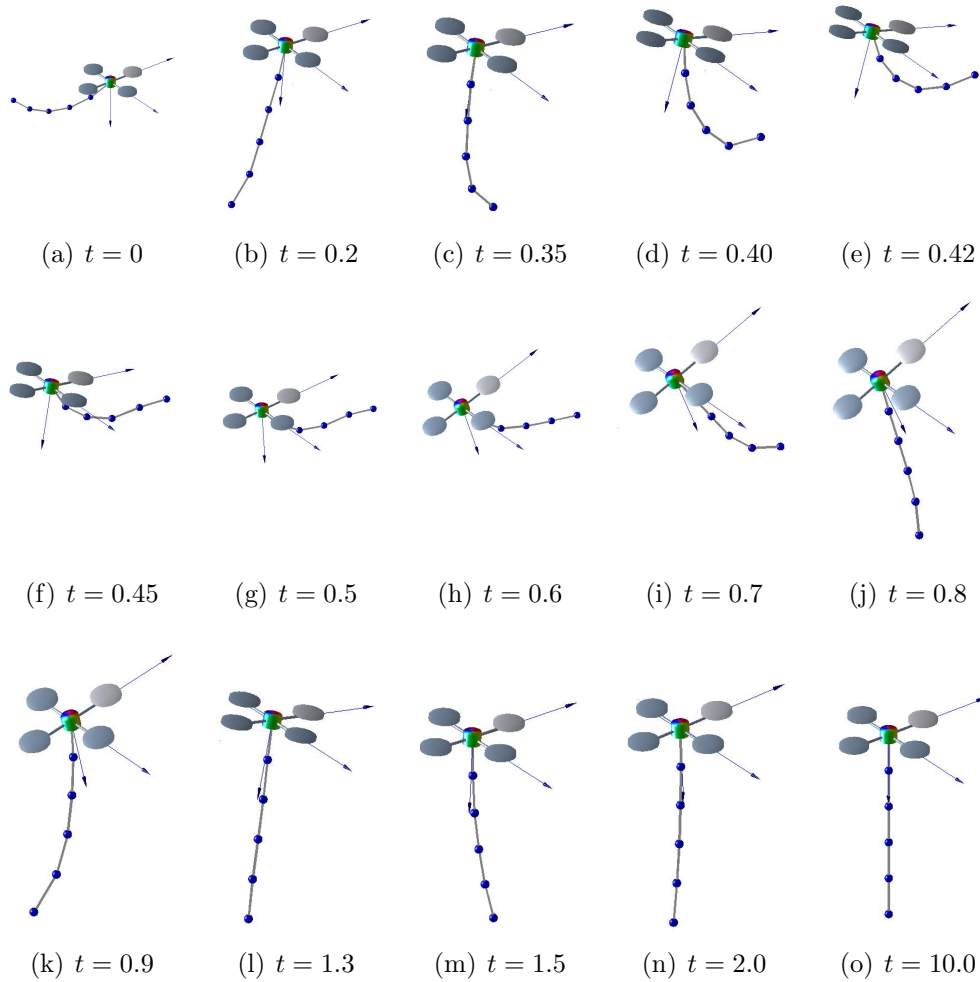


Figure 11: Snapshots of the controlled maneuver

Chapter 4: Multiple Quadrotor UAVs Transporting a Rigid Body

There are various applications for aerial load transportation such as usage in construction, military operations, emergency response, or delivering packages. Load transportation with the cable-suspended load has been studied traditionally for a helicopter [5, 6] or for small unmanned aerial vehicles such as quadrotor UAVs [7, 8, 9].

In most of the prior works, the dynamics of aerial transportation has been simplified due to the inherent dynamic complexities. For example, it is assumed that the dynamics of the payload is considered completely decoupled from quadrotors, and the effects of the payload and the cable are regarded as arbitrary external forces and moments exerted to the quadrotors [11, 12, 13], thereby making it challenging to suppress the swinging motion of the payload actively, particularly for agile aerial transportations.

The complete dynamic model of an arbitrary number of quadrotors transporting a rigid body presented in this chapter where each quadrotor is connected to the rigid body via a flexible cable. Each flexible cable is modeled as an arbitrary number of serially connected links, and it is valid for various masses and lengths. A coordinate free form of equations of motion is derived according to Lagrange mechanics on a nonlinear manifold for the full dynamic model. These sets of equations of motion are presented in a complete and organized manner without any simplification.

Another contribution of this chapter is designing a control system to stabilize the rigid body at desired position. Geometric nonlinear controllers is utilized [41, 28, 45], and they are generalized for the presented model. More explicitly, we show that the rigid body payload is asymptotically transported into a desired location, while aligning all of the links along the vertical direction corresponding to a hanging equilibrium.

The unique property of the proposed control system is that the nontrivial coupling effects between the dynamics of rigid payload, flexible cables, and multiple quadro-

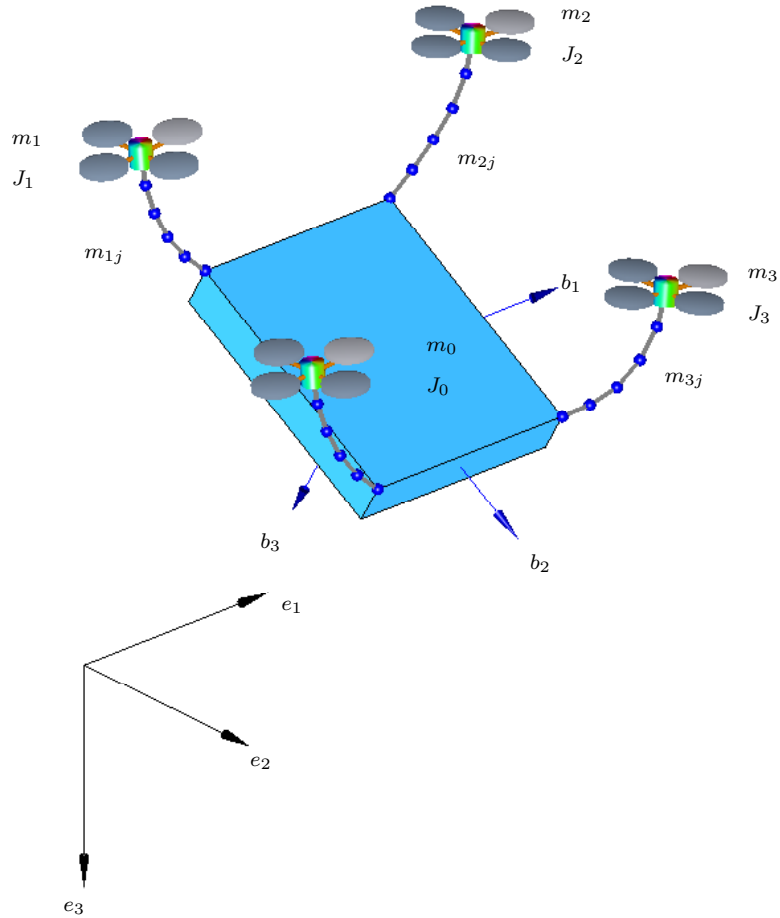


Figure 12: Quadrotor UAVs with a rigid body payload. Cables are modeled as a serial connection of an arbitrary number of links (only 4 quadrotors with 5 links in each cable are illustrated).

tors are explicitly incorporated into control system design, without any simplifying assumption. Another distinct feature is that the equations of motion and the control systems are developed directly on the nonlinear configuration manifold intrinsically. Therefore, singularities of local parameterization are completely avoided to generate agile maneuvers of the payload in a uniform way. In short, the proposed control system is particularly useful for rapid and safe payload transportation in complex terrain, where the position of the payload should be controlled concurrently while suppressing the deformation of the cables.

This chapter is organized as follows. A dynamic model is presented and the problem is formulated at Section 4.1. Control systems are constructed at Sections 4.2

and 4.3, which are followed by numerical examples in Section 4.4.

4.1 Quadrotor Dynamic Model

Consider a rigid body with mass $m_0 \in \mathbb{R}$ and moment of inertia $J_0 \in \mathbb{R}^{3 \times 3}$, being transported with arbitrary n numbers of quadrotors. The location of the mass center of the rigid body is denoted by $x_0 \in \mathbb{R}^3$, and its attitude is given by $R_0 \in \text{SO}(3)$, where the special orthogonal group is given by $\text{SO}(3) = \{R \in \mathbb{R}^{3 \times 3} \mid R^T R = I, \det(R) = 1\}$. Figure 12 illustrates the system with an inertial frame. We choose an inertial frame $\{\vec{e}_1, \vec{e}_2, \vec{e}_3\}$ and body fixed frame $\{\vec{b}_1, \vec{b}_2, \vec{b}_3\}$ attached to the payload. We also consider a body fixed frame attached to the i -th quadrotor $\{\vec{b}_{1_i}, \vec{b}_{2_i}, \vec{b}_{3_i}\}$. In the inertial frame, the third axes \vec{e}_3 points downward with gravity and the other axes are chosen to form an orthonormal frame.

The mass and the moment of inertia of the i -th quadrotor are denoted by $m_i \in \mathbb{R}$ and $J_i \in \mathbb{R}^{3 \times 3}$ respectively. The cable connecting each quadrotor to the rigid body is modeled as an arbitrary numbers of links for each quadrotor with varying masses and lengths. The direction of the j -th link of the i -th quadrotor, measured outward from the quadrotor toward the payload is defined by the unit vector $q_{ij} \in \mathbb{S}^2$, where $\mathbb{S}^2 = \{q \in \mathbb{R}^3 \mid \|q\| = 1\}$, where the mass and length of that link is denoted with m_{ij} and l_{ij} respectively. The number of links in the cable connected to the i -th quadrotor is defined as n_i .

The configuration manifold for this system is given by $\text{SO}(3) \times \mathbb{R}^3 \times (\text{SO}(3)^n) \times (\mathbb{S}^2)^{\sum_{i=1}^n n_i}$. The i -th quadrotor can generate a thrust force of $-f_i R_i e_3 \in \mathbb{R}^3$ with respect to the inertial frame, where $f_i \in \mathbb{R}$ is the total thrust magnitude of the i -th quadrotor. It also generates a moment $M_i \in \mathbb{R}^3$ with respect to its body-fixed frame. Throughout this chapter, the two norm of a matrix A is denoted by $\|A\|$. The standard dot product is denoted by

$x \cdot y = x^T y$ for any $x, y \in \mathbb{R}^3$.

4.1.1 Lagrangian

The kinematics equations for the links, payload, and quadrotors are given by

$$\dot{q}_{ij} = \omega_{ij} \times q_{ij} = \hat{\omega}_{ij} q_{ij}, \quad (70)$$

$$\dot{R}_0 = R_0 \hat{\Omega}_0, \quad (71)$$

$$\dot{R}_i = R_i \hat{\Omega}_i, \quad (72)$$

where $\omega_{ij} \in \mathbb{R}^3$ is the angular velocity of the j -th link in the i -th cable satisfying $q_{ij} \cdot \omega_{ij} = 0$. Also, $\Omega_0 \in \mathbb{R}^3$ is the angular velocity of the payload and $\Omega_i \in \mathbb{R}^3$ is the angular velocity of the i -th quadrotor, expressed with respect to the corresponding body fixed frame. The hat map $\hat{\cdot} : \mathbb{R}^3 \rightarrow \mathfrak{so}(3)$ is defined by the condition that $\hat{x}y = x \times y$ for all $x, y \in \mathbb{R}^3$, and the inverse of the hat map is denoted by the vee map $\vee : \mathfrak{so}(3) \rightarrow \mathbb{R}^3$.

The position of the i -th quadrotor is given by

$$x_i = x_0 + R_0 \rho_i - \sum_{a=1}^{n_i} l_{ia} q_{ia}, \quad (73)$$

where $\rho_i \in \mathbb{R}^3$ is the vector from the center of mass of the rigid body to the point that i -th quadrotor is connected to rigid body via the cable. Similarly the position of the j -th link in the cable connecting the i -th quadrotor to the rigid body is given by

$$x_{ij} = x_0 + R_0 \rho_i - \sum_{a=j+1}^{n_i} l_{ia} q_{ia}. \quad (74)$$

We derive equations of motion according to Lagrangian mechanics. Total

kinetic energy of the system is given by

$$\begin{aligned}
T = & \frac{1}{2}m_0\|\dot{x}_0\|^2 + \sum_{i=1}^n \sum_{j=1}^{n_i} \frac{1}{2}m_{ij}\|\dot{x}_{ij}\|^2 + \frac{1}{2} \sum_{i=1}^n m_i\|\dot{x}_i\|^2 \\
& + \frac{1}{2} \sum_{i=1}^n \Omega_i \cdot J_i \Omega_i + \frac{1}{2} \Omega_0 \cdot J_0 \Omega_0.
\end{aligned} \tag{75}$$

The gravitational potential energy is given by

$$V = -m_0 g e_3 \cdot x_0 - \sum_{i=1}^n m_i g e_3 \cdot x_i - \sum_{i=1}^n \sum_{j=1}^{n_i} m_{ij} g e_3 \cdot x_{ij}, \tag{76}$$

where it is assumed that the unit-vector e_3 points downward along the gravitational acceleration as shown at Figure 12. The corresponding Lagrangian of the system is $L = T - V$.

4.1.2 Euler-Lagrange equations

Coordinate-free form of Lagrangian mechanics on the two-sphere S^2 and the special orthogonal group $SO(3)$ for various multi-body systems has been studied in [61, 62]. The key idea is representing the infinitesimal variation of $R_i \in SO(3)$ in terms of the exponential map

$$\delta R_i = \left. \frac{d}{d\epsilon} \right|_{\epsilon=0} R_i \exp(\epsilon \hat{\eta}_i) = R_i \hat{\eta}_i, \tag{77}$$

for $\eta_i \in \mathbb{R}^3$. The corresponding variation of the angular velocity is given by $\delta \Omega_i = \dot{\eta}_i + \Omega_i \times \eta_i$. Similarly, the infinitesimal variation of $q_{ij} \in S^2$ is given by

$$\delta q_{ij} = \xi_{ij} \times q_{ij}, \tag{78}$$

for $\xi_{ij} \in \mathbb{R}^3$ satisfying $\xi_{ij} \cdot q_{ij} = 0$. This lies in the tangent space as it is perpendicular to q_i . Using these, we obtain the following Euler-Lagrange

equations.

Proposition 8 *By using the above expressions, the equations of motion can be obtained from Hamilton's principle:*

$$\begin{aligned}
& M_T \ddot{x}_0 - \sum_{i=1}^n \sum_{j=1}^{n_i} M_{0ij} l_{ij} \ddot{q}_{ij} - \sum_{i=1}^n M_{iT} R_0 \hat{\rho}_i \dot{\Omega}_0 \\
& = M_T g e_3 + \sum_{i=1}^n -f_i R_i e_3 - \sum_{i=1}^n M_{iT} R_0 \hat{\Omega}_0^2 \rho_i, \tag{79}
\end{aligned}$$

$$\begin{aligned}
& \bar{J}_0 \dot{\Omega}_0 + \sum_{i=1}^n M_{iT} \hat{\rho}_i R_0^T \ddot{x}_0 - \sum_{i=1}^n \sum_{j=1}^{n_i} M_{0ij} l_{ij} \hat{\rho}_i R_0^T \ddot{q}_{ij} \\
& = \sum_{i=1}^n \hat{\rho}_i R_0^T (-f_i R_i e_3 + M_{iT} g e_3) - \hat{\Omega}_0 \bar{J}_0 \Omega_0, \tag{80}
\end{aligned}$$

$$\begin{aligned}
& \sum_{k=1}^{n_i} M_{0ij} l_{ik} \hat{q}_{ij}^2 \ddot{q}_{ik} - M_{0ij} \hat{q}_{ij}^2 \ddot{x}_0 + M_{0ij} \hat{q}_{ij}^2 R_0 \hat{\rho}_i \dot{\Omega}_0 \\
& = M_{0ij} \hat{q}_{ij}^2 R_0 \hat{\Omega}_0^2 \rho_i - \hat{q}_{ij}^2 (M_{0ij} g e_3 - f_i R_i e_3), \tag{81}
\end{aligned}$$

$$J_i \Omega_i + \Omega_i \times J_i \Omega_i = M_i. \tag{82}$$

Here the total mass M_T of the system and the mass of the i -th quadrotor and its flexible cable M_{iT} are defined as

$$M_T = m_0 + \sum_{i=1}^n M_{iT}, \quad M_{iT} = \sum_{j=1}^{n_i} m_{ij} + m_i, \tag{83}$$

and the constants related to the mass of links are given as

$$M_{0ij} = m_i + \sum_{a=1}^{j-1} m_{ia}, \tag{84}$$

The equations of motion can be rearranged in a matrix form as follow

$$\mathbf{N} \ddot{\mathbf{X}} = \mathbf{P} \tag{85}$$

where the state vector $X \in \mathbb{R}^{D_X}$ with $D_X = 6 + 3 \sum_{i=1}^n n_i$ is given by

$$X = [x_0, \Omega_0, q_{1j}, q_{2j}, \dots, q_{nj}]^T, \quad (86)$$

and matrix $\mathbf{N} \in \mathbb{R}^{D_X \times D_X}$ is defined as

$$\mathbf{N} = \begin{bmatrix} M_T I_3 & \mathbf{N}_{x_0 \Omega_0} & \mathbf{N}_{x_0 1} & \mathbf{N}_{x_0 2} & \cdots & \mathbf{N}_{x_0 n} \\ \mathbf{N}_{\Omega_0 x_0} & \bar{J}_0 & \mathbf{N}_{\Omega_0 1} & \mathbf{N}_{\Omega_0 2} & \cdots & \mathbf{N}_{\Omega_0 n} \\ \mathbf{N}_{1 x_0} & \mathbf{N}_{1 \Omega_0} & \mathbf{N}_{qq1} & 0 & \cdots & 0 \\ \mathbf{N}_{2 x_0} & \mathbf{N}_{2 \Omega_0} & 0 & \mathbf{N}_{qq2} & \cdots & 0 \\ \vdots & \vdots & \vdots & \vdots & \vdots & \vdots \\ \mathbf{N}_{n x_0} & \mathbf{N}_{n \Omega_0} & 0 & 0 & \cdots & \mathbf{N}_{qqn} \end{bmatrix}, \quad (87)$$

where the sub-matrices are defined as

$$\begin{aligned} \mathbf{N}_{x_0 \Omega_0} &= - \sum_{i=1}^n M_{iT} R_0 \hat{\rho}_i; \quad \mathbf{N}_{\Omega_0 x_0} = \mathbf{M}_{x_0 \Omega_0}^T, \\ \mathbf{N}_{x_0 i} &= -[M_{0i1} l_{i1} I_3, M_{0i2} l_{i2} I_3, \dots, M_{0in_i} l_{in_i} I_3], \\ \mathbf{N}_{\Omega_0 i} &= -[M_{0i1} l_{i1} \hat{\rho}_i R_0^T, M_{0i2} l_{i2} \hat{\rho}_i R_0^T, \dots, M_{0in_i} l_{in_i} \hat{\rho}_i R_0^T], \\ \mathbf{N}_{i x_0} &= -[M_{0i1} \hat{q}_{i1}^2, M_{0i2} \hat{q}_{i2}^2, \dots, M_{0in_i} \hat{q}_{in_i}^2]^T, \\ \mathbf{N}_{i \Omega_0} &= [M_{0i1} \hat{q}_{i1}^2 R_0 \hat{\rho}_i, M_{0i2} \hat{q}_{i2}^2 R_0 \hat{\rho}_i, \dots, M_{0in_i} \hat{q}_{in_i}^2 R_0 \hat{\rho}_i]^T, \end{aligned} \quad (88)$$

and the sub-matrix $\mathbf{N}_{qqi} \in \mathbb{R}^{3n_i \times 3n_i}$ is given by

$$\mathbf{N}_{qqi} = \begin{bmatrix} -M_{011} l_{i1} I_3 & M_{012} l_{i2} \hat{q}_{i2}^2 & \cdots & M_{01n_i} l_{in_i} \hat{q}_{in_i}^2 \\ M_{021} l_{i1} \hat{q}_{i1}^2 & -M_{022} l_{i2} I_3 & \cdots & M_{02n_i} l_{in_i} \hat{q}_{in_i}^2 \\ \vdots & \vdots & \vdots & \vdots \\ M_{0n_i 1} l_{i1} \hat{q}_{i1}^2 & M_{0n_i 2} l_{i2} \hat{q}_{i2}^2 & \cdots & -M_{0n_i n_i} l_{in_i} I_3 \end{bmatrix}. \quad (89)$$

The $\mathbf{P} \in \mathbb{R}^{D \times D}$ matrix is

$$\mathbf{P} = [P_{x_0}, P_{\Omega_0}, P_{1j}, P_{2j}, \dots, P_{nj}]^T, \quad (90)$$

and sub-matrices of \mathbf{P} matrix are also defined as

$$\begin{aligned} P_{x_0} &= M_T g e_3 + \sum_{i=1}^n -f_i R_i e_3 - \sum_{i=1}^n M_{iT} R_0 \hat{\Omega}_0^2 \rho_i, \\ P_{\Omega_0} &= -\hat{\Omega}_0 \bar{J}_0 \Omega_0 + \sum_{i=1}^n \hat{\rho}_i R_0^T (M_{iT} g e_3 - f_i R_i e_3), \\ P_{ij} &= -\hat{q}_{ij}^2 (-f_i R_i e_3 + M_{0ij} g e_3) + M_{0ij} \hat{q}_{ij}^2 R_0 \hat{\Omega}_0^2 \rho_i + M_{0ij} \|\dot{q}_{ij}\|^2 q_{ij}. \end{aligned}$$

Proof 8 See Appendix A.8

These equations are derived directly on a nonlinear manifold without any simplification. The dynamics of the payload, flexible cables, and quadrotors are considered explicitly, and they avoid singularities and complexities associated to local coordinates.

4.2 Controlled System Design for Simplified Dynamic Model

Let $x_{0_d} \in \mathbb{R}^3$ be the desired position of the payload. The desired attitude of the payload is considered as $R_{0_d} = I_{3 \times 3}$, and the desired direction of links is aligned along the vertical direction. The corresponding location of the i -th quadrotor at this desired configuration is given by

$$x_{i_d} = x_{0_d} + \rho_i - \sum_{a=1}^{n_i} l_{ia} e_3. \quad (91)$$

We wish to design control forces f_i and control moments M_i of quadrotors such that this desired configuration becomes asymptotically stable.

4.2.1 Simplified Dynamic Model

Control forces for each quadrotor is given by $-f_i R_i e_3$ for the given equations of motion (79), (80), (81), (82). As such, the quadrotor dynamics is under-actuated. The total thrust magnitude of each quadrotor can be arbitrary chosen, but the direction of the thrust vector is always along the third body fixed axis, represented by $R_i e_3$. But, the rotational attitude dynamics of the quadrotors are fully actuated, and they are not affected by the translational dynamics of the quadrotors or the dynamics of links.

Based on these observations, in this section, we simplify the model by replacing the $-f_i R_i e_3$ term by a fictitious control input $u_i \in \mathbb{R}^3$, and design an expression for u to asymptotically stabilize the desired equilibrium. In another words, we assume that the attitude of the quadrotor can be instantaneously changed. The effects of the attitude dynamics are studied at the next section.

4.2.2 Linear Control System

The control system for the simplified dynamic model is developed based on the linearized equations of motion. At the desired equilibrium, the position and the attitude of the payload are given by x_{0_d} and $R_0^* = I_3$, respectively, where the superscript $*$ denotes the value of a variable at the desired equilibrium throughout this paper. Also, we have $q_{ij}^* = e_3$ and $R_i^* = I_3$. In this equilibrium configuration, the control input for the i -th quadrotor is

$$u_i^* = -f_i^* R_i^* e_3, \tag{92}$$

where the total thrust is $f_i^* = (M_{iT} + \frac{m_0}{n})g$.

The variation of x_0 is given by

$$\delta x_0 = x_0 - x_{0_d}, \quad (93)$$

and the variation of the attitude of the payload is defined as

$$\delta R_0 = R_0^* \hat{\eta}_0 = \hat{\eta}_0,$$

for $\eta_0 \in \mathbb{R}^3$. The variation of q_{ij} can be written as

$$\delta q_{ij} = \xi_{ij} \times e_3, \quad (94)$$

where $\xi_{ij} \in \mathbb{R}^3$ with $\xi_{ij} \cdot e_3 = 0$. The variation of ω_{ij} is given by $\delta\omega_{ij} \in \mathbb{R}^3$ with $\delta\omega_{ij} \cdot e_3 = 0$. Therefore, the third element of each of ξ_{ij} and $\delta\omega_{ij}$ for any equilibrium configuration is zero, and they are omitted in the following linearized equations. The state vector of the linearized equation is composed of $C^T \xi_{ij} \in \mathbb{R}^2$, where $C = [e_1, e_2] \in \mathbb{R}^{3 \times 2}$. The variation of the control input $\delta u_i \in \mathbb{R}^{3 \times 1}$, is given as $\delta u_i = u_i - u_i^*$.

Proposition 9 *The linearized equations of the simplified dynamic model are given by*

$$\mathbf{M}\ddot{\mathbf{x}} + \mathbf{G}\mathbf{x} = \mathbf{B}\delta u, \quad (95)$$

where the state vector $\mathbf{x} \in \mathbb{R}^{D_x}$ with $D_x = 6 + 2 \sum_{i=1}^n n_i$ is given by

$$\mathbf{x} = \left[\delta x_0, \eta_0, C^T \xi_{1j}, C^T \xi_{2j}, \dots, C^T \xi_{nj} \right],$$

and $\delta u = [\delta u_1^T, \delta u_2^T, \dots, \delta u_n^T]^T \in \mathbb{R}^{3n \times 1}$. The matrix $\mathbf{M} \in \mathbb{R}^{D_x \times D_x}$ are defined as

$$\mathbf{M} = \begin{bmatrix} M_T I_3 & \mathbf{M}_{x_0 \Omega_0} & \mathbf{M}_{x_0 1} & \mathbf{M}_{x_0 2} & \cdots & \mathbf{M}_{x_0 n} \\ \mathbf{M}_{\Omega_0 x_0} & \bar{J}_0 & \mathbf{M}_{\Omega_0 1} & \mathbf{M}_{\Omega_0 2} & \cdots & \mathbf{M}_{\Omega_0 n} \\ \mathbf{M}_{1 x_0} & \mathbf{M}_{1 \Omega_0} & \mathbf{M}_{qq1} & 0 & \cdots & 0 \\ \mathbf{M}_{2 x_0} & \mathbf{M}_{2 \Omega_0} & 0 & \mathbf{M}_{qq2} & \cdots & 0 \\ \vdots & \vdots & \vdots & \vdots & \vdots & \vdots \\ \mathbf{M}_{n x_0} & \mathbf{M}_{n \Omega_0} & 0 & 0 & \cdots & \mathbf{M}_{qqn} \end{bmatrix},$$

where the sub-matrices are defined as

$$\mathbf{M}_{x_0 \Omega_0} = - \sum_{i=1}^n M_{iT} \hat{\rho}_i; \quad \mathbf{M}_{\Omega_0 x_0} = \mathbf{M}_{x_0 \Omega_0}^T,$$

$$\mathbf{M}_{x_0 i} = [M_{0i1} l_{i1} \hat{e}_3 C, M_{0i2} l_{i2} \hat{e}_3 C, \dots, M_{0in_i} l_{in_i} \hat{e}_3 C],$$

$$\mathbf{M}_{\Omega_0 i} = [M_{0i1} l_{i1} \hat{\rho}_i C, M_{0i2} l_{i2} \hat{\rho}_i C, \dots, M_{0in_i} l_{in_i} \hat{\rho}_i C],$$

$$\mathbf{M}_{i x_0} = -[M_{0i1} C^T \hat{e}_3, M_{0i2} C^T \hat{e}_3, \dots, M_{0in_i} C^T \hat{e}_3], \quad (96)$$

$$\mathbf{M}_{i \Omega_0} = [M_{0i1} C^T \hat{e}_3 \hat{\rho}_i, M_{0i2} C^T \hat{e}_3 \hat{\rho}_i, \dots, M_{0in_i} C^T \hat{e}_3 \hat{\rho}_i], \quad (97)$$

and the sub-matrix $\mathbf{M}_{qqi} \in \mathbb{R}^{2n_i \times 2n_i}$ is given by

$$\mathbf{M}_{qqi} = \begin{bmatrix} M_{i11} l_{i1} I_2 & M_{i12} l_{i2} I_2 & \cdots & M_{i1n_i} l_{in_i} I_2 \\ M_{i21} l_{i1} I_2 & M_{i22} l_{i2} I_2 & \cdots & M_{i2n_i} l_{in_i} I_2 \\ \vdots & \vdots & & \vdots \\ M_{in_i 1} l_{i1} I_2 & M_{in_i 2} l_{i2} I_2 & \cdots & M_{in_i n_i} l_{in_i} I_2 \end{bmatrix}. \quad (98)$$

The matrix $\mathbf{G} \in \mathbb{R}^{D_{\mathbf{x}} \times D_{\mathbf{x}}}$ is defined as

$$\mathbf{G} = \begin{bmatrix} 0 & 0 & 0 & 0 & 0 & 0 \\ 0 & \mathbf{G}_{\Omega_0\Omega_0} & 0 & 0 & 0 & 0 \\ 0 & 0 & \mathbf{G}_1 & 0 & 0 & 0 \\ 0 & 0 & 0 & \mathbf{G}_2 & 0 & 0 \\ \vdots & \vdots & \vdots & \vdots & \vdots & \vdots \\ 0 & 0 & 0 & 0 & 0 & \mathbf{G}_n \end{bmatrix},$$

where $\mathbf{G}_{\Omega_0\Omega_0} = \sum_{i=1}^n \frac{m_0}{n} g \hat{\rho}_i \hat{e}_3$ and the sub-matrices $\mathbf{G}_i \in \mathbb{R}^{2n_i \times 2n_i}$ are

$$\mathbf{G}_i = \text{diag}\left[\left(-M_{iT} - \frac{m_0}{n} + M_{0ij}\right)g e_3 I_2\right].$$

The matrix $\mathbf{B} \in \mathbb{R}^{D_{\mathbf{x}} \times 3n}$ is given by

$$\mathbf{B} = \begin{bmatrix} I_3 & I_3 & \cdots & I_3 \\ \hat{\rho}_1 & \hat{\rho}_2 & \cdots & \hat{\rho}_n \\ \mathbf{B}_B & 0 & 0 & 0 \\ 0 & \mathbf{B}_B & 0 & 0 \\ \vdots & \vdots & \vdots & \vdots \\ 0 & 0 & 0 & \mathbf{B}_B \end{bmatrix},$$

where $\mathbf{B}_B = -[C^T \hat{e}_3, C^T \hat{e}_3, \dots, C^T \hat{e}_3]^T$.

Proof 9 See Appendix A.9

We present the following PD-type control system for the linearized dynamics

$$\delta u_i = -K_{x_i} \mathbf{x} - K_{\dot{x}_i} \dot{\mathbf{x}}, \quad (99)$$

for controller gains $K_{x_i}, K_{\dot{x}_i} \in \mathbb{R}^{3 \times D_{\mathbf{x}}}$. Provided that (95) is controllable,

we can choose the combined controller gains $K_x = [K_{x_1}^T, \dots, K_{x_n}^T]^T$, $K_{\dot{x}} = [K_{\dot{x}_1}^T, \dots, K_{\dot{x}_n}^T]^T \in \mathbb{R}^{3n \times D_x}$ such that the equilibrium is asymptotically stable for the linearized equation (95).

4.3 Controlled System Design for Full Dynamic Model

The control system designed at the previous section is based on a simplifying assumption that each quadrotor can generate a thrust along any direction. In the full dynamic model, the direction of the thrust for each quadrotor is parallel to its third body-fixed axis always. In this section, the attitude of each quadrotor is controlled such that the third body-fixed axis becomes parallel to the direction of the ideal control force designed in the previous section. The central idea is that the attitude R_i of the quadrotor is controlled such that its total thrust direction $-R_i e_3$, corresponding to the third body-fixed axis, asymptotically follows the direction of the fictitious control input u_i . By choosing the total thrust magnitude properly, we can guarantee asymptotical stability for the full dynamic model.

Let $A_i \in \mathbb{R}^3$ be the ideal total thrust of the i -th quadrotor that asymptotically stabilize the desired equilibrium. Therefore, we have

$$A_i = u_i^* + \delta u_i = -K_{x_i} \mathbf{x} - K_{\dot{x}_i} \dot{\mathbf{x}} + u_i^*, \quad (100)$$

where f_i^* and u_i^* are the total thrust and control input of each quadrotor at its equilibrium respectively.

From the desired direction of the third body-fixed axis of the i -th quadrotor, namely $b_{3_i} \in \mathbb{S}^2$, is given by

$$b_{3_i} = -\frac{A_i}{\|A_i\|}. \quad (101)$$

This provides a two-dimensional constraint on the three dimensional desired attitude of each quadrotor, such that there remains one degree of freedom. To resolve it, the desired direction of the first body-fixed axis $b_{1_i}(t) \in \mathbf{S}^2$ is introduced as a smooth function of time. Due to the fact that the first body-fixed axis is normal to the third body-fixed axis, it is impossible to follow an arbitrary command $b_{1_i}(t)$ exactly. Instead, its projection onto the plane normal to b_{3_i} is followed, and the desired direction of the second body-fixed axis is chosen to constitute an orthonormal frame [28]. More explicitly, the desired attitude of the i -th quadrotor is given by

$$R_{i_c} = \begin{bmatrix} -\frac{(\hat{b}_{3_i})^2 b_{1_i}}{\|(\hat{b}_{3_i})^2 b_{1_i}\|} & \frac{\hat{b}_{3_i} b_{1_i}}{\|\hat{b}_{3_i} b_{1_i}\|} & b_{3_i} \end{bmatrix}, \quad (102)$$

which is guaranteed to be an element of $\mathfrak{so}(3)$. The desired angular velocity is obtained from the attitude kinematics equation, $\Omega_{i_c} = (R_{i_c}^T \dot{R}_{i_c})^\vee \in \mathbb{R}^3$. Define the tracking error vectors for the attitude and the angular velocity of the i -th quadrotor as

$$e_{R_i} = \frac{1}{2}(R_{i_c}^T R_i - R_i^T R_{i_c})^\vee, \quad e_{\Omega_i} = \Omega_i - R_i^T R_{i_c} \Omega_{i_c}, \quad (103)$$

and a configuration error function on $\text{SO}(3)$ as follows

$$\Psi_i = \frac{1}{2} \text{tr}[\mathbb{I} - R_{i_c}^T R_i]. \quad (104)$$

The thrust magnitude is chosen as the length of u_i , projected on to $-R_i e_3$, and the control moment is chosen as a tracking controller on $\text{SO}(3)$:

$$f_i = -A_i \cdot R_i e_3, \quad (105)$$

$$M_i = -k_R e_{R_i} - k_\Omega e_{\Omega_i} + (R_i^T R_{c_i} \Omega_{c_i})^\wedge J_i R_i^T R_{c_i} \Omega_{c_i} + J_i R_i^T R_{c_i} \dot{\Omega}_{c_i}, \quad (106)$$

where k_R and k_Ω are positive constants. Stability of the corresponding controlled systems for the full dynamic model can be studied by showing the error due to the discrepancy between the desired direction b_{3_i} and the actual direction $R_i e_3$. This stability is shown via a Lyapunov analysis.

Proposition 10 *Consider the full dynamic model defined by (79), (80), (81), (82). For the command x_{0_d} and the desired direction of the first body-fixed axis b_{1_i} , control inputs for quadrotors are designed as (105) and (106). Then, the equilibrium of zero tracking errors for e_{x_0} , \dot{e}_{x_0} , e_{R_0} , e_{Ω_0} , $e_{q_{ij}}$, $e_{\omega_{ij}}$, e_{R_i} , e_{Ω_i} , is exponentially stable.*

Proof 10 *See Appendix A.10*

4.4 Numerical Example

We demonstrate the desirable properties of the proposed control system with numerical examples. Two cases are presented. At the first case, a payload is transported to a desired position from the ground. The second case considers stabilization of a payload with large initial attitude errors.

4.4.1 Stabilization of the Rigid Body

Consider four quadrotors ($n = 4$) connected via flexible cables to a rigid body payload. Initial conditions are chosen as

$$\begin{aligned} x_0(0) &= [1.0, 4.8, 0.0]^T \text{ m}, \quad v_0(0) = 0_{3 \times 1}, \\ q_{ij}(0) &= e_3, \quad \omega_{ij}(0) = 0_{3 \times 1}, \quad R_i(0) = I_{3 \times 3}, \quad \Omega_i(0) = 0_{3 \times 1} \\ R_0(0) &= I_{3 \times 3}, \quad \Omega_0 = 0_{3 \times 1}. \end{aligned}$$

The desired position of the payload is chosen as

$$x_{0_d}(t) = [0.44, 0.78, -0.5]^T \text{ m}. \quad (107)$$

The mass properties of quadrotors are chosen as

$$m_i = 0.755 \text{ kg},$$

$$J_i = \text{diag}[0.557, 0.557, 1.05] \times 10^{-2} \text{ kgm}^2. \quad (108)$$

The payload is a box with mass $m_0 = 0.5 \text{ kg}$, and its length, width, and height are 0.6, 0.8, and 0.2 m, respectively. Each cable connecting the rigid body to the i -th quadrotor is considered to be $n_i = 5$ rigid links. All the links have the same mass of $m_{ij} = 0.01 \text{ kg}$ and length of $l_{ij} = 0.15 \text{ m}$. Each cable is attached to the following points of the payload

$$\rho_1 = [0.3, -0.4, -0.1]^T \text{ m}, \quad \rho_2 = [0.3, 0.4, -0.1]^T \text{ m},$$

$$\rho_3 = [-0.3, -0.4, -0.1]^T \text{ m}, \quad \rho_4 = [-0.3, 0.4, -0.1]^T \text{ m}.$$

Numerical simulation results are presented at Figure 13, which shows the position and velocity of the payload, and its tracking errors. We have also presented the link direction error defined as

$$e_q = \sum_{i=1}^m \sum_{j=1}^{n_i} \|q_{ij} - e_3\|.$$

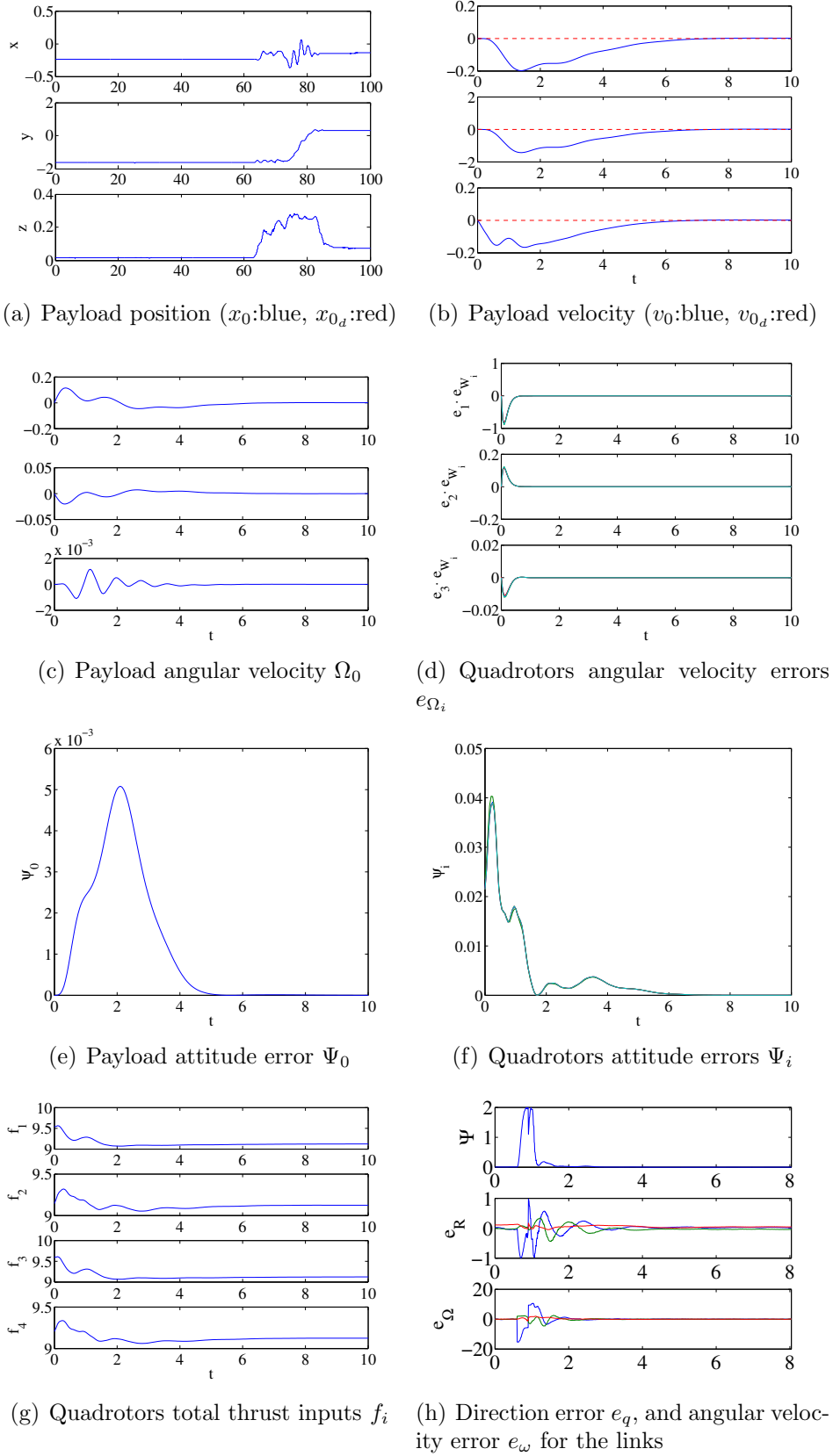
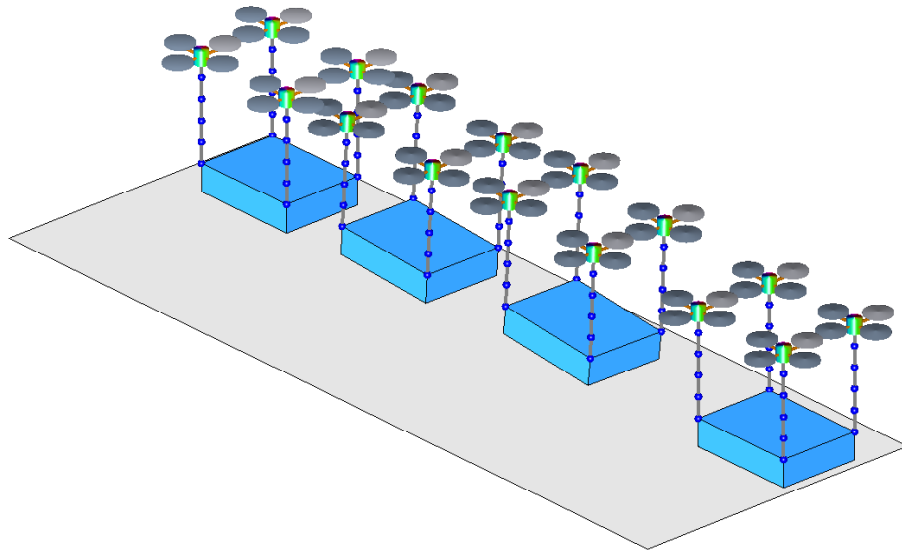
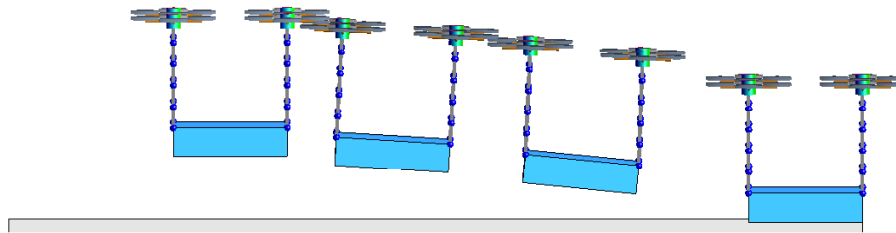


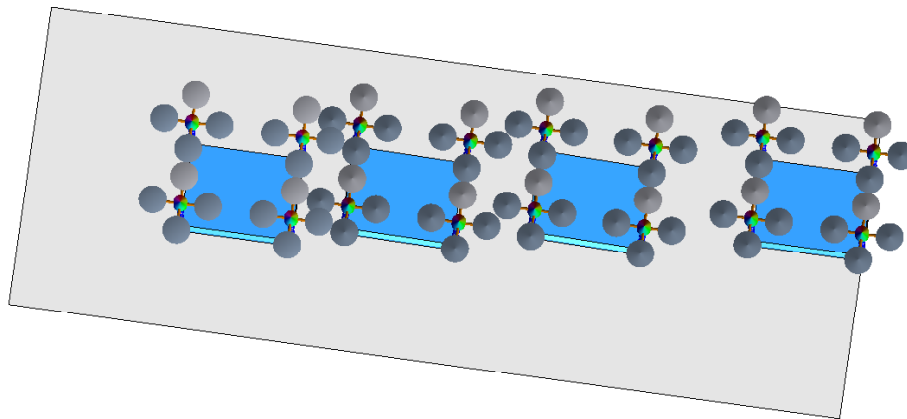
Figure 13: Stabilization of a rigid-body connected to multiple quadrotors



(a) 3D perspective



(b) Side view



(c) Top view

Figure 14: Snapshots of controlled maneuver

4.4.2 Payload Stabilization with Large Initial Attitude Errors

In the second case, we consider large initial errors for the attitude of the payload and quadrotors. Initially, the rigid body is tilted in its b_1 axis by 30 degrees, and the initial direction of the links are chosen such that two cables are curved along the horizontal direction. The initial conditions are given by

$$\begin{aligned} x_0(0) &= [2.4, 0.8, -1.0]^T, \quad v_0(0) = 0_{3 \times 1}, \\ \omega_{ij}(0) &= 0_{3 \times 1}, \quad \Omega_i(0) = 0_{3 \times 1} \\ R_0(0) &= R_x(30^\circ), \quad \Omega_0 = 0_{3 \times 1}, \end{aligned}$$

where $R_x(30^\circ)$ denotes the rotation about the first axis by 30° . The initial attitude of quadrotors are chosen as

$$\begin{aligned} R_1(0) &= R_y(-35^\circ), \quad R_2(0) = I_{3 \times 3}, \\ R_3(0) &= R_y(-35^\circ), \quad R_4(0) = I_{3 \times 3}. \end{aligned}$$

The properties of quadrotors and cables are identical to the previous case. The payload mass is $m = 1.0$ kg, and its length, width, and height are 1.0, 1.2, and 0.2 m, respectively. Figure 15 illustrates the tracking errors, and the total thrust of each quadrotor. Snapshots of the controlled maneuvers is also illustrated at Figure 16. It is shown that the proposed controller is able to stabilize the payload and cables at their desired configuration even from the large initial attitude errors¹.

¹A short animation of this numerical simulation is available at <http://youtu.be/j14tSuHd8oA>.

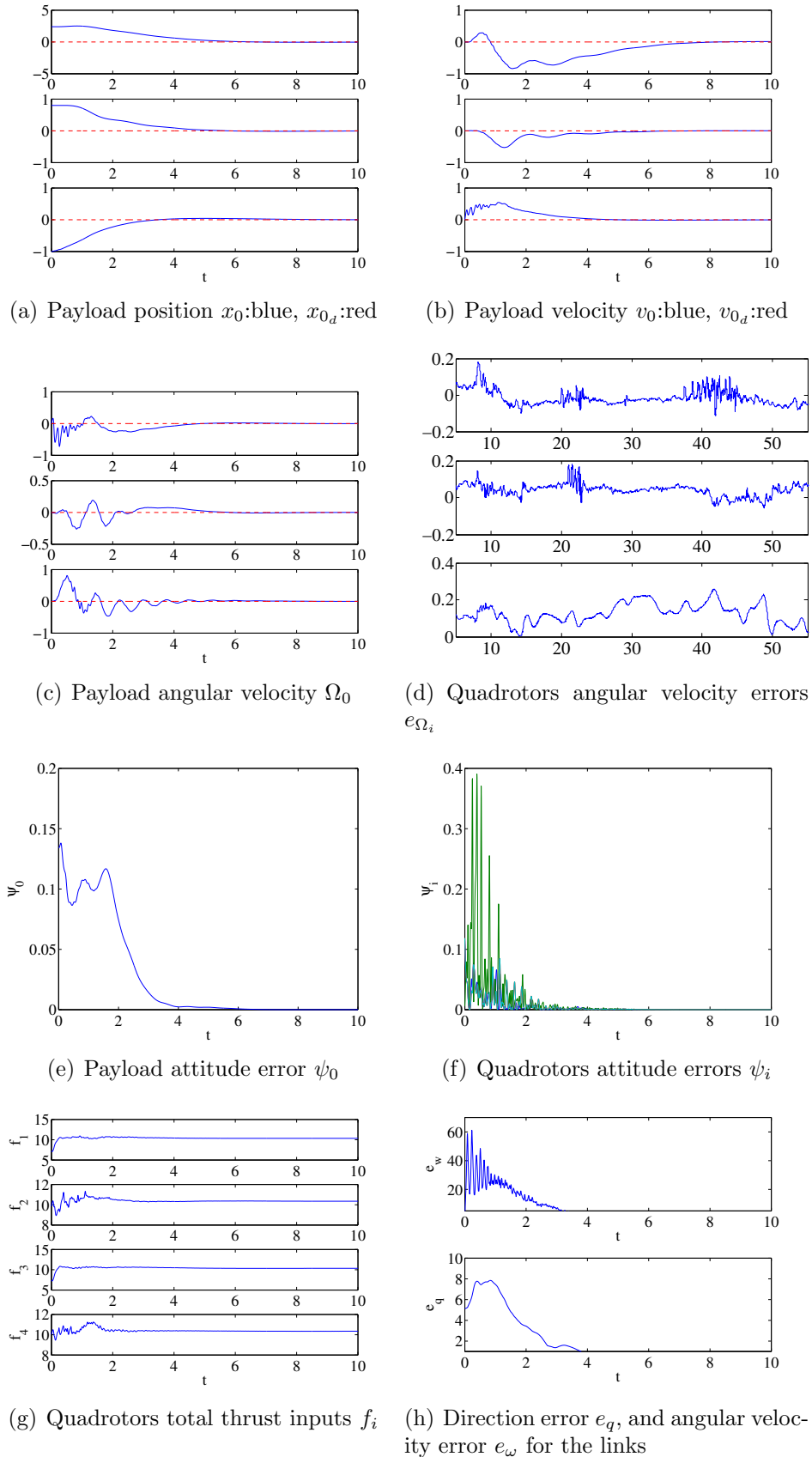


Figure 15: Stabilization of a payload with multiple quadrotors connected with flexible cables. 65

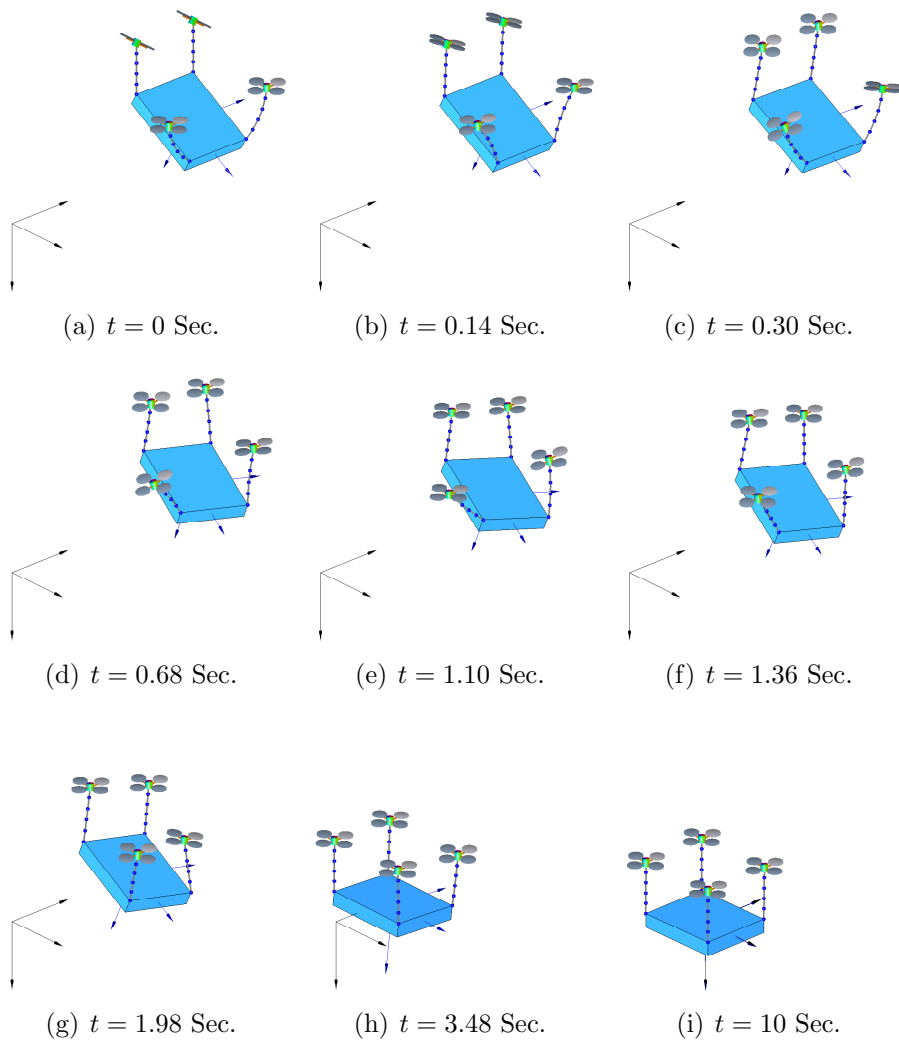


Figure 16: Snapshots of the controlled maneuver.

4.4.3 Two Quadrotors Stabilizing a Rod

The results of this chapter can be specialized to the following system. Consider two quadrotors transporting a rod to a fixed position as shown in Figure 17.

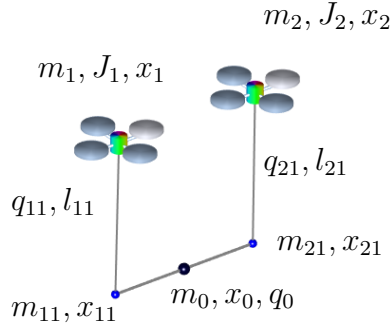


Figure 17: Two quadrotor with a rod

We compare stabilization of the rod with large initial attitude errors both for quadrotors and rod for two cases of with and without the integral term in presence of the fixed disturbances in both rotational and translational dynamics.

The results of this numerical simulation is presented in Figure 18 and 19 for without and with integral cases respectively. Snapshots of this maneuver with the integral term is also illustrated at Figure 20.

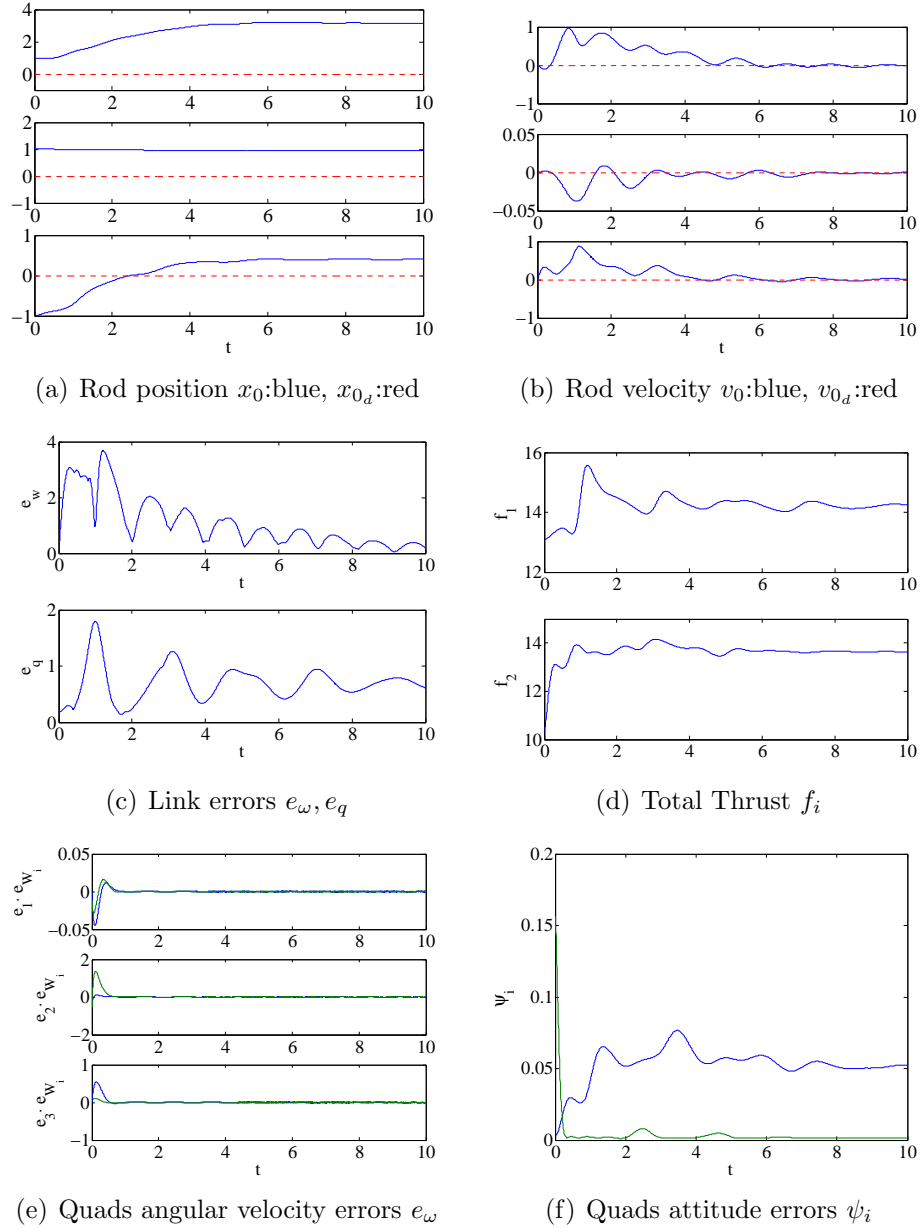


Figure 18: Stabilization of a rod with two quadrotors without Integral term.

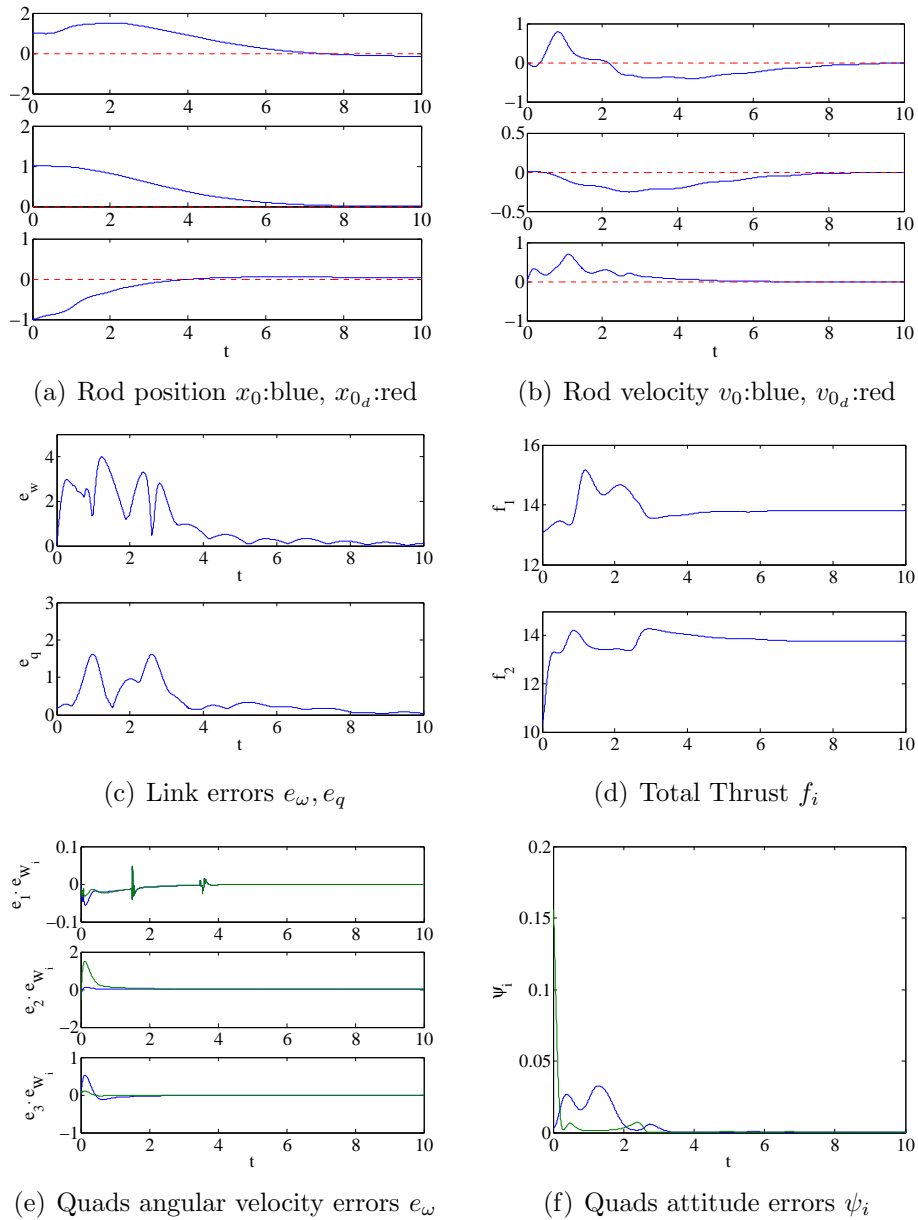


Figure 19: Stabilization of a rod with two quadrotors with Integral term.

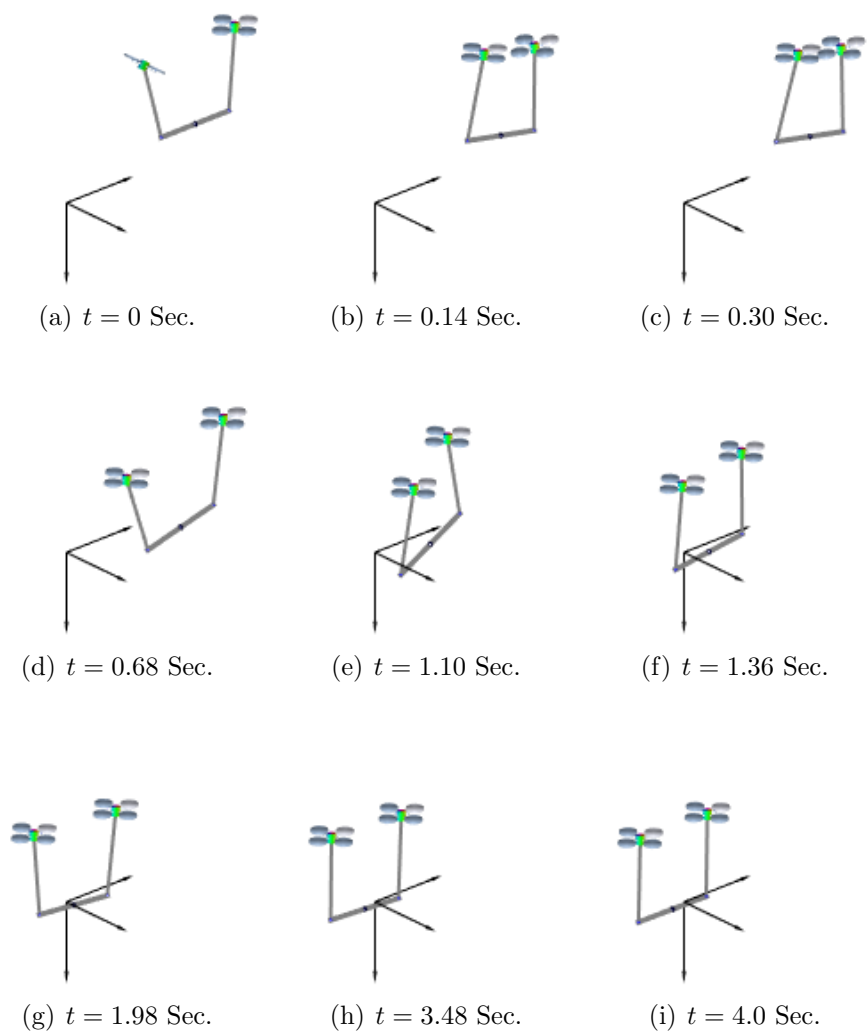


Figure 20: Snapshots of the controlled maneuver for two quadrotors stabilizing a rod.

Chapter 5: Experiment

We develop an experimental testbed with quadrotor UAV's to validate our derivations and simulations. Two quadrotor UAV's are built from scratch by designing every parts followed by developing a software for real-time experiments. The hardware and software development for the experimental part of this dissertation is presented in the following. Finally, the experimental results for some aggressive trajectory tracking and payload transportation are provided.

5.1 CAD Model and Calibration

We developed an accurate CAD model as shown in Figure 21(a) to identify several parameters of the quadrotor, such as moment of inertia and center of mass. Furthermore, a precise rotor calibration is performed for each rotor, with a custom-made thrust stand as shown in Figure 21(b) to determine the relation between the command in the motor speed controller and the actual thrust. For various values of motor speed commands, the corresponding thrust is measured, and those data are fitted with a second order polynomial.

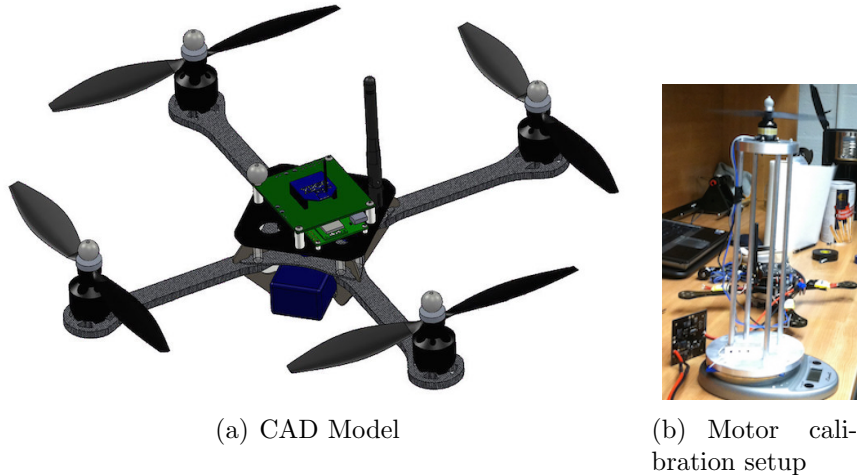


Figure 21: Hardware development for a quadrotor UAV

5.2 Building Quadrotor

The quadrotor UAV developed at the flight dynamics and control laboratory at the George Washington University is shown at Figure 22. The angular velocity is measured from inertial measurement unit (IMU) and the attitude is obtained from IMU data. Position of the UAV is measured from motion capture system (Vicon) as shown in Figure 23 and the velocity is estimated from the measurement. Ground computing system receives the Vicon data and send it to the UAV via XBee. The Gumstix is adopted as micro computing unit on the UAV.

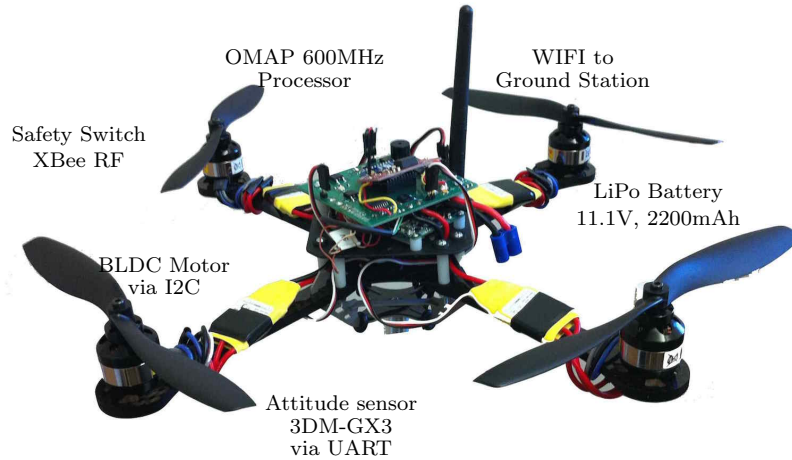


Figure 22: Hardware development



Figure 23: Motion capture Laboratory

5.2.1 Hardware Configuration

Quadrotor is built using several parts as listed bellow. The motors are connected to the circuit board via speed controllers and I2C ports. The IMU is connected to the circuit board via serial ports and the computer module (GUMSTIX) handles the communications and controller computation.

- Gumstix Overo computer-in-module (OMAP 600MHz processor), running a non-realtime Linux operating system. It is connected to a ground station via WIFI (Figure 24(c)).
- Microstrain 3DM-GX3 IMU, connected to Gumstix via UART (Figure 24(b)).
- BL-CTRL 2.0 motor speed controller, connected to Gumstix via I2C (Figure 25(a)).
- Roxxy 2827-35 Brushless DC motors (Figure 25(b)).
- XBee RF module, connected to Gumstix via UART. (Figure 24(a))

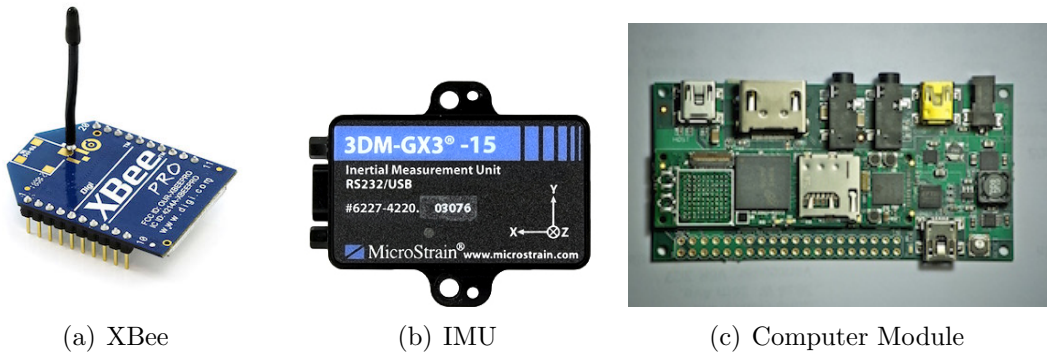


Figure 24: Hardware parts for a quadrotor UAV

Finally, these parts are all connected to the circuit board which has been custom designed and built for the experiment as illustrated in Figure 26 and two quadrotors are prepared for the experiments as shown in Figure 27.

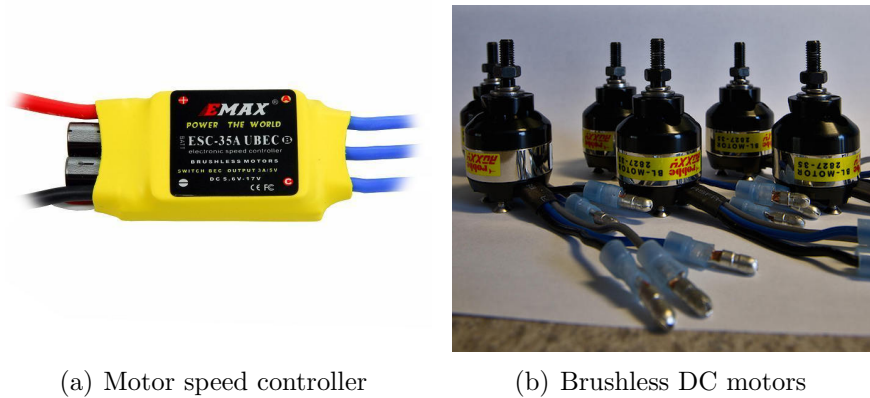


Figure 25: Motors and speed controllers

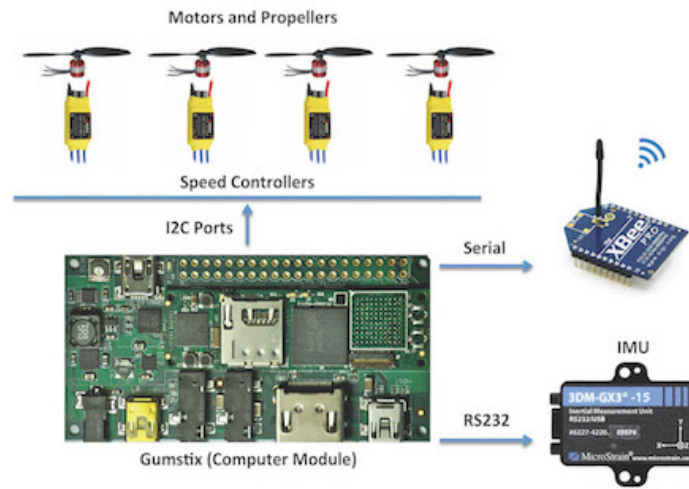
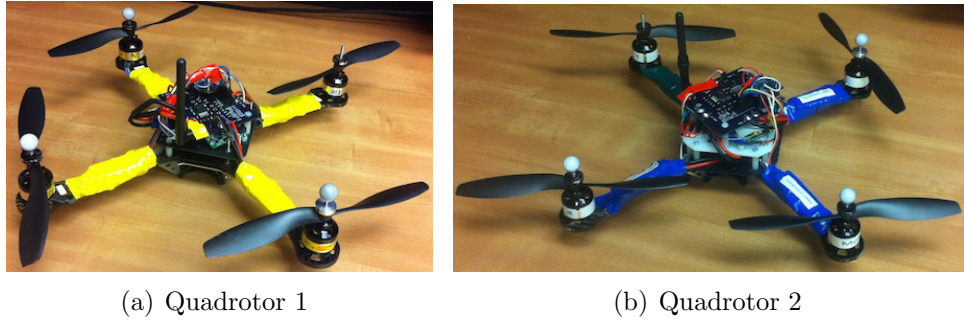


Figure 26: Hardware connections

5.2.2 Software Development

Multi-threaded programming with C/C++ utilized to develop a complete and fast software which runs on the computer module and handles several tasks. It has three main threads, namely Vicon thread, IMU thread, and control thread. The Vicon thread receives the Vicon measurement and estimates linear velocity of the quadrotor. The IMU thread receives the IMU measurement and estimates the attitude. The last thread handles the control outputs at each time step. Also, control outputs are calculated at 120Hz which is fast enough



(a) Quadrotor 1

(b) Quadrotor 2

Figure 27: Quadrotors

to run any kind of aggressive maneuvers. Information flow of the system is illustrated in Figures 28 and 29.

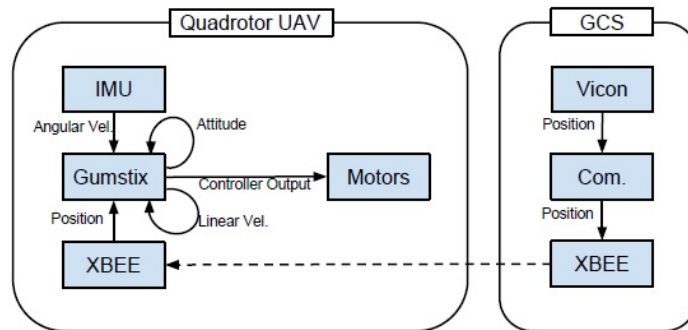


Figure 28: Information flow of overall system

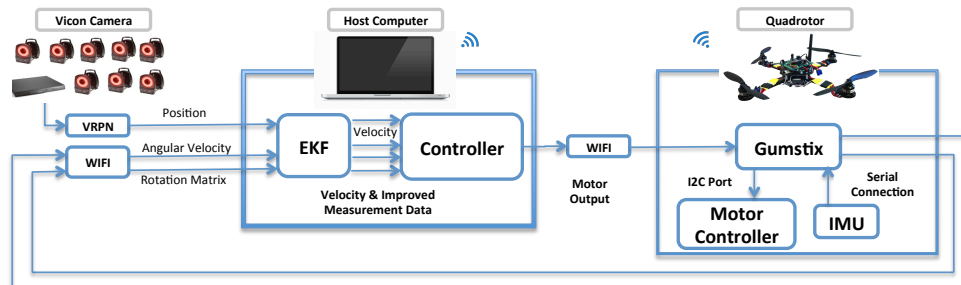


Figure 29: Information flow of overall system

We also need to tune the proportional, derivative, and integral gains for the experiment. By using the numerical simulation, we are able to find an estimate for this gains but they need to be tuned during the experiment in order to get the best performance of the controller.

5.3 Autonomous Trajectory Tracking

5.3.1 Attitude Tracking Test

Experimental results are provided for the attitude tracking control of a hardware system developed in FDCL. To test the attitude dynamics, it is attached to a spherical joint. As the center of rotation is below the center of gravity, there exists a destabilizing gravitational moment, and the resulting attitude dynamics is similar to an inverted rigid body pendulum. The control input is augmented with an additional term to eliminate the effects of the gravity.

The desired attitude command is described by using 3-2-1 Euler angles, i.e. $R_d(t) = R_d(\phi(t), \theta(t), \psi(t))$, where $\phi(t) = \frac{\pi}{9} \sin(\pi t)$, $\theta(t) = \frac{\pi}{9} \cos(\pi t)$, $\psi(t) = 0$. This represents a combined rolling and pitching motion with a period of 2 seconds. The results of the experiment are illustrated at Figures 30 and 31.

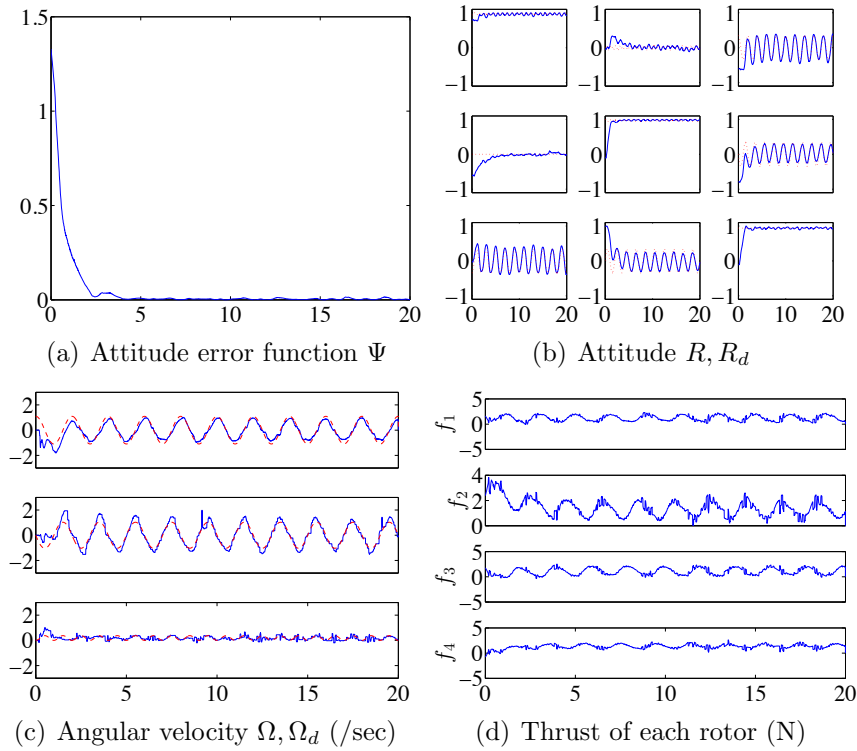


Figure 30: Attitude tracking test(dotted:desired, solid:actual)



Figure 31: Quadrotor on a stand

5.3.2 Lissajous Curve Trajectory Tracking

First, we consider a position tracking mode, where the desired trajectory is defined as the following Lissajous curve,

$$x_d(t) = \begin{cases} x_o - \frac{t}{8}(x_o - x_i) & \text{if } 0 \leq t < 8 \\ [\sin(t - 8) + \frac{\pi}{2}), \sin 2(t - 8), -1.5] \text{ m} & \text{if } 8 \leq t \end{cases}.$$

The quadrotor takes-off from $x_o = [0.2, -2.8, -1.2] \text{m}$ at $t = 0$ sec and flies to the initial position of the Lissajous curve trajectory where is $x_i = [1, 0, 1.5] \text{m}$ by tracking a linear desired trajectory. Then, the quadrotor starts to follow the Lissajous curve trajectory at $t = 8$ sec. There is about 0.15 sec of time delay from the Vicon motion capture system to the Gumstix. However, due to the robustness and stability properties of the proposed controller, position tracking performance shows satisfactory results as shown at Figure 33 and 32.

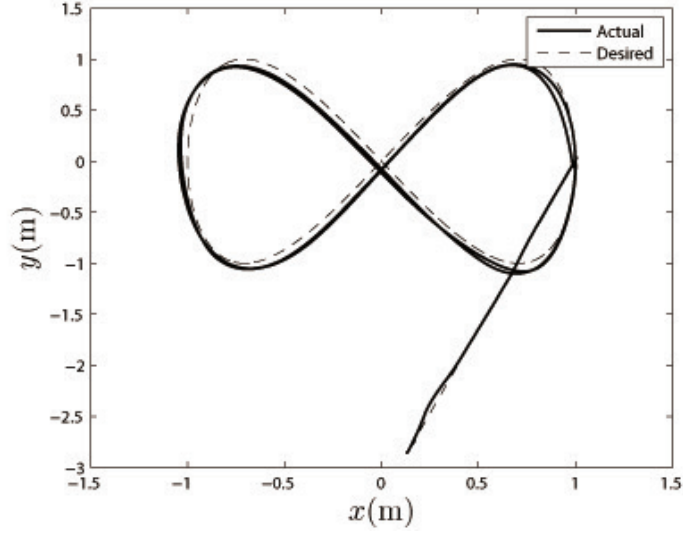


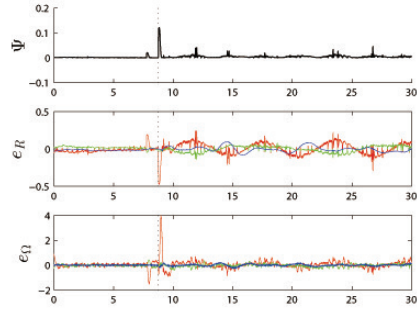
Figure 32: Lissajous curve $x - y$ plane trajectory

5.3.3 Flipping 360 Degree Maneuver

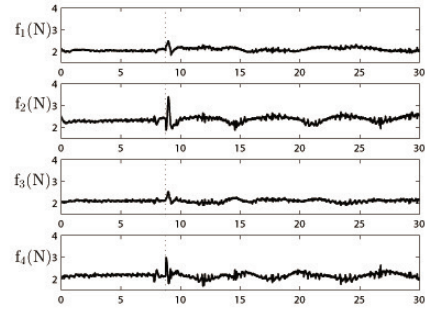
Next, the proposed controller is validated with a flipping maneuver. The quadrotor takes off from a landing platform, increases altitude with constant speed to a constant point, flips 360 degree about its x -axis. As presented in the numerical simulation section, this is a complex maneuver combining a nontrivial pitching maneuver with a yawing motion. It is achieved by concatenating the following two control modes of an attitude tracking same as presented in the numerical simulation to rotate the quadrotor

$$R_d(t) = I + \sin(4\pi t)\hat{e}_r + (1 - \cos(4\pi t))(e_r e_r^T - I), \quad \Omega_d = 5\pi \cdot e_r.$$

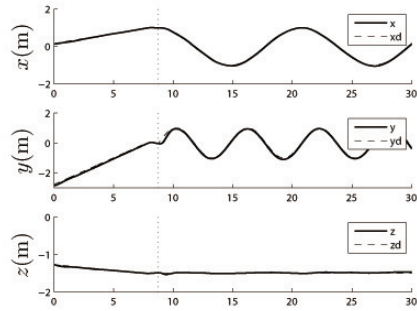
where $e_r = [1, 0, 0]$, and a trajectory tracking mode to make it hover after completing the preceding rotation. As it is clear from the figures, the attitude control part which handles the rotation happens in almost 0.3 seconds and then it switched to the position control mode to make the quadrotor stabilized and hovers to the desired position. Figure 34 and 35 show the experimental



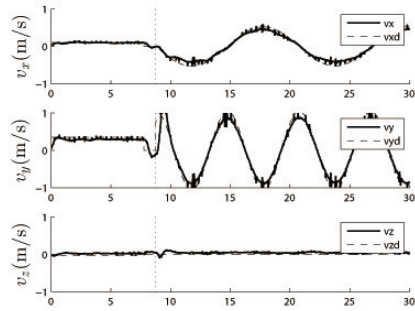
(a) Attitude error variables Ψ, e_R, e_Ω



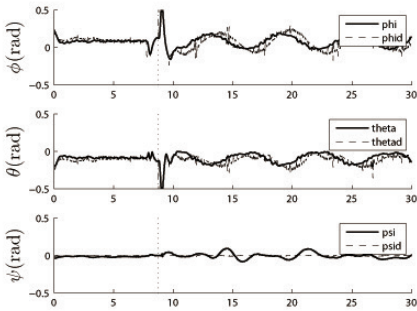
(b) Thrust of each rotor (N)



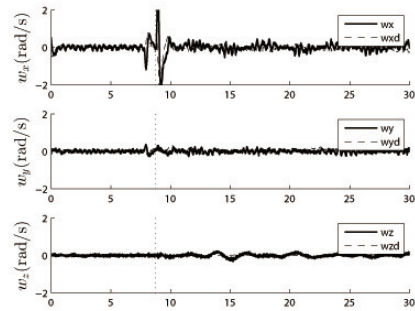
(c) Position (solid line) and desired (dotted line) x, x_d (m)



(d) Linear velocity (m/sec)



(e) Euler angles (rad)



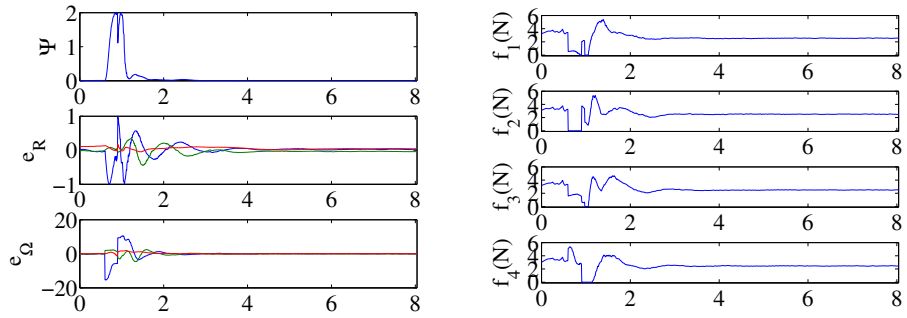
(f) Angular velocity Ω, Ω_d (rad/sec)

Figure 33: Lissajous curve tracking (dotted:desired, solid:actual)

results and snapshots of the flipping maneuver respectively.

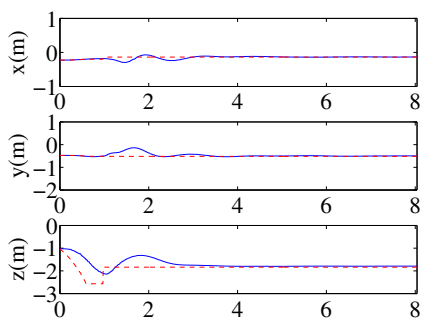
There are several disturbances and modeling errors in this experimental setup, such as errors in mass properties of the quadrotor, processing and communication delay of the motion capture systems, and the dynamics of propellers. Therefore, these experimental illustrate robustness of the proposed control system with respect to various forms of uncertainties and disturbances².

²A short video of the experiments is available at <http://youtu.be/wtn9L6BsYiE>.

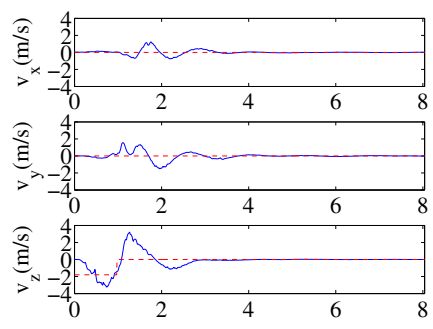


(a) Attitude error variables Ψ, e_R, e_Ω

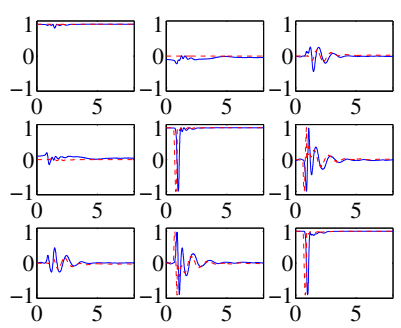
(b) Thrust of each rotor (N)



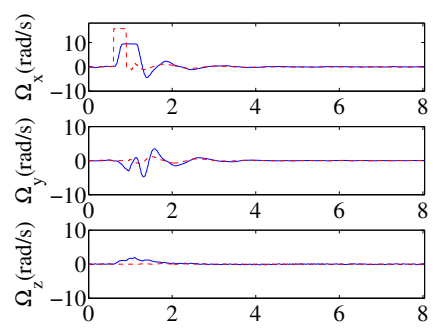
(c) Position x, x_d (m)



(d) Linear velocity (m/sec)



(e) Rotation Matrix



(f) Angular velocity Ω, Ω_d (rad/sec)

Figure 34: Flipping flight test results (dotted:desired, solid:actual)

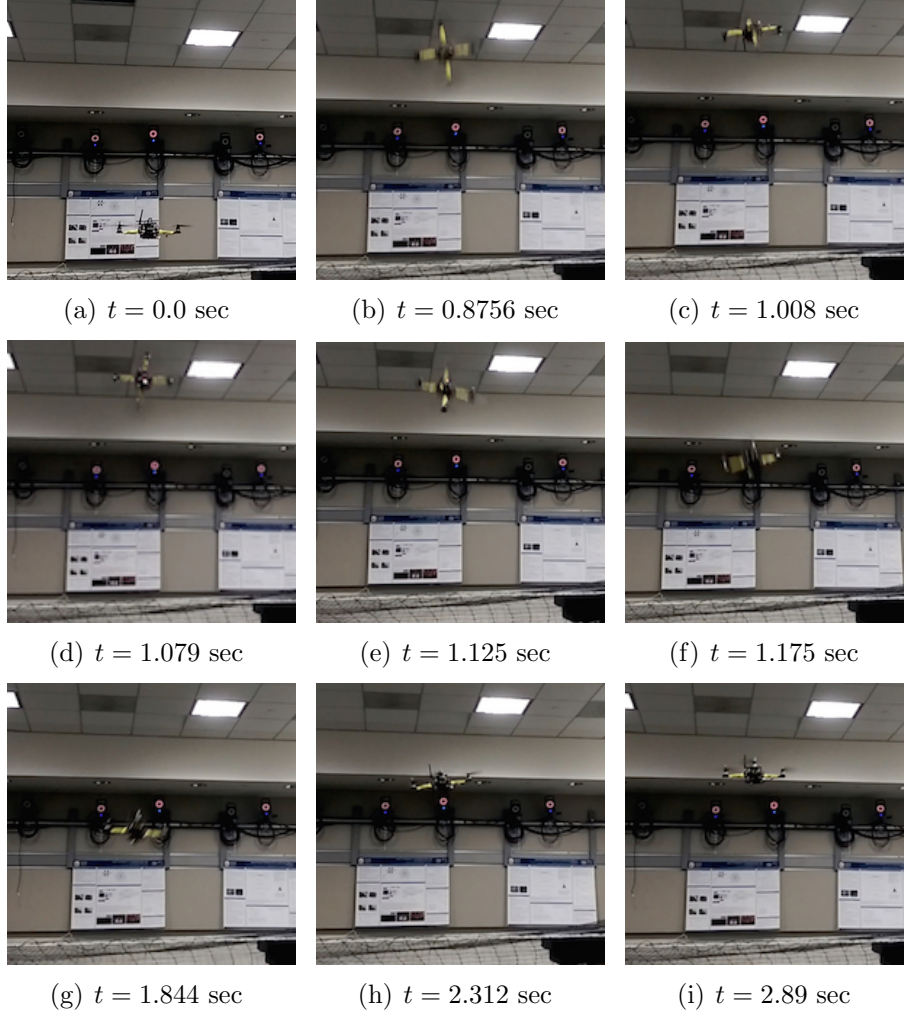


Figure 35: Snapshots for flipping maneuver.

5.4 Payload Stabilization with one Quadrotor

The weight of the entire UAV system is 0.791kg including one battery. A payload with mass of $m_1 = 0.036$ kg is attached to the quadrotor via a cable of length $l_1 = 0.7$ m. The length from the center of the quadrotor to each motor rotational axis is $d = 0.169$ m, the thrust to torque coefficient is $c_{\tau_f} = 0.1056$ m and the moment of inertia is $J = [0.56, 0.56, 1.05] \times 10^{-2}$ kgm².

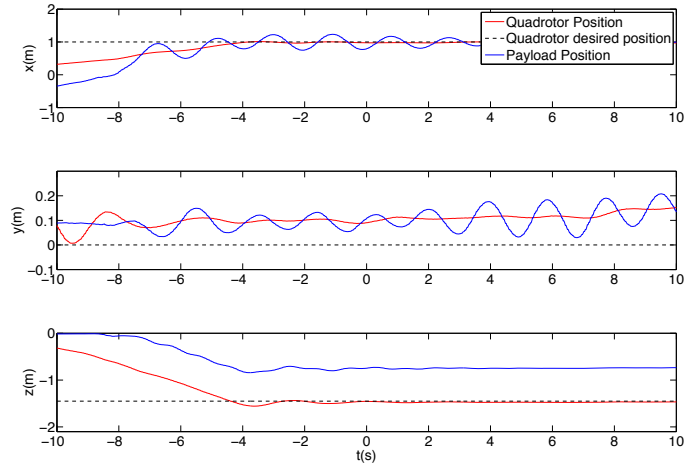
Two cases are considered and compared. For the first case, a position control system developed in [45], for quadrotor UAV that does not include the dynamics of the payload and the link, is applied to hover the quadrotor at the

desired location, and the second case, the proposed control system is used.

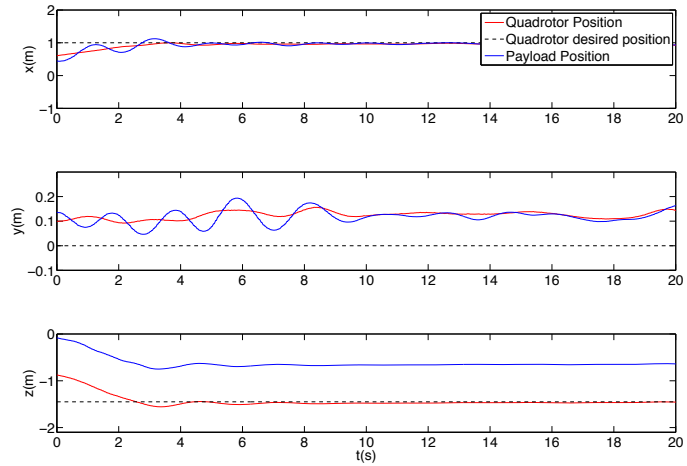
Experimental results are shown at Figures 36 and 38. The position of the quadrotor and the payload is compared with the desired position of the quadrotor at Figure 36, and the deflection angle of the link from the vertical direction are illustrated at Figure 38. It is shown that the proposed control system reduces the undesired oscillation of the link effectively, compared with the quadrotor position control system.³

There are several disturbances and modeling errors in this experimental setup, such as errors in mass properties of the quadrotor, processing and communication delay of the motion capture systems, and ground effects of air flow. Therefore, these experimental illustrate robustness of the proposed control system with respect to various forms of uncertainties and disturbances. Generalizing the presented control system for advanced nonlinear adaptive or robust controls are relegated to future investigation.

³A short video of the experiments is available at <http://youtu.be/RyTnWVbgt34>.



(a) Case I: quadrotor position control system [45]



(b) Case II: proposed control system for quadrotor with suspended payload

Figure 36: Experimental results (x_d :black, x :red, $x + l_1q_1$:blue)

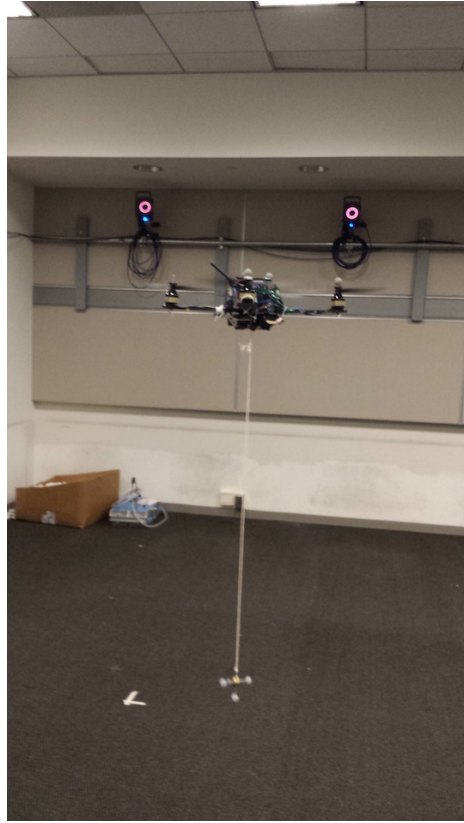
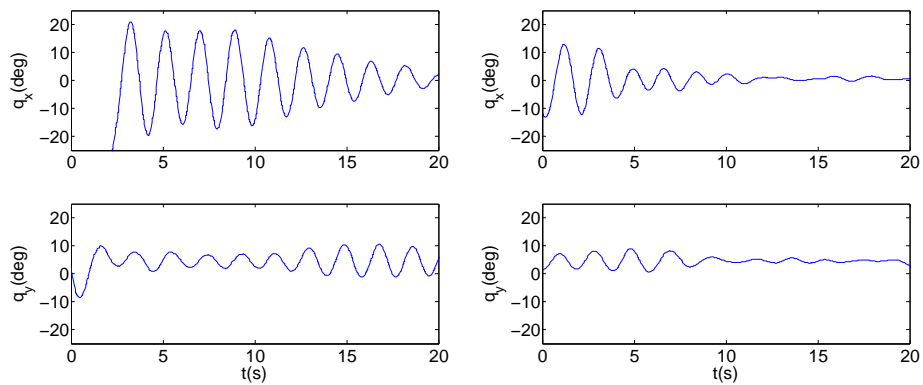


Figure 37: Snapshot of a quadrotor UAV stabilizing a payload



(a) Case I: quadrotor position control [45] (b) Case II: proposed control system for quadrotor with suspended payload

Figure 38: Experimental results: link deflection angles

Chapter 6: Conclusions

We conclude our research and work of this dissertation here. In this section, first a summary of conclusions is given and it is followed by the future work.

6.1 Conclusions

A new nonlinear adaptive control system is proposed for tracking control of quadrotor unmanned aerial vehicles. It is developed directly on the special orthogonal group to avoid complexities and ambiguities that are associated with Euler-angles or quaternions, and the proposed adaptive control term guarantees almost global attractivity for the tracking error variables in the existence of uncertainties.

Euler-Lagrange equations have been derived for multiple cooperative quadrotor UAVs and the chain pendulum to model each flexible cable transporting a rigid body in 3D space. These derivations developed in a remarkably compact form which allows us to choose arbitrary number and any configuration of the links. We developed a geometric nonlinear controller to stabilize the links below the quadrotor in the equilibrium position from any chosen initial condition. We expanded these derivations in such way that there is no need of using local angle coordinate. Rigorous mathematical stability proofs are given without any time-scale separation assumptions and these are verified by mathematical analysis, numerical simulations, and experiments for aggressive maneuvers concurrently.

6.2 Challenges & Future Work

Several limitations and challenges are considered for the proposed dynamic model, controller and experimental testbed. Some of the limitations, important hardware challenges, and future directions are listed below

- Communication is very important in real-time experiments. We need high speed update rate in order to maintain an aggressive maneuver, and any failure in communication causes instability of the system and would lead to incidents.
- Batteries used for the experiment can play an important role in a successful maneuver. They can be drained very soon and it affects the performance of the hardware and the gain tuning process.
- Different sensors are used in real-time experiments. For example, an IMU used to obtain the angular velocities, and Vicon Motion Capture system to obtain the position of the object. In both, sensors provide the noisy data which needed to be filtered or estimated to obtain smooth data. Furthermore, we experienced delay in receiving the data using the Vicon system.
- The flexible cables are considered into the dynamic of the system by modeling them as serially connected links. As more as links get used in the cable, the dynamic model becomes more accurate. However, additional sensors are needed to measure the deformation of the cable accurately.
- The proposed cable model via interconnected lumped masses is readily generalized to uniform mass distribution at each link. Based on the assumption that the diameter of the cable is much smaller than its length, the torsion of the bending moment are not considered in this dissertation.
- Payload stabilization with single and multiple quadrotor UAVs to a fixed position are presented in this work. Dynamics model can be used and new

controller can be extended and designed for tracking time-varying trajectories.

- Experimental results for payload trajectory tracking is another future direction of this dissertation. There are several challenges in running experiments with multiple quadrotors simultaneously and tracking a desired trajectory for a payload with multiple quadrotor UAV's to validate the derivation for time-continuous controller.
- Future directions include extending this research in an outdoor environment to identify the wind effects and verifying the performance of the controller in various weather situations. A GPS system can be installed on the quadrotors instead of the Motion Capture system in a laboratory to identify the position and velocity of the quadrotor.

Bibliography

- [1] Mahony, R., Kumar, V., and Corke, P., 2012. “Multirotor aerial vehicles: Modeling, estimation, and control of a quadrotor”. *IEEE robotics and Automation Magazine*, **19**(3), pp. 20–32.
- [2] Goodarzi, F. A., Lee, D., and Lee, T., 2014. “Geometric stabilization of quadrotor UAV with a payload connected by flexible cable”. In Proceedings of American Control Conference, Portland OR, pp. 4925–4930.
- [3] Goodarzi, F. A., Lee, D., and Lee, T., 2015. “Geometric control of a quadrotor uav transporting a payload connected via flexible cable”. *International Journal of Control, Automation and Systems*, **13**(6).
- [4] Goodarzi, F. A., and Lee, T., 2015. “Dynamics and control of quadrotor uavs transporting a rigid body connected via flexible cables”. In Proceedings of American Control Conference 2015, Chicago IL, pp. 4677–4682.
- [5] Cicolani, L., Kanning, G., and Synnestvedt, R., 1995. “Simulation of the dynamics of helicopter slung load systems”. *Journal of the American Helicopter Society*, **40**(4), pp. 44–61.
- [6] Bernard, M., 2009. “Generic slung load transportation system using small size helicopters”. In Proceedings of the International Conference on Robotics and Automation, pp. 3258–3264.
- [7] Palunko, I., Cruz, P., and Fierro, R., 2012. “Agile load transportation”. *IEEE Robotics and Automation Magazine*, **19**(3), pp. 69–79.
- [8] Michael, N., Fink, J., and Kumar, V., 2011. “Cooperative manipulation and transportation with aerial robots”. *Autonomous Robots*, **30**, pp. 73–86.

- [9] Maza, I., Kondak, K., Bernard, M., and Ollero, A., 2010. “Multi-UAV cooperation and control for load transportation and deployment”. *Journal of Intelligent and Robotic Systems*, **57**, pp. 417–449.
- [10] Mellinger, D., Shomin, M., Michael, N., and Kumar, V., 2013. “Cooperative grasping and transport using multiple quadrotors”. *Distributed Autonomous Robotic Systems, Springer Tracts in Advanced Robotics*, **83**, pp. 545–558.
- [11] Zameroski, D., Starr, G., Wood, J., and Lumia, R., 2008. “Rapid swing-free transport of nonlinear payloads using dynamic programming”. *Journal of Dynamic Systems, Measurement, and Control*, **130**(4), June, p. 041001.
- [12] Schultz, J., and Murphey, T., 2012. “Trajectory generation for underactuated control of a suspended mass”. In *IEEE International Conference on Robotics and Automation*, pp. 123–129.
- [13] Palunko, I., Fierro, R., and Cruz, P., 2012. “Trajectory generation for swing-free maneuvers of a quadrotor with suspended payload: A dynamic programming approach”. In *IEEE International Conference on Robotics and Automation*.
- [14] Cabecinhas, D., Cunha, R., and Silvestre, C., 2009. “Rotorcraft path following control for extended flight envelope coverage”. In *Proceedings of the IEEE Conference on Decision and Control, China*, pp. 3460–3465.
- [15] Mellinger, D., and Kumar, V., 2011. “Minimum snap trajectory generation and control for quadrotors”. In *Proceedings of the International Conference on Robotics and Automation*, pp. 2520–2525.
- [16] Naldi, R., Marconi, L., and Gentili, L., 2009. “Robust takeoff and landing for a class of aerial robots”. In *Proceedings of the IEEE Conference on Decision and Control*, pp. 3436–3441.

- [17] Hua, M., Hamel, T., Morin, P., and Samson, C., 2009. “A control approach for thrust-propelled underactuated vehicles and its application to VTOL drones”. *IEEE Transactions on Automatic Control*, **54**(8), pp. 1834–1853.
- [18] Johnson, N. L., and Leang, K. K., 2013. “Enhanced proportional-derivative control of a micro quadcopter”. In ASME 2013 Dynamic Systems and Control Conference, Paolo Alto.
- [19] M. Hassan Tanveer, S. Faiz Ahmed, D. H. M. K. J., and Warsi, F. A., 2013. “Disturbance and noise rejection controller design for smooth takeoff / landing and altitude stabilization of quad-rotor”. *Journal of Applied Sciences Research*, **5**(9).
- [20] , 2007. “Control of a quadrotor vehicle using sliding mode disturbance observer”. In Proceedings of the 2007 American Control Conference, NY, pp. 5230–5235.
- [21] Hossein Bolandi, Mohammad Rezaei, R. M. H. N., and Smailzadeh, S. M., 2013. “Attitude control of a quadrotor with optimized pid controller”. *Intelligent Control and Automation*, **4**(3), pp. 335–342.
- [22] Sharma, A., and Barve, P. A., 2012. “Controlling of quad-rotor uav using pid controller and fuzzy logic controller”. *International Journal of Electrical, Electronics and Computer Engineering*, **1**(2), pp. 38–41.
- [23] Chao Liu, Sheng Jing Tang, S. Y. Y., and Guo, J., 2013. “Fuzzy sliding-mode control for quad-rotor trajectory tracking”. *The international journal of Unmanned System Technology*, **278**, pp. 1593–1600.
- [24] Addy Wahyudie, T. B. S., and Noura, H., 2013. “Robust pid controller for quad-rotors”. *The international journal of Unmanned System Technology*, **14**.

- [25] Hoffmann, G., Huang, H., Waslander, S., and Tomlin, C., 2007. “Quadrotor helicopter flight dynamics and control: Theory and experiment”. In Proceedings of the AIAA Guidance, Navigation, and Control Conference. AIAA 2007-6461.
- [26] Castillo, P., Albertos, P., Garcia, P., and Lozano, R., 2006. “Simple real-time attitude stabilization of a quadrotor aircraft with bounded signals”. In Proceeding of the IEEE Conference on Decision and Control, San Diego, pp. 1533–1538.
- [27] Lee, T., Leok, M., and McClamroch, N., 2012. “Nonlinear robust tracking control of a quadrotor UAV on $SE(3)$ ”. In Proceeding of the American Control Conference, pp. 4649–4654.
- [28] Lee, T., Leok, M., and McClamroch, N., 2013. “Nonlinear robust tracking control of a quadrotor UAV on $SE(3)$ ”. *Asian Journal of Control*, **15**(2), Mar., pp. 391–408.
- [29] Dydek, Z., Annaswamy, A., and Lavretsky, E., 2012. “Adaptive control of quadrotor uavs: A design trade study with flight evaluations”. *IEEE Transactions on Control Systems Technology*, **21**(4).
- [30] Selfridge, J. M., and Tao, G., 2014. “A multivariable adaptive controller for a quadrotor with guaranteed matching conditions”. *Systems Science and Control Engineering An Open Access Journal*, **2**, pp. 24–33.
- [31] Gianluca Antonelli, Filippo Arrichiello, S. C., and Giordano, P. R., 2013. “Adaptive trajectory tracking for quadrotor mavs in presence of parameter uncertainties and external disturbances”. In IEEE/ASME International Conference on Advanced Intelligent Mechatronics (AIM), Wollongong, Australia, pp. 1337–1342.
- [32] Zhen, H., Qi, X., and Dong, H., 2013. *An Adaptive Block Backstepping Controller for Attitude Stabilization of a Quadrotor Helicopter*, Vol. 8 of 2. Transactions on Systems and Control, april.

- [33] Cabecinhas, D., Cunha, R., and Silvestre, C., 2014. “A nonlinear quadrotor trajectory tracking controller with disturbance rejection”. *Control Engineering Practice*, **26**, pp. 1–10.
- [34] Lee, D., Kim, H., and Sastry, S., 2009. “Feedback linearization vs. adaptive sliding mode control for a quadrotor helicopter”. *Int. Journal of Control, Automation and Systems*, **7**, pp. 1–10.
- [35] B. J. Bialy, J. Klotz, K. B., and Dixon, W. E., 2013. “Lyapunov-based robust adaptive control of a quadrotor uav in the presence of modeling uncertainties”. In *Proceeding of American Control Conference (ACC 2013)*, Washington DC, pp. 13–18.
- [36] Ayoubi, M. A., Goodarzi, F. A., and Banerjee, A., 2011. “Attitude motion of a spinning spacecraft with fuel sloshing and nutation damping”. *The Journal of the Astronautical Sciences*, **58**(4), pp. 551–568.
- [37] Mellinger, D., Michael, N., and Kumar, V., 2012. “Trajectory generation and control for precise aggressive maneuvers with quadrotors”. *International Journal Of Robotics Research*, **31**(5), pp. 664–674.
- [38] Tayebi, A., and McGilvray, S., 2006. “Attitude stabilization of a VTOL quadrotor aircraft”. *IEEE Transactions on Control System Technology*, **14**(3), pp. 562–571.
- [39] Bhat, S., and Bernstein, D., 2000. “A topological obstruction to continuous global stabilization of rotational motion and the unwinding phenomenon”. *Systems and Control Letters*, **39**(1), pp. 66–73.
- [40] Mayhew, C., Sanfelice, R., and Teel, A., 2011. “Quaternion-based hybrid control for robust global attitude tracking”. *IEEE Transactions on Automatic Control*, **56**(11), pp. 2555–2566.

- [41] Lee, T., Leok, M., and McClamroch, N., 2010. “Geometric tracking control of a quadrotor UAV on $SE(3)$ ”. In Proceedings of the IEEE Conference on Decision and Control, pp. 5420–5425.
- [42] Misra, G., Izadi, M., Sanyal, A., and Scheeres, D., 2015. “Coupled orbit-attitude dynamics and relative state estimation of spacecraft near small Solar System bodies”. *Advances in Space Research*.
- [43] Sanyal, A., Izadi, M., and Butcher, E., 2014. “Determination of relative motion of a space object from simultaneous measurements of range and range rate”. In American Control Conference (ACC), Portland, OR, pp. 1607–1612.
- [44] Sanyal, A., Izadi, M., Misra, G., Samiei, E., and Scheeres, D., 2014. “Estimation of dynamics of space objects from visual feedback during proximity operations”. In AIAA Space 2014.
- [45] Goodarzi, F., Lee, D., and Lee, T., 2013. “Geometric nonlinear PID control of a quadrotor UAV on $SE(3)$ ”. In in Proceedings of the European Control Conference, pp. 3845–3850.
- [46] Chaturvedi, N., Sanyal, A., and McClamroch, N., 2011. “Rigid-body attitude control”. *IEEE Control Systems Magazine*, **31**(3), pp. 30–51.
- [47] Izadi, M., and Sanyal, A., 2014. “Rigid body attitude estimation based on the Lagrange–d’Alembert principle”. *Automatica*, **50**(10), pp. 2570–2577.
- [48] Izadi, M., Samiei, E., Sanyal, A., and Kumar, V., 2015. “Comparison of an attitude estimator based on the Lagrange–d’Alembert principle with some state-of-the-art filters”. In Proceedings of the IEEE International Conference on Robotics and Automation, Seattle, WA, IEEE, pp. 2848–2853.

- [49] Lee, T., Sreenath, K., and Kumar, V., 2013. “Geometric control of cooperating multiple quadrotor UAVs with a suspended load”. In Proceedings of the IEEE Conference on Decision and Control. accepted.
- [50] Lee, T., 2014. Geometric control of multiple quadrotor UAVs transporting a cable-suspended rigid body, March.
- [51] Goodarzi, F. A., Lee, D., and Lee, T., 2015. “Geometric adaptive tracking control of a quadrotor unmanned aerial vehicle on $se(3)$ for agile maneuvers”. *Journal of Dynamic Systems, Measurement, and Control*, **137**(9), September, pp. 091007–12.
- [52] Lee, T., Leok, M., and McClamroch, N., 2012. “Dynamics and control of a chain pendulum on a cart”. In Proceedings of the IEEE Conference on Decision and Control, pp. 2502–2508.
- [53] Gillula, J., Hoffmann, G., Huang, H., Vitus, M., and Tomlin, C., 2011. “Applications of hybrid reachability analysis to robotic aerial vehicles”. *The International Journal of Robotics Research*, **30**(3), pp. 335–354.
- [54] Castillo, P., Lozano, R., and Dzul, A., 2005. “Stabilization of a mini rotorcraft with four rotors”. *IEEE Control System Magazine*, pp. 45–55.
- [55] Bullo, F., and Lewis, A., 2005. *Geometric control of mechanical systems*, Vol. 49 of *Texts in Applied Mathematics*. Springer-Verlag, New York. Modeling, analysis, and design for simple mechanical control systems.
- [56] Lee, T., 2013. “Robust adaptive tracking on $SO(3)$ with an application to the attitude dynamics of a quadrotor UAV”. *IEEE Transactions on Control Systems Technology*, **21**(5), pp. 1924–1930.

- [57] Subbarao, K., 2004. “Nonlinear PID-like controllers for rigid-body attitude stabilization”. *Journal of the Astronautical Sciences*, **52**(1-2), pp. 61–74.
- [58] Subbarao, K., and Akella, M., 2004. “Differentiator-free nonlinear proportional-integral controllers for rigid-body attitude stabilization”. *Journal of Guidance, Control, and Dynamics*, **27**(6), pp. 1092–1096.
- [59] Show, L., Juang, J., Lin, C., and Jan, Y., 2002. “Spacecraft robust attitude tracking design: PID control approach”. In *Proceeding of the American Control Conference*, 1360-1365, ed.
- [60] Ioannou, P. A., 1996. *Robust Adaptive Control*. PTR Prentice-Hall.
- [61] Lee, T., 2008. “Computational geometric mechanics and control of rigid bodies”. PhD thesis, University of Michigan.
- [62] Lee, T., Leok, M., and McClamroch, N. H., 2009. “Lagrangian mechanics and variational integrators on two-spheres”. *International Journal for Numerical Methods in Engineering*, **79**(9), pp. 1147–1174.
- [63] Khalil, H., 1996. *Nonlinear Systems*. Prentice Hall.
- [64] Fernando, T., Chandiramani, J., Lee, T., and Gutierrez, H., 2011. “Robust adaptive geometric tracking controls on $so(3)$ with an application to the attitude dynamics of a quadrotor uav”. In *Proceedings of the IEEE Conference on Decision and Control*, 7380-7385, ed.
- [65] Krstic, M., Kanellakopoulos, I., and Kokotovic, P., 1995. *Nonlinear and Adaptive Control Design*. John Wiley and Sons.
- [66] Goodarzi, F., Lee, D., and Lee, T., 2014. “Geometric control of a quadrotor UAV transporting a payload connected via flexible cable”. *ArXiv*.

Appendix- Proofs

A.1 Proof for Proposition 1

The proofs of (i)-(iii) are available at [55, (Chap. 11)]. To show (iv) and (v), let $Q = R_d^T R = \exp \hat{x} \in \text{SO}(3)$ for $x \in \mathbb{R}^3$ from Rodrigues' formula. Using the MATLAB Symbolic Computation Tool, we find

$$\begin{aligned}\Psi &= \frac{1 - \cos \|x\|}{2\|x\|^2} \sum_{(i,j,k) \in \mathfrak{C}} (g_i + g_j)x_k^2, \\ \|e_R\|^2 &= \frac{(1 - \cos \|x\|)^2}{4\|x\|^4} \sum_{(i,j,k) \in \mathfrak{C}} (g_i - g_j)^2 x_i^2 x_j^2 + \frac{\sin^2 \|x\|}{4\|x\|^2} \sum_{(i,j,k) \in \mathfrak{C}} (g_i + g_j)^2 x_k^2,\end{aligned}$$

where $\mathfrak{C} = \{(1, 2, 3), (2, 3, 1), (3, 1, 2)\}$. When $\Psi = 0$, Eq. 12 is trivial. Assuming that $\Psi \neq 0$, therefore $\|x\| \neq 0$, an upper bound of $\frac{\|e_R\|^2}{\Psi}$ is given by

$$\frac{\|e_R\|^2}{\Psi} \leq \frac{1}{2h_1}(1 - \cos \|x\|)h_2 + \frac{1}{2h_1}(1 + \cos \|x\|)h_3 \leq \frac{h_2 + h_3}{h_1},$$

which shows Eq. 12.

Next, we consider (v). When $\Psi = 0$, Eq. 13 is trivial. Hereafter, we assume $\Psi \neq 0$, therefore $R \neq R_d$. At the three remaining critical points of Ψ , the values of Ψ are given by $g_1 + g_2$, $g_2 + g_3$, or $g_3 + g_1$. So, from the given bound $\Psi < \psi$, these three critical points are avoided, and we can guarantee that $e_R \neq 0$ and $\|x\| < \pi$. An upper bound of $\frac{\Psi}{\|e_R\|^2}$ is given by

$$\frac{\Psi}{\|e_R\|^2} \leq \frac{2(1 - \cos \|x\|)}{\sin \|x\|^2} \frac{\sum_{\mathfrak{C}} (g_i + h_j)x_k^2/\|x\|^2}{\sum_{\mathfrak{C}} (g_i + h_j)^2 x_k^2/\|x\|^2} \leq \frac{2}{1 + \cos \|x\|} \frac{h_4}{h_5}, \quad (109)$$

Also, an upper bound of $2 - \psi$ is given by

$$h_1 - \psi < h_1 - \Psi \leq h_1 - \frac{1 - \cos \|x\|}{2} h_1 = \frac{h_1}{2}(1 + \cos \|x\|). \quad (110)$$

Substituting this into Eq. 109, we have

$$\frac{\Psi}{\|e_R\|^2} \leq \frac{h_4 h_1}{h_5 (h_1 - \psi)} = h_2,$$

which shows Eq. 13.

For a given tracking command (R_d, Ω_d) , and current attitude and angular velocity (R, Ω) , we define an attitude error function $\Psi : SO(3) \times SO(3) \in R$ as

$$\Psi(R, R_d) = \frac{1}{2} \text{tr}[I - R_d^T R]. \quad (111)$$

The desired angular velocity can be written as follows

$$\hat{\Omega}_d = R_d^T \dot{R}_d. \quad (112)$$

We take the derivative to find the e_R and e_Ω

$$D\Psi(R, R_d) = -\frac{1}{2} \text{tr}[d(R_d^T R)] = -\frac{1}{2} \text{tr}[R_d^T R \hat{\eta}]. \quad (113)$$

Using

$$\text{tr}(\hat{x}A) = \text{tr}[A\hat{x}] = \frac{1}{2} \text{tr}[\hat{x}(A - A^T)] = -x^T(A - A^T)^\vee, \quad (114)$$

we can conclude

$$\text{tr}[R_d^T R \hat{\eta}] = -\eta(R_d^T R - R_d R^T)^\vee, \quad (115)$$

$$D\Psi(R, R_d) \cdot R \hat{\eta} = \frac{1}{2} (R_d^T R - R^T R_d)^\vee \cdot \eta. \quad (116)$$

We define

$$e_R = \frac{1}{2} (R_d^T R - R^T R_d)^\vee, \quad (117)$$

and

$$\hat{\Omega}_d = R_d^T \dot{R}_d \Rightarrow \dot{R}_d = R_d \hat{\Omega}_d. \quad (118)$$

So we can write and simplify the following equation to find the e_Ω

$$\dot{R} - \dot{R}_d(R^T R) = R\hat{\Omega} - R_d\hat{\Omega}_d R_d^T R = R(\hat{\Omega} - R^T R_d\hat{\Omega}_d R_d^T R). \quad (119)$$

Comparing the above equation with $\dot{R} = R\hat{\Omega}$, we can result in the following equation

$$\hat{e}_\Omega = \hat{\Omega} - R^T R_d\hat{\Omega}_d R_d^T R, \quad (120)$$

or

$$e_\Omega = \Omega - R^T R_d\Omega_d. \quad (121)$$

Now, we try to find an expression for $\dot{\Psi}$ by taking time-derivative of Ψ

$$\dot{\Psi} = \frac{1}{2}tr[-(\frac{d}{dt}R_d^T)R - R_d^T\dot{R}]. \quad (122)$$

Substituting $\dot{R} = R\hat{\Omega}$ and $\dot{R}_d^T = -\hat{\Omega}_d R_d^T$ into the above expression, we would have

$$\dot{\Psi} = -\frac{1}{2}tr[-\hat{\Omega}_d R_d^T R + R_d^T R\hat{\Omega}], \quad (123)$$

and we can rewrite the above equation as follows

$$\dot{\Psi} = \frac{1}{2}e_\Omega^T (R_d^T R - R^T R_d)^\vee, \quad (124)$$

so

$$\dot{\Psi} = e_R \cdot e_\Omega. \quad (125)$$

A.2 Proof for Proposition 2

We first find the error dynamics for e_R, e_Ω , and define a Lyapunov function. Then, we find conditions on control parameters to guarantee the boundedness of tracking errors. Using (3), (4), (24), the time-derivative of Je_Ω can be written as

$$J\dot{e}_\Omega = \{Je_\Omega + d\}^\wedge e_\Omega - k_R e_R - k_\Omega e_\Omega + W_R \tilde{\theta}_R, \quad (126)$$

where $d = (2J - \text{tr}[J]I)R^T R_d \Omega_d \in \mathbb{R}^3$ and $\tilde{\theta}_R = \theta_R - \bar{\theta}_R$. The important property is that the first term of the right hand side is normal to e_Ω , and it simplifies the subsequent Lyapunov analysis. Define a Lyapunov function \mathcal{V}_2 be

$$\mathcal{V}_2 = \frac{1}{2} e_\Omega \cdot Je_\Omega + k_R \Psi(R, R_d) + c_2 e_R \cdot Je_\Omega + \frac{1}{2\gamma_R} \|\tilde{\theta}_R\|^2. \quad (127)$$

From (12), (13), the Lyapunov function \mathcal{V}_2 is bounded as

$$z_2^T M_{21} z_2 + \frac{1}{2\gamma_R} \|\tilde{\theta}_R\|^2 \leq \mathcal{V}_2 \leq z_2^T M_{22} z_2 + \frac{1}{2\gamma_R} \|\tilde{\theta}_R\|^2, \quad (128)$$

where $z_2 = [\|e_R\|, \|e_\Omega\|]^T \in \mathbb{R}^2$, and the matrices M_{21}, M_{22} are given by

$$M_{21} = \frac{1}{2} \begin{bmatrix} k_R & -c_2 \lambda_M \\ -c_2 \lambda_M & \lambda_m \end{bmatrix}, \quad M_{22} = \frac{1}{2} \begin{bmatrix} \frac{2k_R}{2-\psi_2} & c_2 \lambda_M \\ c_2 \lambda_M & \lambda_M \end{bmatrix}. \quad (129)$$

From (13), the upper-bound of (128) is satisfied in the following domain:

$$D_2 = \{(R, \Omega) \in \text{SO}(3) \times \mathbb{R}^3 \mid \Psi(R, R_d) < \psi_2 < 2\}. \quad (130)$$

From (14), (230), the time derivative of \mathcal{V}_2 along the solution of the controlled system is given by

$$\dot{\mathcal{V}}_2 = -k_\Omega \|e_\Omega\|^2 + e_\Omega^T \mathbf{W}_R \tilde{\theta}_R + c_2 \dot{e}_R \cdot J e_\Omega + c_2 e_R \cdot J \dot{e}_\Omega + \frac{1}{\gamma_R} (\tilde{\theta})^T (\dot{\tilde{\theta}}).$$

We have $\dot{\tilde{\theta}}_R = -\dot{\tilde{\theta}}_R$. Substituting (230), the above equation becomes

$$\begin{aligned} \dot{\mathcal{V}}_2 &= -k_\Omega \|e_\Omega\|^2 + c_2 \dot{e}_R \cdot J e_\Omega - c_2 k_R \|e_R\|^2 \\ &\quad + c_2 e_R \cdot ((J e_\Omega + d)^\wedge e_\Omega - k_\Omega e_\Omega) \\ &\quad + \tilde{\theta}_R^T \mathbf{W}_R^T (e_\Omega + c_2 e_R) - \frac{1}{\gamma_R} \tilde{\theta}_R^T \dot{\tilde{\theta}}_R. \end{aligned}$$

By substituting the adaptive law given by (16)

$$\dot{\mathcal{V}}_2 = -k_\Omega \|e_\Omega\|^2 + c_2 \dot{e}_R \cdot J e_\Omega - c_2 k_R \|e_R\|^2 + c_2 e_R \cdot ((J e_\Omega + d)^\wedge e_\Omega - k_\Omega e_\Omega).$$

Since $\|e_R\| \leq 1$, $\|\dot{e}_R\| \leq \|e_\Omega\|$, and $\|d\| \leq B_2$, we have

$$\dot{\mathcal{V}}_2 \leq -z_2^T W_2 z_2, \tag{131}$$

where the matrix $W_2 \in \mathbb{R}^{2 \times 2}$ is given by

$$W_2 = \begin{bmatrix} c_2 k_R & -\frac{c_2}{2} (k_\Omega + B_2) \\ -\frac{c_2}{2} (k_\Omega + B_2) & k_\Omega - 2c_2 \lambda_M \end{bmatrix}.$$

The condition on c_2 given at (237) guarantees that all of matrices M_{21} , W_2 are positive definite. According to the LaSalle-Yoshizawa theorem [65, Theorem A.8], this implies that the zero equilibrium of tracking errors and the estimation error is stable in the sense of Lyapunov, and $e_R, e_\Omega \rightarrow 0$ as $t \rightarrow \infty$. Furthermore $\tilde{\theta}_R$ is uniformly bounded.

A.3 Proof for Proposition 3

We derive the tracking error dynamics and a Lyapunov function for the translational dynamics of a quadrotor UAV, and later it is combined with the stability analysis of the rotational dynamics. The subsequent analysis are developed in the domain D_1

$$D_1 = \{(e_x, e_v, R, e_\Omega) \in \mathbb{R}^3 \times \mathbb{R}^3 \times \text{SO}(3) \times \mathbb{R}^3 \mid \|e_x\| < e_{x_{\max}}, \Psi < \psi_1 < 1\}, \quad (132)$$

Similar to (13), we can show that

$$\frac{1}{2} \|e_R\|^2 \leq \Psi(R, R_c) \leq \frac{1}{2 - \psi_1} \|e_R\|^2. \quad (133)$$

a) Translational Error Dynamics

The time derivative of the position error is $\dot{e}_x = e_v$. The time-derivative of the velocity error is given by

$$m\dot{e}_v = m\ddot{x} - m\ddot{x}_d = mge_3 - fRe_3 - m\ddot{x}_d + W_x\theta_x. \quad (134)$$

Consider the quantity $e_3^T R_c^T R e_3$, which represents the cosine of the angle between $b_3 = Re_3$ and $b_{3_c} = R_c e_3$. Since $1 - \Psi(R, R_c)$ represents the cosine of the eigen-axis rotation angle between R_c and R , we have $e_3^T R_c^T R e_3 \geq 1 - \Psi(R, R_c) > 0$ in D_1 . Therefore, the quantity $\frac{1}{e_3^T R_c^T R e_3}$ is well-defined. To rewrite the error dynamics of e_v in terms of the attitude error e_R , we add and subtract $\frac{f}{e_3^T R_c^T R e_3} R_c e_3$ to the right hand side of (134) to obtain

$$m\dot{e}_v = mge_3 - m\ddot{x}_d - \frac{f}{e_3^T R_c^T R e_3} R_c e_3 - X + W_x\theta_x, \quad (135)$$

where $X \in \mathbb{R}^3$ is defined by

$$X = \frac{f}{e_3^T R_c^T R e_3} ((e_3^T R_c^T R e_3) R e_3 - R_c e_3). \quad (136)$$

Let $A = -k_x e_x - k_v e_v - \mathbb{W}_x \bar{\theta}_x - m g e_3 + m \ddot{x}_d$. Then, from (21), (23), we have $b_{3_c} = R_c e_3 = -A / \|A\|$ and $f = -A \cdot R e_3$. By combining these, we obtain $f = (\|A\| R_c e_3) \cdot R e_3$. Therefore, the third term of the right hand side of (135) can be written as

$$\begin{aligned} -\frac{f}{e_3^T R_c^T R e_3} R_c e_3 &= -\frac{(\|A\| R_c e_3) \cdot R e_3}{e_3^T R_c^T R e_3} \cdot -\frac{A}{\|A\|} = A \\ &= -k_x e_x - k_v e_v - \mathbb{W}_x \bar{\theta}_x - m g e_3 + m \ddot{x}_d. \end{aligned}$$

Substituting this into (135), the error dynamics of e_v can be written as

$$\begin{aligned} m \dot{e}_v &= -k_x e_x - k_v e_v - \mathbb{W}_x \bar{\theta}_x - X + \mathbb{W}_x \theta_x \\ &= -k_x e_x - k_v e_v + \mathbb{W}_x \tilde{\theta}_x - X. \end{aligned} \quad (137)$$

where $\tilde{\theta}_x = \theta_x - \bar{\theta}_x$ is the estimation errors.

b) Lyapunov Candidate for Translation Dynamics

Let a Lyapunov candidate \mathcal{V}_1 be

$$\mathcal{V}_1 = \frac{1}{2} k_x \|e_x\|^2 + \frac{1}{2} m \|e_v\|^2 + c_1 e_x \cdot m e_v + \frac{1}{2\gamma_x} \|\tilde{\theta}_x\|^2. \quad (138)$$

The derivative of \mathcal{V}_1 along the solution of (137) is given by

$$\begin{aligned}
\dot{\mathcal{V}}_1 = & - (k_v - mc_1)\|e_v\|^2 - c_1k_x\|e_x\|^2 \\
& - c_1k_v e_x \cdot e_v + X \cdot \{c_1e_x + e_v\} \\
& + W_x \tilde{\theta}_x \cdot \{e_v + c_1e_x\} - \frac{1}{\gamma_x} \tilde{\theta}_x^T \dot{\theta}_x.
\end{aligned} \tag{139}$$

For the first case of the adaptive law given by (25), the last two terms of (139) are cancelled out. Also for the second case [60] that $\dot{\theta}_x = \gamma_x(I - \frac{\bar{\theta}_x \bar{\theta}_x^T}{\bar{\theta}_x^T \bar{\theta}_x})W_x^T(e_v + c_1e_x)$, we obtain

$$\begin{aligned}
\dot{\mathcal{V}}_1 = & - (k_v - mc_1)\|e_v\|^2 - c_1k_x\|e_x\|^2 \\
& - c_1k_v e_x \cdot e_v + X \cdot \{c_1e_x + e_v\} \\
& + \tilde{\theta}_x^T \frac{\bar{\theta}_x \bar{\theta}_x^T}{\bar{\theta}_x^T \bar{\theta}_x} W_x^T(e_v + c_1e_x).
\end{aligned} \tag{140}$$

In the above equation, the last term on the right hand side is always negative since $\bar{\theta}_x^T W_x^T(e_v + c_1e_x) > 0$ and $\tilde{\theta}_x^T \bar{\theta}_x \leq 0$. Therefore for both cases of (25), we obtain

$$\dot{\mathcal{V}}_1 \leq - (k_v - mc_1)\|e_v\|^2 - c_1k_x\|e_x\|^2 - c_1k_v e_x \cdot e_v + X \cdot \{c_1e_x + e_v\}. \tag{141}$$

The last term of the above equation corresponds to the effects of the attitude tracking error on the translational dynamics. We find a bound of X , defined at (136), to show stability of the coupled translational dynamics and rotational dynamics in the subsequent Lyapunov analysis. Since $f = \|A\|(e_3^T R_c^T R e_3)$, we have

$$\begin{aligned}
\|X\| & \leq \|A\| \|(e_3^T R_c^T R e_3) R e_3 - R_c e_3\| \\
& \leq (k_x \|e_x\| + k_v \|e_v\| + B_{W_x} B_\theta + B_1) \times \|(e_3^T R_c^T R e_3) R e_3 - R_c e_3\|.
\end{aligned}$$

The last term $\|(e_3^T R_c^T R e_3) R e_3 - R_c e_3\|$ represents the sine of the angle between $b_3 = R e_3$ and $b_{3_c} = R_c e_3$, since $(b_{3_c} \cdot b_3) b_3 - b_{3_c} = b_3 \times (b_3 \times b_{3_c})$. The magnitude of the attitude error vector, $\|e_R\|$ represents the sine of the eigen-axis rotation angle between R_c and R (see [41]). Therefore, $\|(e_3^T R_c^T R e_3) R e_3 - R_c e_3\| \leq \|e_R\|$ in D_1 . It follows that

$$\begin{aligned} \|(e_3^T R_d^T R e_3) R e_3 - R_d e_3\| &\leq \|e_R\| = \sqrt{\Psi(2 - \Psi)} \\ &\leq \left\{ \sqrt{\psi_1(2 - \psi_1)} \triangleq \alpha \right\} < 1. \end{aligned} \quad (142)$$

Therefore, X is bounded by

$$\begin{aligned} \|X\| &\leq (k_x \|e_x\| + k_v \|e_v\| + B_{W_x} B_\theta + B_1) \|e_R\| \\ &\leq (k_x \|e_x\| + k_v \|e_v\| + B_{W_x} B_\theta + B_1) \alpha. \end{aligned} \quad (143)$$

Substituting (143) into (141),

$$\begin{aligned} \dot{\mathcal{V}}_1 &\leq -(k_v(1 - \alpha) - mc_1) \|e_v\|^2 - c_1 k_x (1 - \alpha) \|e_x\|^2 \\ &\quad + c_1 k_v (1 + \alpha) \|e_x\| \|e_v\| \\ &\quad + \|e_R\| \{ (B_{W_x} B_\theta + B_1) (c_1 \|e_x\| + \|e_v\|) + k_x \|e_x\| \|e_v\| \}. \end{aligned} \quad (144)$$

In the above expression for $\dot{\mathcal{V}}_1$, there is a third-order error term, namely $k_x \|e_R\| \|e_x\| \|e_v\|$. Using (142), it is possible to choose its upper bound as $k_x \alpha \|e_x\| \|e_v\|$ similar to other terms, but the corresponding stability analysis becomes complicated, and the initial attitude error should be reduced further. Instead, we restrict our analysis to the domain D_1 defined in (242), and its upper bound is chosen as $k_x e_{x_{\max}} \|e_R\| \|e_v\|$.

c) Lyapunov Candidate for the Complete System

Let $\mathcal{V} = \mathcal{V}_1 + \mathcal{V}_2$ be the Lyapunov candidate of the complete system. Define $z_1 = [\|e_x\|, \|e_v\|]^T$, $z_2 = [\|e_R\|, \|e_\Omega\|]^T \in \mathbb{R}^2$, and

$$\mathcal{V}_A = \frac{1}{2\gamma_x} \|\theta_x - \bar{\theta}_x\|^2 + \frac{1}{2\gamma_R} \|\theta_R - \bar{\theta}_R\|^2.$$

Using (243), the bound of the Lyapunov candidate \mathcal{V} can be written as

$$z_1^T M_{11} z_1 + z_2^T M_{21} z_2 + \mathcal{V}_A \leq \mathcal{V} \leq z_1^T M_{12} z_1 + z_2^T M'_{22} z_2 + \mathcal{V}_A, \quad (145)$$

where the matrices $M_{11}, M_{12}, M_{21}, M_{22}$ are given by

$$M_{11} = \frac{1}{2} \begin{bmatrix} k_x & -mc_1 \\ -mc_1 & m \end{bmatrix}, \quad M_{12} = \frac{1}{2} \begin{bmatrix} k_x & mc_1 \\ mc_1 & m \end{bmatrix},$$

$$M_{21} = \frac{1}{2} \begin{bmatrix} k_R & -c_2 \lambda_M \\ -c_2 \lambda_M & \lambda_m \end{bmatrix}, \quad M_{22} = \frac{1}{2} \begin{bmatrix} \frac{2k_R}{2-\psi_1} & c_2 \lambda_M \\ c_2 \lambda_M & \lambda_M \end{bmatrix}.$$

Using (236) and (144), the time-derivative of \mathcal{V} is given by

$$\dot{\mathcal{V}} \leq -z_1^T W_1 z_1 + z_1^T W_{12} z_2 - z_2^T W_2 z_2 \leq -z^T W z \quad (146)$$

where $z = [z_1, z_2]^T \in \mathbb{R}^2$, and the matrices $W_1, W_{12}, W_2 \in \mathbb{R}^{2 \times 2}$ are defined at (29)-(31). The matrix $W \in \mathbb{R}^{2 \times 2}$ is given by

$$W = \begin{bmatrix} \lambda_m(W_1) & -\frac{1}{2} \|W_{12}\|_2 \\ -\frac{1}{2} \|W_{12}\|_2 & \lambda_m(W_2) \end{bmatrix}.$$

The conditions given at (237), (27), (28) guarantee that all of matrices $M_{11}, M_{12}, M_{21}, M_{22}, W$ are positive definite. According to the LaSalle-Yoshizawa theorem [65, Theorem A.8],

this implies that the zero equilibrium of tracking errors and the estimation errors is stable in the sense of Lyapunov, and tracking errors asymptotically converge to zero. Furthermore, estimation errors are uniformly bounded.

A.4 Proof for Proposition 4

According to the proof of Proposition 2, the attitude tracking errors asymptotically decrease to zero, and therefore, they enter the region given by (26) in a finite time t^* , after which the results of Proposition 3 can be applied to yield attractiveness. The remaining part of the proof is showing that the tracking error $z_1 = [\|e_x\|, \|e_v\|]^T$ is bounded in $t \in [0, t^*]$. This is similar to the proof given at [28].

A.5 Proof for Proposition 5

From (38) and (40), the Lagrangian is given by

$$\begin{aligned}
L = & \frac{1}{2}M_{00}\|\dot{x}\|^2 + \dot{x} \cdot \sum_{i=1}^n M_{0i}\dot{q}_i + \frac{1}{2} \sum_{i,j=1}^n M_{ij}\dot{q}_i \cdot \dot{q}_j \\
& + \sum_{i=1}^n \sum_{a=i}^n m_a g l_i e_3 \cdot q_i + M_{00} g e_3 \cdot x + \frac{1}{2} \Omega^T J \Omega,
\end{aligned} \tag{147}$$

The derivatives of the Lagrangian are given by

$$\begin{aligned}
\mathbf{D}_x L &= M_{00} g e_3, \\
\mathbf{D}_{\dot{x}} L &= M_{00} \dot{x} + \sum_{i=1}^n M_{0i} \dot{q}_i,
\end{aligned}$$

where $\mathbf{D}_x L$ represents the derivative of L with respect to x . From the variation of the angular velocity given after (77), we have

$$\mathbf{D}_{\Omega} L \cdot \delta \Omega = J \Omega \cdot (\dot{\eta} + \Omega \times \eta) = J \Omega \cdot \dot{\eta} - \eta \cdot (\Omega \times J \Omega). \tag{148}$$

Similarly from (78), the derivative of the Lagrangian with respect to q_i is given by

$$\mathbf{D}_{q_i} L \cdot \delta q_i = \sum_{a=i}^n m_a g l_i e_3 \cdot (\xi_i \times q_i) = - \sum_{a=i}^n m_a g l_i \hat{e}_3 q_i \cdot \xi_i.$$

The variation of \dot{q}_i is given by

$$\delta \dot{q}_i = \dot{\xi}_i \times q_i + \xi_i \times \dot{q}_i.$$

Using this, the derivative of the Lagrangian with respect to \dot{q}_i is given by

$$\begin{aligned} \mathbf{D}_{\dot{q}_i} L \cdot \delta \dot{q}_i &= (M_{i0} \dot{x} + \sum_{j=1}^n M_{ij} \dot{q}_j) \cdot \delta \dot{q}_i \\ &= (M_{i0} \dot{x} + \sum_{j=1}^n M_{ij} \dot{q}_j) \cdot (\dot{\xi}_i \times q_i + \xi_i \times \dot{q}_i) \\ &= \hat{q}_i (M_{i0} \dot{x} + \sum_{j=1}^n M_{ij} \dot{q}_j) \cdot \dot{\xi}_i + \hat{q}_i (M_{i0} \dot{x} + \sum_{j=1}^n M_{ij} \dot{q}_j) \cdot \xi_i. \end{aligned}$$

Let \mathfrak{G} be the action integral, i.e., $\mathfrak{G} = \int_{t_0}^{t_f} L dt$. From the above expressions for the derivatives of the Lagrangian, the variation of the action integral can be written as

$$\begin{aligned} \delta \mathfrak{G} &= \int_{t_0}^{t_f} \{ M_{00} \dot{x} + \sum_{i=1}^n M_{0i} \dot{q}_i \} \cdot \delta \dot{x} + M_{00} g e_3 \cdot \delta x \\ &\quad + \sum_{i=1}^n \{ \hat{q}_i (M_{i0} \dot{x} + \sum_{j=1}^n M_{ij} \dot{q}_j) \} \cdot \dot{\xi}_i \\ &\quad + \sum_{i=1}^n \{ \hat{q}_i (M_{i0} \dot{x} + \sum_{j=1}^n M_{ij} \dot{q}_j) - \sum_{a=i}^n m_a g l_i \hat{e}_3 q_i \} \cdot \xi_i \\ &\quad + J \Omega \cdot \dot{\eta} - \eta \cdot (\Omega \times J \Omega) dt. \end{aligned}$$

Integrating by parts and using the fact that variations at the end points vanish, this reduces to

$$\begin{aligned} \delta \mathfrak{E} = & \int_{t_0}^{t_f} \{M_{00}g e_3 - M_{00}\ddot{x} - \sum_{i=1}^n M_{0i}\ddot{q}_i\} \cdot \delta x \\ & + \sum_{i=1}^n \left\{ -\hat{q}_i (M_{i0}\ddot{x} + \sum_{j=1}^n M_{ij}\ddot{q}_j) - \sum_{a=i}^n m_a g l_i \hat{e}_3 q_i \right\} \cdot \xi_i \\ & - \eta \cdot (J\dot{\Omega} + \Omega \times J\Omega) dt. \end{aligned}$$

According to the Lagrange-d'Alembert principle, the variation of the action integral is equal to the negative of the virtual work done by the external force and moment, namely

$$- \int_{t_0}^{t_f} (-f R e_3 + \Delta_x) \cdot \delta x + (M + \Delta_R) \cdot \eta dt, \quad (149)$$

and we obtain (43) and (45). As ξ_i is perpendicular to q_i , we also have

$$-\hat{q}_i^2 (M_{i0}\ddot{x} + \sum_{j=1}^n M_{ij}\ddot{q}_j) + \sum_{a=i}^n m_a g l_i \hat{q}_i^2 e_3 = 0. \quad (150)$$

Equation (150) is rewritten to obtain an explicit expression for \ddot{q}_i . As $q_i \cdot \dot{q}_i = 0$, we have $\dot{q}_i \cdot \dot{q}_i + q_i \cdot \ddot{q}_i = 0$. Using this, we have

$$-\hat{q}_i^2 \ddot{q}_i = -(q_i \cdot \ddot{q}_i) q_i + (q_i \cdot q_i) \ddot{q}_i = (\dot{q}_i \cdot \dot{q}_i) q_i + \ddot{q}_i.$$

Substituting this equation into (150), we obtain (44). This can be slightly rewritten in terms of the angular velocities. Since $\dot{q}_i = \omega_i \times q_i$ for the angular velocity ω_i

satisfying $q_i \cdot \omega_i = 0$, we have

$$\begin{aligned}\ddot{q}_i &= \dot{\omega}_i \times q_i + \omega_i \times (\omega_i \times q_i) \\ &= \dot{\omega}_i \times q_i - \|\omega_i\|^2 q_i = -\hat{q}_i \dot{\omega}_i - \|\omega_i\|^2 q_i.\end{aligned}$$

Using this and the fact that $\dot{\omega}_i \cdot q_i = 0$, we obtain (47).

A.6 Proof for Proposition 6

The variations of x , u and q are given by (51) and (52). From the kinematics equation $\dot{q}_i = \omega_i \times q_i$, $\delta \dot{q}_i$ is given by

$$\delta \dot{q}_i = \dot{\xi}_i \times e_3 = \delta \omega_i \times e_3 + 0 \times (\xi_i \times e_3) = \delta \omega_i \times e_3.$$

Since both sides of the above equation is perpendicular to e_3 , this is equivalent to $e_3 \times (\dot{\xi}_i \times e_3) = e_3 \times (\delta \omega_i \times e_3)$, which yields

$$\dot{\xi}_i - (e_3 \cdot \dot{\xi}_i) e_3 = \delta \omega_i - (e_3 \cdot \delta \omega_i) e_3.$$

Since $\xi_i \cdot e_3 = 0$, we have $\dot{\xi}_i \cdot e_3 = 0$. As $e_3 \cdot \delta \omega_i = 0$ from the constraint, we obtain the linearized equation for the kinematics equation:

$$\dot{\xi}_i = \delta \omega_i. \tag{151}$$

Substituting these into (47), and ignoring the higher order terms, we obtain (53).

See [66] for details.

A.7 Proof for Proposition 7

We first show stability of the rotational dynamics, and later it is combined with the stability analysis of the translational dynamics of quad rotor and the rotational dynamics of links.

a) Attitude Error Dynamics

Here, attitude error dynamics for e_R, e_Ω are derived and we find conditions on control parameters to guarantee the boundedness of attitude tracking errors. The time-derivative of $J e_\Omega$ can be written as

$$J \dot{e}_\Omega = \{J e_\Omega + d\}^\wedge e_\Omega - k_R e_R - k_\Omega e_\Omega - k_I e_I + \Delta_R, \quad (152)$$

where $d = (2J - \text{tr}[J]I)R^T R_d \Omega_d \in \mathbb{R}^3$ [64]. The important property is that the first term of the right hand side is normal to e_Ω , and it simplifies the subsequent Lyapunov analysis.

b) Stability for Attitude Dynamics

Define a configuration error function on $\text{SO}(3)$ as follows

$$\Psi = \frac{1}{2} \text{tr}[\|I - R_c^T R\|]. \quad (153)$$

We introduce the following Lyapunov function

$$\mathcal{V}_2 = \frac{1}{2} e_\Omega \cdot J \dot{e}_\Omega + k_R \Psi(R, R_d) + c_2 e_R \cdot e_\Omega + \frac{1}{2} k_I \|e_I - \frac{\Delta_R}{k_I}\|^2. \quad (154)$$

Consider a domain D_2 given by

$$D_2 = \{(R, \Omega) \in \text{SO}(3) \times \mathbb{R}^3 \mid \Psi(R, R_d) < \psi_2 < 2\}. \quad (155)$$

In this domain we can show that \mathcal{V}_2 is bounded as follows [64]

$$z_2^T M_{21} z_2 + \frac{k_I}{2} \|e_I - \frac{\Delta_R}{k_I}\|^2 \leq \mathcal{V}_2 \leq z_2^T M_{22} z_2 + \frac{k_I}{2} \|e_I - \frac{\Delta_R}{k_I}\|^2, \quad (156)$$

where $z_2 = [\|e_R\|, \|e_\Omega\|]^T \in \mathbb{R}^2$ and the matrices M_{21} , M_{22} are given by

$$M_{21} = \frac{1}{2} \begin{bmatrix} k_R & -c_2 \lambda_M \\ -c_2 \lambda_M & \lambda_m \end{bmatrix}, M_{22} = \frac{1}{2} \begin{bmatrix} \frac{2k_R}{2-\psi_2} & c_2 \lambda_M \\ c_2 \lambda_M & \lambda_M \end{bmatrix}, \quad (157)$$

The time derivative of \mathcal{V}_2 along the solution of the controlled system is given by

$$\dot{\mathcal{V}}_2 = -k_\Omega \|e_\Omega\|^2 - e_\Omega \cdot (k_I e_I - \Delta_R) + c_2 \dot{e}_R \cdot J e_\Omega + c_2 e_R \cdot J \dot{e}_\Omega + (k_I e_I - \Delta_R) \dot{e}_I.$$

We have $\dot{e}_I = c_2 e_R + e_\Omega$ from (67). Substituting this and (230), the above equation becomes

$$\dot{\mathcal{V}}_2 = -k_\Omega \|e_\Omega\|^2 + c_2 \dot{e}_R \cdot J e_\Omega - c_2 k_R \|e_R\|^2 + c_2 e_R \cdot ((J e_\Omega + d)^\wedge e_\Omega - k_\Omega e_\Omega).$$

We have $\|e_R\| \leq 1$, $\|\dot{e}_R\| \leq \|e_\Omega\|$ [64], and choose a constant B_2 such that $\|d\| \leq B_2$.

Then we have

$$\dot{\mathcal{V}}_2 \leq -z_2^T W_2 z_2, \quad (158)$$

where the matrix $W_2 \in \mathbb{R}^{2 \times 2}$ is given by

$$W_2 = \begin{bmatrix} c_2 k_R & -\frac{c_2}{2} (k_\Omega + B_2) \\ -\frac{c_2}{2} (k_\Omega + B_2) & k_\Omega - 2c_2 \lambda_M \end{bmatrix}.$$

The matrix W_2 is a positive definite matrix if

$$c_2 < \min\left\{\frac{\sqrt{k_R\lambda_m}}{\lambda_M}, \frac{4k_\Omega}{8k_R\lambda_M + (k_\Omega + B_2)^2}\right\}. \quad (159)$$

This implies that

$$\dot{V}_2 \leq -\lambda_m(W_2)\|z_2\|^2, \quad (160)$$

which shows stability of attitude dynamics.

c) Translational Error Dynamics

We derive the tracking error dynamics and a Lyapunov function for the translational dynamics of a quadrotor UAV and the dynamics of links. Later it is combined with the stability analyses of the rotational dynamics. This proof is based on the Lyapunov method presented in Theorem 3.6 and 3.7 [63]. From (51), (43), (53), and (105), the linearized equation of motion for the controlled full dynamic model is given by

$$\mathbf{M}\ddot{\mathbf{x}} + \mathbf{G}\dot{\mathbf{x}} = \mathbf{B}(-fRe_3 - M_{00}ge_3) + \mathbf{g}(\mathbf{x}, \dot{\mathbf{x}}) + \mathbf{B}\Delta_x, \quad (161)$$

and $\mathbf{g}(\mathbf{x}, \dot{\mathbf{x}})$ is higher order term. The subsequent analyses are developed in the domain D_1

$$D_1 = \{(\mathbf{x}, \dot{\mathbf{x}}, R, e_\Omega) \in \mathbb{R}^{2n+3} \times \mathbb{R}^{2n+3} \times \mathbf{SO}(3) \times \mathbb{R}^3 \mid \Psi < \psi_1 < 1\}. \quad (162)$$

In the domain D_1 , we can show that

$$\frac{1}{2}\|e_R\|^2 \leq \Psi(R, R_c) \leq \frac{1}{2 - \psi_1}\|e_R\|^2. \quad (163)$$

Consider the quantity $e_3^T R_c^T R e_3$, which represents the cosine of the angle between $b_3 = R e_3$ and $b_{3_c} = R_c e_3$. Since $1 - \Psi(R, R_c)$ represents the cosine of the eigen-axis rotation angle between R_c and R , we have $e_3^T R_c^T R e_3 \geq 1 - \Psi(R, R_c) > 0$ in D_1 . Therefore, the quantity $\frac{1}{e_3^T R_c^T R e_3}$ is well-defined. We add and subtract $\frac{f}{e_3^T R_c^T R e_3} R_c e_3$ to the right hand side of (239) to obtain

$$\mathbf{M}\ddot{\mathbf{x}} + \mathbf{G}\mathbf{x} = \mathbf{B}\left(\frac{-f}{e_3^T R_c^T R e_3} R_c e_3 - X - M_{00}g e_3 + \Delta_x\right) + \mathbf{g}(\mathbf{x}, \dot{\mathbf{x}}), \quad (164)$$

where $X \in \mathbb{R}^3$ is defined by

$$X = \frac{f}{e_3^T R_c^T R e_3} ((e_3^T R_c^T R e_3) R e_3 - R_c e_3). \quad (165)$$

The first term on the right hand side of (164) can be written as

$$-\frac{f}{e_3^T R_c^T R e_3} R_c e_3 = -\frac{(\|A\| R_c e_3) \cdot R e_3}{e_3^T R_c^T R e_3} \cdot -\frac{A}{\|A\|} = A. \quad (166)$$

Substituting this and (57) into (164)

$$\mathbf{M}\ddot{\mathbf{x}} + \mathbf{G}\mathbf{x} = \mathbf{B}(-K_x \mathbf{x} - K_{\dot{x}} \dot{\mathbf{x}} - K_z \text{sat}_{\sigma}(e_{\mathbf{x}}) - X + \Delta_x) + \mathbf{g}(\mathbf{x}, \dot{\mathbf{x}}), \quad (167)$$

This can be rearranged as

$$\begin{aligned} \ddot{\mathbf{x}} = & -(\mathbf{M}^{-1}\mathbf{G} + \mathbf{M}^{-1}\mathbf{B}K_x)\mathbf{x} - (\mathbf{M}^{-1}\mathbf{B}K_{\dot{x}})\dot{\mathbf{x}} \\ & - \mathbf{M}^{-1}\mathbf{B}X - \mathbf{M}^{-1}\mathbf{B}K_z \text{sat}_{\sigma}(e_{\mathbf{x}}) + \mathbf{M}^{-1}\mathbf{g}(\mathbf{x}, \dot{\mathbf{x}}) + \mathbf{M}^{-1}\mathbf{B}\Delta_x. \end{aligned} \quad (168)$$

Using the definitions for \mathbb{A} , \mathbb{B} , and z_1 presented before, the above expression can be rearranged as

$$\dot{z}_1 = \mathbb{A}z_1 + \mathbb{B}(-\mathbf{B}X + \mathbf{g}(\mathbf{x}, \dot{\mathbf{x}}) - \mathbf{B}K_z \text{sat}_{\sigma}(e_{\mathbf{x}}) + \mathbf{B}\Delta_x). \quad (169)$$

d) Lyapunov Candidate for Translation Dynamics

From the linearized control system developed at section 3, we use matrix P to introduce the following Lyapunov candidate for translational dynamics

$$\mathcal{V}_1 = z_1^T P z_1 + 2 \int_{p_{eq}}^{e_x} (\mathbf{B}K_z \text{sat}_\sigma(\mu) - \mathbf{B}\Delta_x) \cdot d\mu. \quad (170)$$

The last integral term of the above equation is positive definite about the equilibrium point $e_x = p_{eq}$ where

$$p_{eq} = \left[\frac{\Delta_x}{k_z}, 0, 0, \dots \right], \quad (171)$$

if

$$\delta < k_z \sigma, \quad (172)$$

considering the fact that $\text{sat}_\sigma y = y$ if $y < \sigma$. The time derivative of the Lyapunov function using the Leibniz integral rule is given by

$$\dot{\mathcal{V}}_1 = \dot{z}_1^T P z_1 + z_1^T P \dot{z}_1 + 2\dot{e}_x \cdot (\mathbf{B}K_z \text{sat}_\sigma(e_x) - \mathbf{B}\Delta_x). \quad (173)$$

Since $\dot{e}_x^T = ((PB)^T z_1)^T = z_1^T PB$ from (58), the above expression can be written as

$$\dot{\mathcal{V}}_1 = \dot{z}_1^T P z_1 + z_1^T P \dot{z}_1 + 2z_1^T PB(\mathbf{B}K_z \text{sat}_\sigma(e_x) - \mathbf{B}\Delta_x). \quad (174)$$

Substituting (249) into (174), it reduces to

$$\dot{\mathcal{V}}_1 = z_1^T (\mathbf{A}^T P + P\mathbf{A}) z_1 + 2z_1^T PB(-\mathbf{B}X + \mathbf{g}(\mathbf{x}, \dot{\mathbf{x}})). \quad (175)$$

Let $c_3 = 2\|P\mathbf{B}\mathbf{B}\|_2 \in \mathbb{R}$ and using $\mathbf{A}^T P + P\mathbf{A} = -Q$, we have

$$\dot{\mathcal{V}}_1 \leq -z_1^T Q z_1 + c_3 \|z_1\| \|X\| + 2z_1^T P \mathbf{B} g(\mathbf{x}, \dot{\mathbf{x}}). \quad (176)$$

The second term on the right hand side of the above equation corresponds to the effects of the attitude tracking error on the translational dynamics. We find a bound of X , defined at (245), to show stability of the coupled translational dynamics and rotational dynamics in the subsequent Lyapunov analysis. Since

$$f = \|A\| (e_3^T R_c^T R e_3), \quad (177)$$

we have

$$\|X\| \leq \|A\| \|(e_3^T R_c^T R e_3) R e_3 - R_c e_3\|. \quad (178)$$

The last term $\|(e_3^T R_c^T R e_3) R e_3 - R_c e_3\|$ represents the sine of the angle between $b_3 = R e_3$ and $b_{3c} = R_c e_3$, since $(b_{3c} \cdot b_3) b_3 - b_{3c} = b_3 \times (b_3 \times b_{3c})$. The magnitude of the attitude error vector, $\|e_R\|$ represents the sine of the eigen-axis rotation angle between R_c and R . Therefore, $\|(e_3^T R_c^T R e_3) R e_3 - R_c e_3\| \leq \|e_R\|$ in D_1 . It follows that

$$\begin{aligned} \|(e_3^T R_c^T R e_3) R e_3 - R_c e_3\| &\leq \|e_R\| = \sqrt{\Psi(2 - \Psi)} \\ &\leq \{\sqrt{\psi_1(2 - \psi_1)} \triangleq \alpha\} < 1, \end{aligned} \quad (179)$$

therefore

$$\begin{aligned} \|X\| &\leq \|A\| \|e_R\| \\ &\leq \|A\| \alpha. \end{aligned} \quad (180)$$

We also use the following properties

$$\lambda_{\min}(Q)\|z_1\|^2 \leq z_1^T Q z_1. \quad (181)$$

Note that $\lambda_{\min}(Q)$ is real and positive since Q is symmetric and positive definite.

Then, we can simplify (254) as given

$$\dot{V}_1 \leq -\lambda_{\min}(Q)\|z_1\|^2 + c_3\|z_1\|\|A\|\|e_R\| + 2z_1^T P B g(\mathbf{x}, \dot{\mathbf{x}}). \quad (182)$$

We find an upper boundary for

$$A = -K_x \mathbf{x} - K_{\dot{\mathbf{x}}} \dot{\mathbf{x}} - K_z \text{sat}_{\sigma}(e_{\mathbf{x}}) + M_{00} g e_3, \quad (183)$$

by defining

$$\|M_{00} g e_3\| \leq B_1, \quad (184)$$

for a given positive constant B_1 . We use the following properties where for any matrix

$A \in \mathbb{R}^{m \times n}$

$$\|A\|_2 \leq \sqrt{mn} \|A\|_{\max}, \quad (185)$$

where $\|A\|_{\max} = \max\{a_{mn}\}$. The third term on the right hand side of (259) can be bounded as

$$\| -K_z \text{sat}_{\sigma}(e_{\mathbf{x}}) \| \leq \|K_z\| \| \text{sat}_{\sigma}(e_{\mathbf{x}}) \| \leq \|K_z\| \sqrt{2n+3}\sigma, \quad (186)$$

where

$$\|K_z\| \leq \sqrt{3(2n+3)}\|K_z\|_{\max},$$

and similarly

$$\|K_{\mathbf{x}}\| \leq \sqrt{3(2n+3)}\|K_{\mathbf{x}}\|_{\max},$$

$$\|K_{\dot{\mathbf{x}}}\| \leq \sqrt{3(2n+3)}\|K_{\dot{\mathbf{x}}}\|_{\max}.$$

We define $K_{\max}, K_{z_m} \in \mathbb{R}$

$$K_{\max} = \max\{\|K_{\mathbf{x}}\|_{\max}, \|K_{\dot{\mathbf{x}}}\|_{\max}\} \sqrt{3(2n+3)},$$

$$K_{z_m} = \sqrt{3(2n+3)}\|K_z\|_{\max},$$

and then the upper bound of A is given by

$$\|A\| \leq K_{\max}(\|\mathbf{x}\| + \|\dot{\mathbf{x}}\|) + \sigma K_{z_m} + B_1 \quad (187)$$

$$\leq 2K_{\max}\|z_1\| + (B_1 + \sigma K_{z_m}), \quad (188)$$

and substitute (261) into (182)

$$\begin{aligned} \dot{V}_1 &\leq -(\lambda_{\min}(Q) - 2c_3 K_{\max} \alpha) \|z_1\|^2 \\ &\quad + c_3 (B_1 + \sigma K_{z_m}) \|z_1\| \|e_R\| + 2z_1^T P \mathbf{B} \mathbf{g}(\mathbf{x}, \dot{\mathbf{x}}). \end{aligned} \quad (189)$$

e) Lyapunov Candidate for the Complete System

Let $\mathcal{V} = \mathcal{V}_1 + \mathcal{V}_2$ be the Lyapunov function for the complete system. The time derivative of \mathcal{V} is given by

$$\dot{\mathcal{V}} = \dot{\mathcal{V}}_1 + \dot{\mathcal{V}}_2. \quad (190)$$

Substituting (263) and (238) into the above equation

$$\begin{aligned} \dot{\mathcal{V}} \leq & -(\lambda_{\min}(Q) - 2c_3K_{\max}\alpha)\|z_1\|^2 + 2z_1^T P B \mathbf{g}(\mathbf{x}, \dot{\mathbf{x}}) \\ & + c_3(B_1 + \sigma K_{z_m})\|z_1\|\|e_R\| - \lambda_m(W_2)\|z_2\|^2, \end{aligned} \quad (191)$$

and using $\|e_R\| \leq \|z_2\|$, it can be written as

$$\begin{aligned} \dot{\mathcal{V}} \leq & -(\lambda_{\min}(Q) - 2c_3K_{\max}\alpha)\|z_1\|^2 + 2z_1^T P B \mathbf{g}(\mathbf{x}, \dot{\mathbf{x}}) \\ & + c_3(B_1 + \sigma K_{z_m})\|z_1\|\|z_2\| - \lambda_m(W_2)\|z_2\|^2. \end{aligned} \quad (192)$$

Also, the $2z_1^T P B \mathbf{g}(\mathbf{x}, \dot{\mathbf{x}})$ term in the above equation is indefinite. The function $\mathbf{g}(\mathbf{x}, \dot{\mathbf{x}})$ satisfies

$$\frac{\|\mathbf{g}(\mathbf{x}, \dot{\mathbf{x}})\|}{\|z_1\|} \rightarrow 0 \quad \text{as} \quad \|z_1\| \rightarrow 0. \quad (193)$$

Then, for any $\gamma > 0$ there exists $r > 0$ such that

$$\|\mathbf{g}(\mathbf{x}, \dot{\mathbf{x}})\| < \gamma\|z_1\|, \quad \forall \|z_1\| < r, \quad (194)$$

so,

$$2z_1^T P B \mathbf{g}(\mathbf{x}, \dot{\mathbf{x}}) \leq 2\gamma\|P\|_2\|z_1\|^2. \quad (195)$$

Substituting the above equation into (266)

$$\begin{aligned} \dot{\mathcal{V}} \leq & -(\lambda_{\min}(Q) - 2c_3K_{\max}\alpha)\|z_1\|^2 + 2\gamma\|P\|_2\|z_1\|^2 \\ & + c_3(B_1 + \sigma K_{z_m})\|z_1\|\|z_2\| - \lambda_m(W_2)\|z_2\|^2, \end{aligned} \quad (196)$$

we obtain

$$\dot{\mathcal{V}} \leq -z^T W z + 2\gamma\|P\|_2\|z_1\|^2, \quad (197)$$

where $z = [z_1, z_2]^T \in \mathbb{R}^2$ and

$$W = \begin{bmatrix} \lambda_{\min}(Q) - 2c_3K_{\max}\alpha & -\frac{c_3(B_1 + \sigma K_{z_m})}{2} \\ -\frac{c_3(B_1 + \sigma K_{z_m})}{2} & \lambda_m(W_2) \end{bmatrix}. \quad (198)$$

By using $\|z_1\| \leq \|z\|$, we obtain

$$\dot{\mathcal{V}} \leq -(\lambda_{\min}(W) - 2\gamma\|P\|_2)\|z\|^2. \quad (199)$$

Choosing $\gamma < (\lambda_{\min}(W))/2\|P\|_2$, ensures that $\dot{\mathcal{V}}$ is negative semi-definite. This implies that the zero equilibrium of tracking errors is stable in the sense of Lyapunov and \mathcal{V} is non-increasing. Therefore all of error variables z_1 , z_2 and integral control terms e_I , e_x are uniformly bounded. Also, from Lasalle-Yoshizawa theorem [63, Thm 3.4], we have $z \rightarrow 0$ as $t \rightarrow \infty$.

A.8 Proof for Proposition 8

a) Kinetic Energy

The kinetic energy of the whole system is composed of the kinetic energy of quadrotors, cables and the rigid body, as

$$T = \frac{1}{2}m_0\|\dot{x}_0\|^2 + \sum_{i=1}^n \sum_{j=1}^{n_i} \frac{1}{2}m_{ij}\|\dot{x}_{ij}\|^2 + \frac{1}{2} \sum_{i=1}^n m_i\|\dot{x}_i\|^2 + \frac{1}{2} \sum_{i=1}^n \Omega_i \cdot J_i \Omega_i + \frac{1}{2} \Omega_0 \cdot J_0 \Omega_0. \quad (200)$$

Substituting the derivatives of (73) and (74) into the above expression we have

$$\begin{aligned} T = & \frac{1}{2}m_0\|\dot{x}_0\|^2 + \sum_{i=1}^n \sum_{j=1}^{n_i} \frac{1}{2}m_{ij}\|\dot{x}_0 + \dot{R}_0\rho_i - \sum_{a=j+1}^{n_i} l_{ia}\dot{q}_{ia}\|^2 \\ & + \frac{1}{2} \sum_{i=1}^n m_i\|\dot{x}_0 + \dot{R}_0\rho_i - \sum_{a=1}^{n_i} l_{ia}\dot{q}_{ia}\|^2 + \frac{1}{2} \sum_{i=1}^n \Omega_i \cdot J_i \Omega_i + \frac{1}{2} \Omega_0 \cdot J_0 \Omega_0. \end{aligned} \quad (201)$$

We expand the above expression as follow

$$\begin{aligned} T = & \frac{1}{2}(m_0\|\dot{x}_0\|^2 + \sum_{i=1}^n \sum_{j=1}^{n_i} m_{ij}\|\dot{x}_0\|^2 + \sum_{i=1}^n m_i\|\dot{x}_0\|^2) \\ & + \frac{1}{2} \sum_{i=1}^n (\sum_{j=1}^{n_i} m_{ij}\|\dot{R}_0\rho_i\|^2 + m_i\|\dot{R}_0\rho_i\|^2) \\ & + \sum_{i=1}^n (\sum_{j=1}^{n_i} m_{ij}\dot{x}_0 \cdot \dot{R}_0\rho_i + m_i\dot{x}_0 \cdot \dot{R}_0\rho_i) \\ & + \frac{1}{2} \sum_{i=1}^n (\sum_{j=1}^{n_i} m_{ij}\|\sum_{a=j+1}^{n_i} l_{ia}\dot{q}_{ia}\|^2 + m_i\|\sum_{a=1}^{n_i} l_{ia}\dot{q}_{ia}\|^2) \\ & - \sum_{i=1}^n (\sum_{j=1}^{n_i} m_{ij}\dot{x}_0 \cdot \sum_{a=j+1}^{n_i} l_{ia}\dot{q}_{ia} + \dot{x}_0 \cdot \sum_{a=1}^{n_i} l_{ia}\dot{q}_{ia}) \\ & - \sum_{i=1}^n (\sum_{j=1}^{n_i} m_{ij}\dot{R}_0\rho_i \cdot \sum_{a=j+1}^{n_i} l_{ia}\dot{q}_{ia} + m_i\dot{R}_0\rho_i \cdot \sum_{a=1}^{n_i} l_{ia}\dot{q}_{ia}) \\ & + \frac{1}{2} \sum_{i=1}^n \Omega_i \cdot J_i \Omega_i + \frac{1}{2} \Omega_0 \cdot J_0 \Omega_0, \end{aligned} \quad (202)$$

and substituting (83), (84), it is rewritten as

$$\begin{aligned}
T = & \frac{1}{2}M_T\|\dot{x}_0\|^2 + \frac{1}{2}\sum_{i=1}^n M_{iT}\|\dot{R}_0\rho_i\|^2 + \sum_{i=1}^n (M_{iT}\dot{x}_0 \cdot \dot{R}_0\rho_i) \\
& + \sum_{i=1}^n \sum_{j,k=1}^{n_i} M_{0ij}l_{ik}\dot{q}_{ij} \cdot \dot{q}_{ik} - \sum_{i=1}^n (\dot{x}_0 \cdot \sum_{j=1}^{n_i} M_{0ij}l_{ij}\dot{q}_{ij}) \\
& - \sum_{i=1}^n (\dot{R}_0\rho_i \cdot \sum_{j=1}^{n_i} M_{0ij}l_{ij}\dot{q}_{ij}) \\
& + \frac{1}{2}\sum_{i=1}^n \Omega_i \cdot J_i\Omega_i + \frac{1}{2}\Omega_0 \cdot J_0\Omega_0.
\end{aligned} \tag{203}$$

b) Potential Energy

We can derive the potential energy expression by considering the gravitational forces on each part of system as given

$$V = -m_0ge_3 \cdot x_0 - \sum_{i=1}^n m_i ge_3 \cdot x_i - \sum_{i=1}^n \sum_{j=1}^{n_i} m_{ij}ge_3 \cdot x_{ij}. \tag{204}$$

Using (73) and (74), we obtain

$$\begin{aligned}
V = & -m_0ge_3 \cdot x_0 - \sum_{i=1}^n m_i ge_3 \cdot (x_0 + R_0\rho_i - \sum_{a=1}^{n_i} l_{ia}q_{ia}) \\
& - \sum_{i=1}^n \sum_{j=1}^{n_i} m_{ij}ge_3 \cdot (x_0 + R_0\rho_i - \sum_{a=j+1}^{n_i} l_{ia}q_{ia}),
\end{aligned} \tag{205}$$

and utilizing (84), we can simplify the potential energy as

$$V = -M_Tge_3 \cdot x_0 - \sum_{i=1}^n M_{iT}ge_3 \cdot R_0\rho_i + \sum_{i=1}^n \sum_{j=1}^{n_i} M_{0ij}l_{ij}q_{ij} \cdot e_3. \tag{206}$$

c) Derivatives of Lagrangian

We develop the equation of motion for the Lagrangian $L = T - V$. The derivatives of the Lagrangian are given by

$$D_{\dot{x}_0} L = M_T \dot{x}_0 + \sum_{i=1}^n M_{iT} \dot{R}_0 \rho_i - \sum_{i=1}^n \sum_{j=1}^{n_i} M_{0ij} l_{ij} \dot{q}_{ij}, \quad (207)$$

$$D_{x_0} L = M_T g e_3, \quad (208)$$

$$D_{\dot{q}_{ij}} L = \sum_{i=1}^n \sum_{j=1}^{n_i} M_{0ij} l_{ik} \dot{q}_{ik} - \sum_{i=1}^n M_{0ij} l_{ij} (\dot{x}_0 + \dot{R}_0 \rho_i), \quad (209)$$

$$D_{q_{ij}} L = - \sum_{i=1}^n M_{0ij} l_{ij} e_3, \quad (210)$$

where $D_{\dot{x}_0}$ denote the derivative with respect to \dot{x}_0 , and other derivatives are defined similarly. We also have

$$D_{\Omega_0} L = J_0 \Omega_0 + \sum_{i=1}^n M_{iT} \hat{\rho}_i R_0^T \dot{x}_0 - \sum_{i=1}^n \sum_{j=1}^{n_i} M_{0ij} l_{ij} \hat{\rho}_i R_0^T \dot{q}_{ij} - \sum_{i=1}^n M_{iT} \hat{\rho}_i^2 \Omega_0, \quad (211)$$

$$D_{\Omega_0} L = \bar{J}_0 \Omega_0 + \sum_{i=1}^n \hat{\rho}_i R_0^T (M_{iT} \dot{x}_0 - \sum_{j=1}^{n_i} M_{0ij} l_{ij} \dot{q}_{ij}), \quad (212)$$

$$D_{\Omega_i} L = \sum_{i=1}^n J_i \Omega_i, \quad (213)$$

where \bar{J}_0 is defined as

$$\bar{J}_0 = J_0 - \sum_{i=1}^n M_{iT} \hat{\rho}_i^2. \quad (214)$$

The derivation of the Lagrangian with respect to R_0 is given by

$$\begin{aligned}
D_{R_0}L \cdot \delta R_0 &= \sum_{i=1}^n M_{iT} R_0 \hat{\eta}_0 \hat{\Omega}_0 \rho_i \cdot \dot{x}_0 \\
&\quad - \sum_{i=1}^n R_0 \hat{\eta}_0 \hat{\Omega}_0 \rho_i \cdot \sum_{j=1}^{n_i} M_{0ij} l_{ij} \dot{q}_{ij} \\
&\quad + \sum_{i=1}^n M_{iT} g e_3 \cdot R_0 \hat{\eta}_0 \rho_i,
\end{aligned} \tag{215}$$

which can be rewritten as

$$D_{R_0}L \cdot \delta R_0 = d_{R_0} \cdot \eta_0, \tag{216}$$

where

$$d_{R_0} = \sum_{i=1}^n (((\widehat{\Omega}_0 \rho_i R_0^T (M_{iT} \dot{x}_0) - \sum_{j=1}^{n_i} M_{0ij} l_{ij} \dot{q}_{ij}) + M_{iT} g \hat{\rho}_i R_0^T e_3)). \tag{217}$$

d) Lagrange-d'Alembert Principle

Consider $\mathfrak{G} = \int_{t_0}^{t_f} L$ be the action integral. Using the equations derived in previous section, the infinitesimal variation of the action integral can be written as

$$\begin{aligned}
\delta \mathfrak{G} &= \int_{t_0}^{t_f} D_{\dot{x}_0} L \cdot \delta \dot{x}_0 + D_{x_0} \cdot \delta x_0 \\
&\quad + D_{\Omega_0} L (\dot{\eta}_0 + \Omega_0 \times \eta_0) + d_{R_0} L \cdot \eta_0 \\
&\quad + \sum_{i=1}^n \sum_{j=1}^{n_i} D_{\dot{q}_{ij}} L (\dot{\xi}_{ij} \times q_{ij} + \xi_{ij} \times \dot{q}_{ij}) \\
&\quad + \sum_{i=1}^n \sum_{j=1}^{n_i} D_{q_{ij}} L \cdot (\xi_{ij} \times q_{ij}) \\
&\quad + \sum_{i=1}^n D_{\Omega_i} L \cdot (\dot{\eta}_i + \Omega_i \times \eta_i).
\end{aligned} \tag{218}$$

The total thrust at the i -th quadrotor with respect to the inertial frame is denoted by $u_i = -f_i R_i e_3 \in \mathbb{R}^3$ and the total moment at the i -th quadrotor is defined as $M_i \in \mathbb{R}^3$. The corresponding virtual work is given by

$$\delta W = \int_{t_0}^{t_f} \sum_{i=1}^n u_i \cdot \{ \delta x_0 + R_0 \hat{\eta}_0 \rho_i - \sum_{j=1}^{n_i} l_{ij} \dot{\xi}_{ij} \times q_{ij} \} + M_i \cdot \eta_i dt. \quad (219)$$

According to Lagrange-d'Alembert principle, we have $\delta \mathfrak{G} = -\delta W$ for any variation of trajectories with fixed end points. By using integration by parts and rearranging, we obtain the following Euler-Lagrange equations

$$\frac{d}{dt} D_{\dot{x}_i} L - D_{x_0} L = \sum_{i=1}^n u_i, \quad (220)$$

$$\frac{d}{dt} D_{\Omega_0} + \Omega_0 \times D_{\Omega_0} - d_{R_0} = \sum_{i=1}^n \hat{\rho}_i R_0^T u_i, \quad (221)$$

$$\hat{q}_{ij} \frac{d}{dt} D_{\dot{q}_{ij}} L - \hat{q}_{ij} D_{q_i} L = -l_{ij} \hat{q}_{ij} u_i, \quad (222)$$

$$\frac{d}{dt} D_{\Omega_i} L + \Omega_i \times D_{\Omega_i} L = M_i. \quad (223)$$

Substituting the derivatives of Lagrangians into the above expression and rearranging, the equations of motion are given by (79), (80), (81), (82).

A.9 Proof for Proposition 9

The variations of x and q are given by (93) and (94). From the kinematics equation $\dot{q}_{ij} = \omega_{ij} \times q_{ij}$ and

$$\delta \dot{q}_{ij} = \dot{\xi}_{ij} \times e_3 = \delta \omega_{ij} \times e_3 + 0 \times (\xi_{ij} \times e_3) = \delta \omega_{ij} \times e_3.$$

Since both sides of the above equation is perpendicular to e_3 , this is equivalent to $e_3 \times (\dot{\xi}_{ij} \times e_3) = e_3 \times (\delta\omega_{ij} \times e_3)$, which yields

$$\dot{\xi}_{ij} - (e_3 \cdot \dot{\xi}_{ij})e_3 = \delta\omega_{ij} - (e_3 \cdot \delta\omega_{ij})e_3.$$

Since $\xi_{ij} \cdot e_3 = 0$, we have $\dot{\xi}_{ij} \cdot e_3 = 0$. As $e_3 \cdot \delta\omega_{ij} = 0$ from the constraint, we obtain the linearized equation for the kinematics equation of the link

$$\dot{\xi}_{ij} = \delta\omega_{ij}. \quad (224)$$

The infinitesimal variation of $R_0 \in \text{SO}(3)$ in terms of the exponential map

$$\delta R_0 = \left. \frac{d}{d\epsilon} \right|_{\epsilon=0} R_0 \exp(\epsilon \hat{\eta}_0) = R_0 \hat{\eta}_0, \quad (225)$$

for $\eta_0 \in \mathbb{R}^3$. Substituting these into (79), (80), and (81), and ignoring the higher order terms, we obtain the following sets of linearized equations of motion

$$M_T \delta \ddot{x}_0 - \sum_{i=1}^n M_{iT} \hat{\rho}_i \delta \dot{\Omega}_0 + \sum_{i=1}^n \sum_{j=1}^{n_i} M_{0ij} l_{ij} \hat{e}_3 C(C^T \ddot{\xi}_{ij}) = \sum_{i=1}^n \delta u_i \quad (226)$$

$$\sum_{i=1}^n M_{iT} \hat{\rho}_i \delta \ddot{x}_0 + \bar{J}_0 \delta \dot{\Omega}_0 + \sum_{i=1}^n \sum_{j=1}^{n_i} M_{0ij} l_{ij} \hat{\rho}_i \hat{e}_3 C(C^T \ddot{\xi}_{ij}) + \sum_{i=1}^n \frac{m_0}{n} g \hat{\rho}_i \hat{e}_3 \eta_0 = \sum_{i=1}^n \hat{\rho}_i \delta u_i \quad (227)$$

$$\begin{aligned} & -M_{0ij} C^T \hat{e}_3 \delta \ddot{x}_0 + M_{0ij} C^T \hat{e}_3 \hat{\rho}_i \delta \dot{\Omega}_0 + \sum_{k=1}^{n_i} M_{0ij} l_{ik} I_2(C^T \ddot{\xi}_{ij}) \\ & = -C^T \hat{e}_3 \delta u_i + \left(-M_{iT} - \frac{m_0}{n} + M_{0ij}\right) g e_3 I_2(C^T \xi_{ij}) \end{aligned} \quad (228)$$

$$\dot{\eta}_i = \delta \Omega_i, \quad \dot{\eta}_0 = \delta \Omega_0, \quad J_i \delta \Omega_i = \delta M_i, \quad (229)$$

which can be written in a matrix form as presented in (95). See [66] for detailed derivations for a similar dynamic system. We used $C^T \hat{e}_3^2 C = -I_2$ to simplify these

derivations.

A.10 Proof for Proposition 10

We first show stability of the rotational dynamics of each quadrotor, and later it is combined with the stability analysis for the remaining parts.

a) Attitude Error Dynamics

Here, attitude error dynamics for e_{R_i} , e_{Ω_i} are derived and we find conditions on control parameters to guarantee the boundedness of attitude tracking errors. The time-derivative of $J_i e_{\Omega_i}$ can be written as

$$J_i \dot{e}_{\Omega_i} = \{J_i e_{\Omega_i} + d_i\}^\wedge e_{\Omega_i} - k_R e_{R_i} - k_\Omega e_{\Omega_i}, \quad (230)$$

where $d_i = (2J_i - \text{tr}[[J_i]I])R_i^T R_{i_d} \Omega_{i_d} \in \mathbb{R}^3$ [45]. The important property is that the first term of the right hand side is normal to e_{Ω_i} , and it simplifies the subsequent Lyapunov analysis.

b) Stability for Attitude Dynamics

Define a configuration error function on $\text{SO}(3)$ as follows

$$\Psi_i = \frac{1}{2} \text{tr}[[I - R_{i_c}^T R_i]. \quad (231)$$

We introduce the following Lyapunov function

$$\mathcal{V}_2 = \sum_{i=1}^n \mathcal{V}_{2_i}, \quad (232)$$

where

$$\mathcal{V}_{2_i} = \frac{1}{2}e_{\Omega_i} \cdot J_i \dot{e}_{\Omega_i} + k_R \Psi_i(R_i, R_{d_i}) + c_{2_i} e_{R_i} \cdot e_{\Omega_i}. \quad (233)$$

Consider a domain D_2 given by

$$D_2 = \{(R_i, \Omega_i) \in \text{SO}(3) \times \mathbb{R}^3 \mid \Psi_i(R_i, R_{d_i}) < \psi_{2_i} < 2\}. \quad (234)$$

In this domain we can show that \mathcal{V}_2 is bounded as follows [45]

$$z_{2_i}^T M_{i_{21}} z_{2_i} \leq \mathcal{V}_{2_i} \leq z_{2_i}^T M_{i_{22}} z_{2_i}, \quad (235)$$

and $z_{2_i} = [\|e_{R_i}\|, \|e_{\Omega_i}\|]^T \in \mathbb{R}^2$. Matrices $M_{i_{21}}$, $M_{i_{22}}$ are given by

$$M_{i_{21}} = \frac{1}{2} \begin{bmatrix} k_R & -c_{2_i} \lambda_{M_i} \\ -c_{2_i} \lambda_{M_i} & \lambda_{m_i} \end{bmatrix},$$

$$M_{i_{22}} = \frac{1}{2} \begin{bmatrix} \frac{2k_R}{2-\psi_{2_i}} & c_{2_i} \lambda_{M_i} \\ c_{2_i} \lambda_{M_i} & \lambda_{M_i} \end{bmatrix},$$

The time derivative of \mathcal{V}_2 along the solution of the controlled system is given by

$$\dot{\mathcal{V}}_2 = \sum_{i=1}^n -k_{\Omega} \|e_{\Omega_i}\|^2 + c_{2_i} \dot{e}_{R_i} \cdot J_i e_{\Omega_i} + c_{2_i} e_{R_i} \cdot J_i \dot{e}_{\Omega_i}.$$

Substituting (230), the above equation becomes

$$\begin{aligned} \dot{\mathcal{V}}_2 &= \sum_{i=1}^n -k_{\Omega} \|e_{\Omega_i}\|^2 + c_{2_i} \dot{e}_{R_i} \cdot J_i e_{\Omega_i} - c_{2_i} k_R \|e_{R_i}\|^2 \\ &\quad + c_{2_i} e_{R_i} \cdot ((J_i e_{\Omega_i} + d_i)^\wedge e_{\Omega_i} - k_{\Omega} e_{\Omega_i}). \end{aligned}$$

We have $\|e_{R_i}\| \leq 1$, $\|\dot{e}_{R_i}\| \leq \|e_{\Omega_i}\|$ [64], and choose a constant B_{2_i} such that $\|d_i\| \leq B_{i_2}$. Then we have

$$\dot{\mathcal{V}}_2 \leq - \sum_{i=1}^n z_{2_i}^T W_{2_i} z_{2_i}, \quad (236)$$

where the matrix $W_{2_i} \in \mathbb{R}^{2 \times 2}$ is given by

$$W_{2_i} = \begin{bmatrix} c_{2_i} k_R & -\frac{c_{2_i}}{2} (k_\Omega + B_{2_i}) \\ -\frac{c_{2_i}}{2} (k_\Omega + B_{2_i}) & k_\Omega - 2c_{2_i} \lambda_{M_i} \end{bmatrix}.$$

The matrix W_{2_i} is a positive definite matrix if

$$c_{2_i} < \min \left\{ \frac{\sqrt{k_R \lambda_{m_i}}}{\lambda_{M_i}}, \frac{4k_\Omega}{8k_R \lambda_{M_i} + (k_\Omega + B_{i_2})^2} \right\}. \quad (237)$$

This implies that

$$\dot{\mathcal{V}}_2 \leq - \sum_{i=1}^n \lambda_m(W_{2_i}) \|z_{2_i}\|^2, \quad (238)$$

which shows stability of the attitude dynamics of quadrotors.

c) Error Dynamics of the Payload and Links

We derive the tracking error dynamics and a Lyapunov function for the translational dynamics of a payload and the dynamics of links. Later it is combined with the stability analyses of the rotational dynamics. From (79), (95), (100), and (105), the equation of motion for the controlled dynamic model is given by

$$\mathbf{M}\ddot{\mathbf{x}} + \mathbf{G}\mathbf{x} = \mathbf{B}(u - u^*) + \mathbf{g}(\mathbf{x}, \dot{\mathbf{x}}), \quad (239)$$

where

$$u = \begin{bmatrix} u_1 \\ u_2 \\ \vdots \\ u_n \end{bmatrix}, \quad u^* = \begin{bmatrix} -(M_{1T} + \frac{m_0}{n})ge_3 \\ -(M_{2T} + \frac{m_0}{n})ge_3 \\ \vdots \\ -(M_{nT} + \frac{m_0}{n})ge_3 \end{bmatrix}, \quad (240)$$

and $\mathbf{g}(\mathbf{x}, \dot{\mathbf{x}})$ corresponds to the higher order terms. As $u_i = -f_i R_i e_3$ for the full dynamic model, $\delta u = u - u^*$ is given by

$$\delta u = \begin{bmatrix} -f_1 R_1 e_3 + (M_{1T} + \frac{m_0}{n})ge_3 \\ -f_2 R_2 e_3 + (M_{2T} + \frac{m_0}{n})ge_3 \\ \vdots \\ -f_n R_n e_3 + (M_{nT} + \frac{m_0}{n})ge_3 \end{bmatrix}. \quad (241)$$

The subsequent analyses are developed in the domain D_1

$$D_1 = \{(\mathbf{x}, \dot{\mathbf{x}}, R_i, e_{\Omega_i}) \in \mathbb{R}^{D_x} \times \mathbb{R}^{D_x} \times \text{SO}(3) \times \mathbb{R}^3 \mid \Psi_i < \psi_{1_i} < 1\}. \quad (242)$$

In the domain D_1 , we can show that

$$\frac{1}{2} \|e_{R_i}\|^2 \leq \Psi_i(R_i, R_{c_i}) \leq \frac{1}{2 - \psi_{1_i}} \|e_{R_i}\|^2. \quad (243)$$

Consider the quantity $e_3^T R_{c_i}^T R_i e_3$, which represents the cosine of the angle between $b_{3_i} = R_i e_3$ and $b_{3_{c_i}} = R_{c_i} e_3$. Since $1 - \Psi_i(R_i, R_{c_i})$ represents the cosine of the eigen-axis rotation angle between R_{c_i} and R_i , we have $e_3^T R_{c_i}^T R_i e_3 \geq 1 - \Psi_i(R_i, R_{c_i}) > 0$ in D_1 . Therefore, the quantity $\frac{1}{e_3^T R_{c_i}^T R_i e_3}$ is well-defined. We add and subtract $\frac{f_i}{e_3^T R_{c_i}^T R_i e_3} R_{c_i} e_3$

to the right hand side of (241) to obtain

$$\delta u = \begin{bmatrix} \frac{-f_1}{e_3^T R_{c_1}^T R_{1e_3}} R_{c_1} e_3 - X_1 + (M_{1T} + \frac{m_0}{n}) g e_3 \\ \frac{-f_2}{e_3^T R_{c_2}^T R_{2e_3}} R_{c_2} e_3 - X_2 + (M_{2T} + \frac{m_0}{n}) g e_3 \\ \vdots \\ \frac{-f_n}{e_3^T R_{c_n}^T R_{ne_3}} R_{c_n} e_3 - X_n + (M_{nT} + \frac{m_0}{n}) g e_3 \end{bmatrix}. \quad (244)$$

where $X_i \in \mathbb{R}^3$ is defined by

$$X_i = \frac{f_i}{e_3^T R_{c_i}^T R_{ie_3}} ((e_3^T R_{c_i}^T R_{ie_3}) R_{ie_3} - R_{c_i} e_3). \quad (245)$$

Using

$$-\frac{f_i}{e_3^T R_{c_i}^T R_{ie_3}} R_{c_i} e_3 = -\frac{(\|A_i\| R_{c_i} e_3) \cdot R_{ie_3}}{e_3^T R_{c_i}^T R_{ie_3}} \cdot -\frac{A_i}{\|A_i\|} = A_i, \quad (246)$$

the equation (244) becomes

$$\delta u = \begin{bmatrix} A_1 - X_1 + (M_{1T} + \frac{m_0}{n}) g e_3 \\ A_2 - X_2 + (M_{2T} + \frac{m_0}{n}) g e_3 \\ \vdots \\ A_n - X_n + (M_{nT} + \frac{m_0}{n}) g e_3 \end{bmatrix}. \quad (247)$$

Substituting (100) into the above equation, (239) becomes

$$\mathbf{M}\ddot{\mathbf{x}} + \mathbf{G}\dot{\mathbf{x}} = \mathbf{B}(-K_{\mathbf{x}}\mathbf{x} - K_{\dot{\mathbf{x}}}\dot{\mathbf{x}} - X) + \mathbf{g}(\mathbf{x}, \dot{\mathbf{x}}), \quad (248)$$

where $X = [X_1^T, X_2^T, \dots, X_n^T]^T \in \mathbb{R}^{3n}$. It is rewritten in the following matrix form

$$\dot{z}_1 = \mathbf{A}z_1 + \mathbf{B}(\mathbf{B}X + \mathbf{g}(\mathbf{x}, \dot{\mathbf{x}})), \quad (249)$$

where $z_1 = [\mathbf{x}, \dot{\mathbf{x}}]^T \in \mathbb{R}^{2D_x}$ and

$$\mathbf{A} = \begin{bmatrix} 0 & I \\ -\mathbf{M}^{-1}(\mathbf{G} + \mathbf{B}K_x) & -\mathbf{M}^{-1}\mathbf{B}K_{\dot{x}} \end{bmatrix}, \mathbf{B} = \begin{bmatrix} 0 \\ \mathbf{M}^{-1} \end{bmatrix}. \quad (250)$$

We can also choose K_x and $K_{\dot{x}}$ such that $\mathbf{A} \in \mathbb{R}^{2D_x \times 2D_x}$ is Hurwitz. Then for any positive definite matrix $Q \in \mathbb{R}^{2D_x \times 2D_x}$, there exist a positive definite and symmetric matrix $P \in \mathbb{R}^{2D_x \times 2D_x}$ such that $\mathbf{A}^T P + P\mathbf{A} = -Q$ according to [63, Thm 3.6].

d) Lyapunov Candidate for Simplified Dynamics

From the linearized control system developed at section 3, we use matrix P to introduce the following Lyapunov candidate for translational dynamics

$$\mathcal{V}_1 = z_1^T P z_1. \quad (251)$$

The time derivative of the Lyapunov function using the Leibniz integral rule is given by

$$\dot{\mathcal{V}}_1 = \dot{z}_1^T P z_1 + z_1^T P \dot{z}_1. \quad (252)$$

Substituting (249) into above expression

$$\dot{\mathcal{V}}_1 = z_1^T (\mathbf{A}^T P + P\mathbf{A}) z_1 + 2z_1^T P \mathbf{B} (\mathbf{B}X + \mathbf{g}(\mathbf{x}, \dot{\mathbf{x}})). \quad (253)$$

Let $c_3 = 2\|P\mathbf{B}\mathbf{B}\|_2 \in \mathbb{R}$ and using $\mathbf{A}^T P + P\mathbf{A} = -Q$, we have

$$\dot{\mathcal{V}}_1 \leq -z_1^T Q z_1 + c_3 \|z_1\| \|X\| + 2z_1^T P \mathbf{B} \mathbf{g}(\mathbf{x}, \dot{\mathbf{x}}). \quad (254)$$

The second term on the right hand side of the above equation corresponds to the effects of the attitude tracking error on the translational dynamics. We find a bound of X_i , defined at (245), to show stability of the coupled translational dynamics and rotational dynamics in the subsequent Lyapunov analysis. Since

$$f_i = \|A_i\|(e_3^T R_{c_i}^T R_i e_3), \quad (255)$$

we have

$$\|X_i\| \leq \|A_i\| \|(e_3^T R_{c_i}^T R_i e_3) R_i e_3 - R_{c_i} e_3\|. \quad (256)$$

The last term $\|(e_3^T R_{c_i}^T R_i e_3) R_i e_3 - R_{c_i} e_3\|$ represents the sine of the angle between $b_{3_i} = R_i e_3$ and $b_{3_{c_i}} = R_{c_i} e_3$, since $(b_{3_{c_i}} \cdot b_{3_i}) b_{3_i} - b_{3_{c_i}} = b_{3_i} \times (b_{3_i} \times b_{3_{c_i}})$. The magnitude of the attitude error vector, $\|e_{R_i}\|$ represents the sine of the eigen-axis rotation angle between R_{c_i} and R_i . Therefore, $\|(e_3^T R_{c_i}^T R_i e_3) R_i e_3 - R_{c_i} e_3\| \leq \|e_{R_i}\|$ in D_1 . It follows that

$$\begin{aligned} \|(e_3^T R_{c_i}^T R_i e_3) R_i e_3 - R_{c_i} e_3\| &\leq \|e_{R_i}\| = \sqrt{\Psi_i(2 - \Psi_i)} \\ &\leq \{\sqrt{\psi_{1_i}(2 - \psi_{1_i})} \triangleq \alpha_i\} < 1, \end{aligned} \quad (257)$$

therefore

$$\begin{aligned} \|X_i\| &\leq \|A_i\| \|e_{R_i}\| \\ &\leq \|A_i\| \alpha_i. \end{aligned} \quad (258)$$

We find an upper boundary for

$$A_i = -K_{\mathbf{x}} \mathbf{x} - K_{\dot{\mathbf{x}}} \dot{\mathbf{x}} + u_i^*, \quad (259)$$

by defining

$$\|u_i^*\| \leq B_{1_i}, \quad (260)$$

for a given positive constant B_1 . defining $K_{max} \in \mathbb{R}$

$$K_{max} = \max\{\|K_{\mathbf{x}}\|, \|K_{\dot{\mathbf{x}}}\|\},$$

and then the upper bound of A is given by

$$\begin{aligned} \|A_i\| &\leq K_{max}(\|\mathbf{x}\| + \|\dot{\mathbf{x}}\|) + B_1 \\ &\leq 2K_{max}\|z_1\| + B_1. \end{aligned} \quad (261)$$

Using the above steps we can show that

$$\begin{aligned} \|X\| &\leq \sum_{i=1}^n ((2K_{max}\|z_1\| + B_1)\|e_{R_i}\|) \\ &\leq (2K_{max}\|z_1\| + B_1)\alpha, \end{aligned} \quad (262)$$

where $\alpha = \sum_{i=1}^n \alpha_i$. Then, we can simplify (254) as

$$\dot{\mathcal{V}}_1 \leq -(\lambda_{\min}(Q) - 2c_3K_{max}\alpha)\|z_1\|^2 + \sum_{i=1}^n c_3B_1\|z_1\|\|e_{R_i}\| + 2z_1^T P B \mathbf{g}(\mathbf{x}, \dot{\mathbf{x}}). \quad (263)$$

e) Lyapunov Candidate for the Complete System

Let $\mathcal{V} = \mathcal{V}_1 + \mathcal{V}_2$ be the Lyapunov function for the complete system. The time derivative of \mathcal{V} is given by

$$\dot{\mathcal{V}} = \dot{\mathcal{V}}_1 + \dot{\mathcal{V}}_2. \quad (264)$$

Substituting (263) and (238) into the above equation

$$\begin{aligned} \dot{\mathcal{V}} \leq & -(\lambda_{\min}(Q) - 2c_3K_{\max}\alpha)\|z_1\|^2 + 2z_1^T P B \mathbf{g}(\mathbf{x}, \dot{\mathbf{x}}) \\ & + \sum_{i=1}^n c_3 B_1 \|z_1\| \|e_{R_i}\| - \sum_{i=1}^n \lambda_m(W_{2_i}) \|z_{2_i}\|^2, \end{aligned} \quad (265)$$

and using $\|e_{R_i}\| \leq \|z_{2_i}\|$, it can be written as

$$\begin{aligned} \dot{\mathcal{V}} \leq & -(\lambda_{\min}(Q) - 2c_3K_{\max}\alpha)\|z_1\|^2 + 2z_1^T P B \mathbf{g}(\mathbf{x}, \dot{\mathbf{x}}) \\ & + \sum_{i=1}^n c_3 B_1 \|z_1\| \|z_{2_i}\| - \sum_{i=1}^n \lambda_m(W_{2_i}) \|z_{2_i}\|^2. \end{aligned} \quad (266)$$

The $2z_1^T P B \mathbf{g}(\mathbf{x}, \dot{\mathbf{x}})$ term in the above equation is indefinite. The function $\mathbf{g}(\mathbf{x}, \dot{\mathbf{x}})$ satisfies

$$\frac{\|\mathbf{g}(\mathbf{x}, \dot{\mathbf{x}})\|}{\|z_1\|} \rightarrow 0 \quad \text{as} \quad \|z_1\| \rightarrow 0.$$

Then, for any $\gamma > 0$ there exists $r > 0$ such that

$$\|\mathbf{g}(\mathbf{x}, \dot{\mathbf{x}})\| < \gamma \|z_1\| \quad \forall \|z_1\| < r.$$

Therefore

$$2z_1^T P B \mathbf{g}(\mathbf{x}, \dot{\mathbf{x}}) \leq 2\gamma \|P\|_2 \|z_1\|^2. \quad (267)$$

Substituting the above inequality into (266)

$$\begin{aligned} \dot{\mathcal{V}} \leq & -(\lambda_{\min}(Q) - 2c_3K_{\max}\alpha)\|z_1\|^2 + 2\gamma \|P\|_2 \|z_1\|^2 \\ & + \sum_{i=1}^n c_3 B_1 \|z_1\| \|z_{2_i}\| - \sum_{i=1}^n \lambda_m(W_{2_i}) \|z_{2_i}\|^2, \end{aligned} \quad (268)$$

and rearranging

$$\begin{aligned}\dot{\mathcal{V}} \leq & - \sum_{i=1}^n \left(\frac{\lambda_{\min}(Q) - 2c_3K_{\max}\alpha}{n} \|z_1\|^2 \right. \\ & \left. - c_3B_1\|z_1\|\|z_{2_i}\| + \lambda_m(W_{2_i})\|z_{2_i}\|^2 \right) \\ & + 2\gamma\|P\|_2\|z_1\|^2,\end{aligned}\tag{269}$$

we obtain

$$\dot{\mathcal{V}} \leq - \sum_{i=1}^n (\mathbf{z}_i^T W_i \mathbf{z}_i) + 2\gamma\|P\|_2\|z_1\|^2,\tag{270}$$

where $\mathbf{z}_i = [\|z_1\|, \|z_{2_i}\|]^T \in \mathbb{R}^2$ and

$$W_i = \begin{bmatrix} \frac{\lambda_{\min}(Q) - 2c_3K_{\max}\alpha}{n} & -\frac{c_3B_{1_i}}{2} \\ -\frac{c_3B_{1_i}}{2} & \lambda_m(W_{2_i}) \end{bmatrix}.\tag{271}$$

By using $\|z_1\| \leq \|\mathbf{z}_i\|$, we obtain

$$\dot{\mathcal{V}} \leq - \sum_{i=1}^n \left(\lambda_{\min}(W_i) - \frac{2\gamma\|P\|_2}{n} \right) \|\mathbf{z}_i\|^2.\tag{272}$$

Choosing $\gamma < n(\lambda_{\min}(W_i))/2\|P\|_2$, and

$$\lambda_m(W_{2_i}) > \frac{n\|\frac{c_3B_{1_i}}{2}\|^2}{\lambda_{\min}(Q) - 2c_3K_{\max}\alpha},\tag{273}$$

ensures that $\dot{\mathcal{V}}$ is negative definite. Then, the zero equilibrium is exponentially stable.